NMR Study of Polymer Blends : Polymer/Polymer and Polymer/Lithium-Salt Blends

by

Atsushi Asano

January 1994

Department of Polymer Science,
Faculty of Science, Hokkaido University

(1)

NMR Study of Polymer Blends:

Polymer/Polymer and Polymer/Lithium-Salt Blends

by

Atsushi Asano

January 1994

A Dissertation submitted to

Department of Polymer Science,

Faculty of Science, Hokkaido University

Sapporo 060 Japan

in fulfillment of the degree of Doctor of Science

Preface

Since polymer blends have superior physical and/or chemical properties, and since they can be easily obtained by mixing two or more different components, they are nowadays widely used in industry. In order to develop new materials of high performance, it is requisite to study the interaction between the components, structure, and dynamics of blends.

In 1974 and 1975, pioneering studies of morphology and phase-separation process of polystyrene/poly(vinyl methyl ether) blends were done by Nishi, et al. using the broad line ^{1}H NMR spectroscopy. In 1981, Schaefer, et al. first applied the solid-state high-resolution ^{13}C NMR spectroscopy (eg. CP/MAS) to polymer blends to study the morphology and miscibility.

This doctoral dissertation presents a structural investigation in a molecular level of polymer blends by the high-resolution NMR technique. Topics investigated here are the interaction, miscibility, molecular motion, and phase-separation process of polymer/polymer blends. Polycarbonate/poly(methyl methacrylate) and polystyrene/poly(vinyl methyl ether) blends are studied. The morphology and mobility of Li^{+}-ion of poly(ethylene oxide)/$LiClO_4$ blend are studied. This blend shows ionic conductivity in the solid state. The results obtained here will be useful for understanding the structure and physical property of polymer blends and for exploiting new synthetic polymeric materials.

Atsushi Asano (Sapporo, January 1994)

Contents

Chapter 1 General Introduction

1.1 Polymer/Polymer Blends

Polymer/polymer blends are widely used for engineering purposes. The research of polymer/polymer blends has been progressively developed. The physical and/or chemical properties of polymer/polymer blends mainly depend on its miscibility and/or phase structure. In particular, the homo- or heterogeneous domain size (morphology), the molecular dynamics, the fluctuation of composition, and the interphase (or interface) between component polymers affect the physical property. In order to exploit new polymer materials, we need such information.

Thermodynamic properties of polymer blend have been extensively studied.[1] Polymer/polymer blends are miscible (homogeneous), if the free energy of mixing ΔG_m is negative. Such a condition is encountered for only a few polymer pairs. The entropy of mixing ΔS_m of polymers is nearly zero and the enthalpy of mixing ΔH_m is, in general, positive.[1] Thus, the value of $\Delta G_m=\Delta H_m-T\Delta S_m$ is positive, T the absolute temperature. However, when an exothermic interaction exists between two polymers, ΔH_m is negative. Therefore, if a specific inter-polymer interaction is operative between two polymers, they can be in close proximity, resulting in a miscible state.

The miscibility (morphology) and phase-separation process of polymer/polymer blends have been studied by differential scanning calorimetry (DSC),[2] light scattering,[3] fluorescence emission,[4] Fourier transform infrared spectroscopy (FT-IR),[5] small angle X-ray scattering (SAXS, wide angle X-ray diffraction; WAXD),[6] scanning and transmission electron microscopes (SEM and TEM),[7] and so on. Besides advantages, these measurements have some limitations for study of polymer/polymer blend. DSC is useful for determining a miscible polymer pair, but can not detect the domain size. It is not sensitive to phase-separation on a smaller scale. Light scattering and SAXS can examine change of domain size on a larger scale. It is difficult to determine the composition in each domain. Fluorescence emission study gives information on a scale of 20-30 Å, but component polymer must be labeled by fluorescent anthracene units. This limits polymer/polymer blends to be analyzed. SEM and TEM require a cured sample for observation. FT-IR can detect a polymer-polymer interaction, i.e., hydrogen bonding, through the red-shift of absorption. FT-IR is, however, not sensitive to change in domain size.

Recent development of high-resolution solid-state NMR techniques has enabled us to characterize the heterogeneity in polymers.[8] In most cases, the heterogeneity manifests itself in the magnetic relaxation phenomenon. The most significant magnetic relaxation in solid polymers is governed by the ^{1}H dipole-dipole interaction, which is a function of inter-proton distance.[9] Examination of relaxation phenomena such as ^{1}H spin-diffusion can

reveal the spatial proximity and the heterogeneous structure of polymer/polymer blends in the solid state.[10-13] The ^{13}C cross-polarization/magic-angle-spinning (CP/MAS)[14] solid-state NMR spectroscopy is very useful for characterizing homo- or heterogeneity in polymer/polymer blends.[15,16] Stejskal, *et al.* showed an advantage of the use of well-resolved spectra of a dilute spin such as ^{13}C nucleus to monitor the ^{1}H relaxation behavior.[15] This method is quite powerful to study miscibility (morphology) and phase-separated domain structure in polymer/polymer blends.

Table 1-1 lists polymer/polymer blends investigated by NMR methods in 1973 to 1993. Those are mainly collected from papers published in *Macromolecules* and *Polymer*. For twenty years, about one hundred papers were published and seventy kinds of polymer/polymer blends are studied by NMR. In particular, for last four years (1990-1993), more than half of those papers were published. This indicates that polymer/polymer blends are very important materials in more recent years for industry (technology) and science, and that NMR measurements can reveal easily and clearly the domain structure of polymer/polymer blends.

Table 1-1 List of polymer/polymer blends examined by NMR techniques which were published in *Macromolecules* and *Polymer* in 1973 to 1993; Polymer/polymer blends published in other journals are also included

Polymer I	Polymer II	Reference Number
PS	PVME	1 - 10
PS	PMMA	11, 12
PS	PBMA	13
PS	PPO	14 - 17
P2(4)MS	PPO	15
PS	PB	18, 19
PS	PVPy	20
PS	PVIZ	20
PS	PEA	20, 21
PS	PDMAA	22
PS	PAc	23
PS	PS-d_8	24
PS	PC	25
PS	PU	26
PVF_2	PMMA	27 - 31
PVF_2	PEMA	28
PVPh	PMMA	32, 33
PVAc	PMMA	34
PVC	PMMA	4, 35, 36
PVC	PCHMA	36
PVC	PBZMA	36
PVC	PTEGMA	37
PC	PMMA	38, 39
PU	PMMA	40
PEO	PMMA	41 - 43
PEO	PVC	44
PVA	PMAA	45
PVA	PAA	45
PVA	PVP	46, 47
PMA	PVAc	48
PMA	PVPh	32
PDMAA	PVPh	22, 49
PVMK	PVPh	50
PEO	PVPh	51
PC	PET	52, 53
PC	PBT	54
PAr	PBT	55, 56
PENDC	PET	57
Nylon66	PBZT	58
Nylon6	PS	59
Nylon6	Li-SPS	60
Nylon6	Zn-SPS	61
PCL	PVC	62
POT	PPO	63
PEI	PBI	58, 64
PEI	PAEK	65
PES	PIm	66
PES	PPS	67
PBI	PIm	68
PI	PVE	69
PI	PB	70
PI	PChP	71
PI	epo-PI	71
PE	PAc	72
PHPM	PDMAA	73
PECMA	PNBEA	74
PDMS	Silicone	75
PDMS	PDMS-d_6	76
PU	PU-d_6	76
PS-PAN	PMMA	77
PS-PVPh	PMMA	78
PS-PVPh	PBMA	79
PVPy-PEA	PS	20
PVIZ-PEA	PS	20
PS-PSSA	PMMA-PVPy	11, 80
PS-PSSA	PDMAA	22
PS-PSSA	PU	81
PS-PVPh	PDMAA	22
PS-PAAMA	PEA-PMVPyI	21
PS-PSSNa	PEA-PMVPyI	21
PENDC-PHBZA	PET	57
Vectra-A	PET	82
PDMS-PDPS	Silicone	75
PS-PB	PS	83
SBR	PB	84

Continued.

Continued.

Continued.

Abbreviations :

PS : Polystyrene, PVME: Poly(vinyl methyl ether), PMMA : Poly(methyl methacrylate), PBMA : Poly(butyl methacrylate), PPO : Poly(2,6-dimethyl-1,4-phenylene oxide), P2(4)MS : Poly(2-methyl styrene) or Poly(4-methylstyrene), PB : Polybutadiene, PVPy : Poly(4-vinylpyridine), PVIZ : Poly(N-vinylimidazole), PEA : Poly(ethyl acrylate), PDMAA : Poly(N,N-dimethylacrylamid), PAc : Poly acetylene, PC : Polycarbonate, PU : Polyurethane, PVF2 : Poly(vinylidene fluoride), PEMA : Poly(ethyl methacrylate), PVPh : Poly(4-vinyl phenol), PVAc : Poly(vinyl acetate), PVC : Poly(vinyl chloride), PCHMA : Poly(cyclohexyl methacrylate), PBZMA : Poly(benzyl methacrylate), PTEGMA : Poly(tetraethylene glycol dimethacrylate), PEO : Poly(ethylene oxide), PVA : Poly(vinyl alcohol), PMAA : Poly(methacrylic acid), PAA : Poly(acrylic acid), PVP : Poly(N-vinyl-2-pyrrolidone), PMA : Poly(methyl acrylate), PVMK : Poly(vinyl methyl ketone), PET : Poly(ethylene terephthalate), PBT : Poly(butylene terephthalate), PAr : Polyarylate, PENDC : Poly(ethylene naphthalene dicarboxylate), PBZT: Poly(benz[a,d]dithiazol-2,6-diyl-1,4-phenylene), Nylon6 : Poly(ε-caprolactam), Li-SPS : lithium salt of sulfonated PS, Zn-SPS : zinc salt of SPS, PCL : Poly(ε-caprolactone), POT : Poly(3-octylthiophene), PEI : Poly(ether imide), PBI : Poly benzimidazole, PAEK : Poly(aryl ether ketone), PES : Poly(ether sulphone), PIm : Polyimide, PPS : Poly(phenylene sulphide), PI : Polyisoprene, PVE : Poly(vinyl ethylene), PChP : Polychloroprene, epo-PI : epoxidized PI, PE : Polyethylene, PHPM : Poly([1-hydroxy-2,6-phenylene]methylene), PECMA : Poly([N-ethylcarbazol-3-yl]methyl acetate), PNBEA : Poly(2-[{3,5-dinitrobenzoyl}oxy]ethyl acetate), PDMS : Poly(dimethylsiloxane), PS-PAN : PS-co-Polyacrylonitrile (copolymer), PSSA : Poly(styrene sulfonic acid), PAAMA : Poly(tetraalkylammonium methacrylate), PMVPyI : Poly(N-methyl-4-vinyl pyridinium iodide), PSSNa : Poly(sodium styrenesulfonate), PHBZA : Poly(p-hydroxybenzoic acid), Vectra-A : Poly(p-hydroxybenzoic acid-co-p-hydroxynaphthoic acid), PDPS : Poly(diphenylsiloxane), SBR : styrene-butadiene rubbers

References for Table 1-1

1. (a)Kwei,T.K.;Nishi,T.;Roberts,R.F. *Macromolecules*, 1974, *7*, 667.
   (b)Nishi,T.;Wang,T.T.;Kwei,T.K. *Macromolecules*, 1975, *8*, 227.
2. Kaplan,S. *ACS Polym. Prep.*, 1984, *25*, 356.
3. (a)Caravatti,P.;Neuenschwander,P.;Ernst,R.R. *Macromolecules*, 1985, *18*, 119.
   (b)Caravatti,P.;Neuenschwander,P.;Ernst,R.R. *Macromolecules*, 1986, *19*, 1889.
4. Parmer,J.F.;Dickinson,L.C.;Chien,J.C.W.;Porter,R.S. *Macromolecules*, 1987, *20*, 2308.
5. Gobbi,G.C.;Silvestri,R.;Russell,T.P.;Lyerla,J.R.;Fleming,W.W.;Nishi,T. *J. Polym. Sci., Part C, Polym. Lett.*, 1987, *25*, 61.
6. Crowther,M.W.;Cabasso,I.;Levy,G.C. *Macromolecules*, 1988, *21*, 2924.
7. (a)Mirau,P.A.;Tanaka,H.;Bovey,F.A. *Macromolecules*, 1988, *21*, 2929.
   (b)Mirau,P.A.;Bovey,F.A. *Macromolecules*, 1990, *23*, 4548.
   (c)White,J.L.;Mirau,P.A. *Macromolecules*, 1993, *26*, 3049.
8. Chu,C.-W.;Dickinson,L.C.;Chien,J.C.W. *J. Appl. Polym. Sci.*, 1990, *41*, 2311.
9. Takegoshi,K.;Hikichi,K. *J. Chem. Phys.*, 1991, *94*, 3200.
10. Menestrel,C.Le;Kenwright,A.M.;Sergot,P.;Laupretre,F.; Monnerie,L. *Macromolecules*, 1992, *25*, 3020.
11. Zhang,X.;Natansohn,A.;Eisenberg,A. *Macromolecules*, 1990, *23*, 412.
12. (a)Spiess,H.W. *Makromol. Chem., Macromol. Symp.*, 1991, *50*, 241.
    (b)Clauss,J.;Schmidt-Rohr,K.;Spiess,H.W. *Acta Polymer*, 1993, *44*, 1.
13. Campbell,G.C.;VanderHart,D.L.;Feng,Yi;Han,C.C. *Macromolecules*, 1992, *25*, 2107.
14. Stejskal,E.O.;Schaefer,J.;Sefcik,M.D.;McKay,R.A. *Macromolecules*, 1981, *14*, 275.
15. Dickinson,L.C.;Yang,H.;Chu,C.-W.;Stein,R.S.;Chien,J.C.W. *Macromolecules*, 1987, *20*, 1757.
16. (a)Kambour,R.P.;Kelly,J.M.;McKinley,B.J.;Cauley,B.J.;Inglefield,P.T.; Jones,A.A. *Macromolecules*, 1988, *21*, 2937.
    (b)Chin,Y.H.;Zhang,C.;Wang,P.;Inglefield,P.T.;Jones,A.A.; Kambour,R.P.;Bendler,J.T.;White,D.M. *Macromolecules*, 1992, *25*, 3031.
    (c)Chin,Y.H.;Inglefield,P.T.;Jones,A.A. *Macromolecules*, 1993, *26*, 5372.
    (d)Pavlovskaya,G.;Hansen,M.;Jones,A.A.;Inglefield,P.T. *Macromolecules*, 1993, *26*, 6310.

17. Feng,H.;Feng,Z.;Ruan,H.;Shen,L. *Macromolecules*, 1992, *25*, 5981.
18. Cory,D.G.;Boer,J.C.de;Veeman,W.S. *Macromolecules*, 1989, *22*, 1618.
19. Segre,A.L.;Capitani,D.;Fiordiponti,P.;Cantini,P.L.; Callaioli,A.;Ferrando,A.;Nocci,R. *Eur. Polym. J.*, 1992, *28*, 1165.
20. Crick,D.E.;Alexandratos,S.D. *Macromolecules*, 1993, *26*, 3267.
21. Zhang,X.;Eisenberg,A. *J. Polym. Sci., Part B, Polym. Phys.*, 1990, *28*, 1841.
22. Kelts,L.W.;Landry,C.J.T.;Teegarden,D.M. *Macromolecules*, 1993, *26*, 2941.
23. Dumais,J.J.;Jelinski,L.W.;Galvin,M.E.;Dybowsi,C.;Brown,C.E.; Kovacic,P. *Macromolecules*, 1989, *22*, 612.
24. VanderHart,D.L.;Manders,W.F.;Stein,R.S.;Herman,W. *Macromolecules*, 1987, *20*, 1724.
25. (a)Afewori,M.;McKay,R.A.;Schaefer,J. *Macromolecules*, 1992, *25*, 4084.
(b)Afewori,M.;Schaefer,J. *Macromolecules*, 1992, *25*, 4092.
(c)Afewori,M.;Schaefer,J. *Macromolecules*, 1992, *25*, 4097.
(d)Afewori,M.;Vega,S.;Schaefer,J. *Macromolecules*, 1992, *25*, 4100.
26. Russell,T.P.;Lee,D.S.;Nishi,T.;Kim,S.C. *Macromolecules*, 1993, *26*, 1922.
27. Bovey,F.A.;Shilling,F.C.;Kwei,T.K.;Frisch,H.L. *Macromolecules*, 1977, *10*, 559.
28. Douglass,D.C.;McBrierty,V.J. *Macromolecules*, 1978, *11*, 766.
29. Tekely,P.;Laupretre,F.;Monnerie,L. *Polymer*, 1985, *26*, 1081.
30. (a)Douwel,C.H.K.;Maas,W.E.J.R.;Veeman,W.S.;Buning,G.H.W.;Vankan,J.M.J. *Macromolecules*, 1990, *23*, 406.
(b)Maas,W.E.J.R.;Heijden,W.A.C.v.d.;Veeman,W.S.;Vankan,J.M.J.Buning,G.H.W. *J. Chem. Phys.*, 1991, *95*, 4698.
(c)Eijkelenboom,A.P.A.M.;Maas,W.E.J.R.;Veeman,W.S.;Buning,G.H.W.; Vankan,J.M.J. *Macromolecules*, 1992, *25*, 4511.
(d)Papavoine,C.H.M.;Maas,W.E.J.R.;Veeman,W.S.;Buning,G.H.W.;Vankan,J.M.J. *Macromolecules*, 1993, *26*, 6611.
31. Grinsted,R.A.;Koenig,J.L. *J. Polym. Sci., Part B, Polym. Phys.*, 1990, *28*, 177.
32. (a)Zhang,X.;Takegoshi,K.;Hikichi,K. *Macromolecules*, 1991, *24*, 5756.
(b)Zhang,X.;Takegoshi,K.;Hikichi,K. *Macromolecules*, 1991, *25*, 4871.
33. Zumbulyadis,N.;Landry,C.J.T.;Long,T.E. *Macromolecules*, 1993, *26*, 2647.
34. Schenk,W.;Reichert,D.;Schneider,H. *Polymer*, 1990, *31*, 329.
35. Albert,B.;Jerome,R.;Teyssie,P.;Smyth,G.;Boyle,N.G.;McBrierty,V.J. *Macromolecules*, 1985, *18*, 388. [CORRECTION] *Macromolecules*, 1985, *18*, 1640.
36. Parmer,J.F.;Dickinson,L.C.;Chien,J.C.W.;Porter,R.S. *Macromolecules*, 1989, *22*, 1078.
37. Davis,D.D.;Slichter,W.P. *Macromolecules*, 1973, *6*, 728.
38. Landry,C.J.T.;Henrichs,P.M. *Macromolecules*, 1989, *22*, 2157.
39. (a)Asano,A.;Takegoshi,K.;Hikichi,K. *Polym. J.* 1992, *24*, 473.
(b)Asano,A.;Takegoshi,K.;Hikichi,K. *Polym. J.* 1992, *24*, 555.
40. Parizel,N.;Meyer,G.;Weill,G. *Polymer*, 1993, *34*, 2495.
41. Martuscelli,E.;Demma,G. *Polym. Commun.*, 1983, *24*, 266.
42. Marco,C.;Fatou,J.G.;Gomez,M.A.;Tanaka,H.;Tonelli,A.E. *Macromolecules*, 1990, *23*, 2183.
43. Brosseau,C.;Guillermo,A.;Cohen-Addad,J.P. *Polymer*, 1992, *33*, 2076.
44. Marco,C.;Gomez,M.A.;Fatou,J.G.;Etxeberria,A.;Elorza,M.M.;Iruin,J.J. *Eur. Polym. J.*, 1993, *11*, 1477.
45. (a)Zhang,X.;Takegoshi,K.;Hikichi,K. *Polym. J.*, 1991, *23*, 79.
(b)Zhang,X.;Takegoshi,K.;Hikichi,K. *Polym. J.*, 1991, *23*, 87.
(c)Zhang,X.;Takegoshi,K.;Hikichi,K. *Polymer*, 1992, *33*, 718.
46. Zhang,X.;Takegoshi,K.;Hikichi,K. *Polymer*, 1992, *33*, 712.
47. Feng,H.;Geng,Z.;Shen,L. *Polymer*, 1993, *34*, 2516.
48. Takegoshi,K.;Ohya,Y.;Hikichi,K. *Polym. J.*, 1993, *25*, 59.
49. Suzuki, T.;Pearce,E.M.;Kwei,T.K. *Polym. Commun.*, 1992, *33*, 198.
50. C.Qin;Pires,A.T.N.;Belfiore,L.A. *Macromolecules*, 1991, *24*, 666.
51. (a)Zhang,X.;Takegoshi,K.;Hikichi,K. *Macromolecules*, 1992, *25*, 2336.
(b)Zhang,X.;Takegoshi,K.;Hikichi,K. *Macromolecules*, 1993, *26*, 2198.
52. (a)Linder,M.;Henrichs,P.M.;Hewitt,J.M.;Massa,D.J. *J. Chem. Phys.*, 1985, *82*, 1585.
(b)Henrichs,P.M.;Tribone,J.;Massa,D.J.;Hewitt,J.M. *Macromolecules*, 1988, *21*, 1282.
53. Zheng,W.G.;Wan,Z.H.;Qi,Z.N.;Wang,F.S. *Polymer*, 1993, *34*, 4982.
54. Velden,G.v.d.;Kolfschoten-Smitsmans,G.;Veermans,A. *Polym. Commun.*, 1987, *28*, 169.
55. Valero,M.;Iruin,J.J.;Espinosa,E.;Fernandez-Berridi,M.J. *Polym. Commun.*, 1990, *31*, 127.
56. Huo,P.P.;Cebe,P. *Macromolecules*, 1993, *26*, 5561.
57. Guo,M.;Zachmann,H.G. *Polymer*, 1993, *34*, 2503.
58. VanderHart,D.L. *Makromol. Chem., Macromol. Symp.*, 1990, *34*, 125.
59. Schmidt,P.;Dybal,J.;Straka,J.;Schneider,B. *Makromol. Chem.*,

1993, *194*, 1757.
60. Gao,Z.;Molnar,A.;Morin,F.G.;Eisenberg,A. *Macromolecules*, 1992, *25*, 6460.
61. Kwei,T.K.;Dai,Y.K.;Lu,X.;Weiss,R.A. *Macromolecules*, 1993, *26*, 6583.
62. Albert,B.;Jerome,R.;Teyssie,P.;Smyth,G.;McBrierty,V.J. *Macromolecules*, 1984, *17*, 2552.
63. Schantz,S.;Ljungqvist,N. *Macromolecules*, 1993, *26*, 6517.
64. Campbell,G.C.;VanderHart,D.L. *J. Magn. Reson.*, 1992, *96*, 69.
65. Schmidt-Rohr,K.;Clauss,J.;Blumich,B.;Spiess,H.W. *Magn. Reson. Chem.*, 1990, *28*, S3.
66. Grobelny,J.;Rice,D.M.;Karasz,F.E.;MacKnight,W.J. *Polym. Commun.*, 1990, *31*, 86.
67. Zhang,X.;Wang,Y. *Polymer*, 1989, *60*, 1867.
68. Grobelny,J.;Rice,D.M.;Karasz,F.E.;MacKnight,W.J. *Macromolecules*, 1990, *23*, 2139.
69. (a)Miller,J.B.;McGrath,K.J.;Roland,C.M.;Trask,C.A.;Garroway,A.N. *Macromolecules*, 1990, *23*, 4543.
(b)Roland,C.M.;Miller,J.B.;McGrath,K.J. *Macromolecules*, 1993, *26*, 4967.
70. Walton,J.H.;Miller,J.B.;Roland,C.M.;Nagode,J.B. *Macromolecules*, 1993, *26*, 4052.
71. Walton,J.H.;Miller,J.B.;Roland,C.M. *J. Polym. Sci., Part B, Polym. Phys.*, 1992, *30*, 527.
72. Maresch,G.G.;Kendrich,R.D.;Yannoni,C.S. *Macromolecules*, 1988, *21*, 3523.
73. Yang,T.P.;Pearce,E.M.;Kwei,T.K.;Yang,N.L. *Macromolecules*, 1989, *22*, 1813.
74. Natansohn,A.;Simmons,A. *Macromolecules*, 1989, *22*, 4426.
75. Newmark,R.A.;Copley,B.C. *Macromolecules*, 1984, *17*, 1973.
76. Sotta,P.;Deloche,B.;Herz,J.;Lapp,A.;Durand,D.;Rabadeux,J.-C. *Macromolecules*, 1987, *20*, 2769.
77. McBrierty,V.J.;Douglass,D.C.;Kwei,T.K. *Macromolecules*, 1978, *11*, 1265.
78. Jong,L.;Pearce,E.M.;Kwei,T.K. *Polymer*, 1993, *34*, 48.
79. Jong,L.;Pearce,E.M.;Kwei,T.K.;Dickinson,L.C. *Macromolecules*, 1990, *23*, 5071.
80. Natansohn,A.;Eisenberg,A. *Macromolecules*, 1987, *20*, 323.
81. Natansohn,A.;Rutkowska,M.;Eisenberg,A. *Polymer*, 1987, *28*, 885.
82. Tang,P.;Reimer,J.A.;Denn,M.M. *Macromolecules*, 1993, *26*, 4269.
83. Schaefer,J.;Sefcik,M.D.;Stejskal,E.O.;McKay,R.A. *Macromolecules*, 1981, *14*, 188.
84. Sarkar,S.N.;Komoroski,R.A. *Macromolecules*, 1992, *25*, 1420.

In this dissertation, we investigate two kinds of polymer/polymer blends using mainly the CP/MAS ^{13}C NMR technique. One is bisphenol A polycarbonate/poly(methyl methacrylate) blend (PC/PMMA) and another is polystyrene/poly(vinyl methyl ether) blend (PS/PVME). The phase diagram of both polymer/polymer blends exhibits lower critical solution temperature (LCST) behavior. The glass transition temperature T_g of PC/PMMA blend is higher than 110℃,[2(c)] that of PS/PVME blends at PS contents less than 60wt% is lower than 0℃.[2(a)]

In chapter 2, we describe how the interacted region, the heterogeneous domain, and compositional change in each phase-separated domain are detected by NMR techniques. We introduce the nuclear Overhauser effect (NOE) and ^{13}C spin-lattice relaxation time (^{13}C-T_1) in solution, ^{1}H spin-diffusion and ^{1}H spin-lattice relaxation times both in the laboratory ($T_{1\rho H}$) and the rotating (T_{1H}) frames in solid.

In chapter 3, polymer-polymer interaction in solution of PC/PMMA blend is investigated. The inter-polymer ^{1}H NOE can be observed, suggesting that PC and PMMA in solution are in close contact with each other. We measure ^{13}C-T_1 of the mixture and pure polymers in solution. The temperature dependence of ^{13}C-T_1 is affected by mixing only for the phenyl and the methoxy carbon resonances. It is concluded that the phenyl group of PC and the methoxy group of PMMA interact with each other in solution.

Furthermore, the miscibility and the phase-separation of PC/PMMA blends are studied by examining T_{1H} and $T_{1\rho H}$ in solid. The observation is done indirectly through the high-resolution

solid-state CP/MAS ^{13}C resonance. The blends are found to be homogeneous on a scale of 200-300 Å, but heterogeneous on a scale of 20-30 Å. The phase diagram is obtained by analyzing the recovery curve of ^{1}H relaxation of blends heated at various temperatures for 30min. The kinetics of the phase-separation is also discussed, and found to be initiated by spinodal decomposition; the phase-separation rate is $3.6\times10^{-2}min^{-1}$.

In chapter 4, we investigate the miscibility of PS/PVME blend in the solid state. We examine T_{1H} and $T_{1\rho H}$ at various temperatures. At temperatures lower than T_g of the blend, observed T_{1H} of PS and PVME as well as $T_{1\rho H}$ are the same each other, showing that PS/PVME=5:5 blend is miscible on a scale of 20-30 Å. At temperatures much higher than T_g, the observed ^{1}H relaxation curve ($T_{1\rho H}$) of PS apparently differs from that of PVME. They are multiple-exponential. The analysis of multiple-exponential decays shows that the ^{1}H cross-relaxation rate between PS and PVME is $\sim1000s^{-1}$ at 38℃. This cross-relaxation rate is so slow that $T_{1\rho H}$ values of PS and PVME do not coincide with each other. This is attributed to fast molecular motion of PVME.

Above the LCST, the phase-separation occurs; the ^{1}H relaxation curves differ markedly from those of homogeneous blend. We analyze the ^{1}H relaxation curve of each component polymer, and obtain the stoichiometry in phase-separated domains. We found that the phase-separation at 140℃ of PS/PVME=5:5 blend is initiated by the spinodal decomposition; phase-separation rate is $0.5min^{-1}$.

1.2 Polymer/Lithium-Salt Blends

Polymer/lithium(Li)-salt blend is a useful and important material in the future, because it exhibits a high ionic conductivity in the solid state. The most famous system of polymer/Li-salt blends is poly(ethylene oxide) (PEO) with Li-salt.[17] For example, the ionic conductivity of PEO/$LiClO_4$ blends at higher than 50℃ is more than $10^{-5}\Omega^{-1}cm^{-1}$.[18-21] Since PEO is a semicrystalline polymer, PEO/Li-salt blend shows various complicated phases. Robitaille and Fauteux studied PEO/Li-salt blends by wide angle X-ray scattering and polarized light optical microscopy, and suggested that PEO/Li-salt blend can be in various states, that is, crystalline and amorphous phases of PEO/Li-salt complex and those of pure PEO.[21]

At temperatures higher than the melting point, the ionic conductivity of blends at low Li-salt concentrations is an order of $10^{-3}\Omega^{-1}cm^{-1}$.[18-21] Such high conductivity suggests that PEO/Li-salt blend is in an amorphous phase and that an interaction between Li^{+}-ion and PEO in the crystalline phase is weak. The interaction between ion and polymer depends on the morphology, the ionic polarity, and so on.[22]

The solid-state NMR technique enables us to examine the morphology of heterogeneous polymer blends. The ^{13}C CP/MAS, the ^{7}Li spectra, and the ^{1}H relaxation behavior can reveal the conformation, the stoichiometry, and the domain size of heterogeneous blend. Furthermore, ^{13}C and ^{7}Li relaxation rates directly depend on the mobility of polymer chain and Li^{+}-ion,

respectively. They provide information on the mobility of Li^+-ion.

In chapter 5, $PEO/LiClO_4$ blend is examined by ^{13}C CP/MAS and ^7Li NMR. We assign ^{13}C CP/MAS spectra. The observed spectra are fitted with three or four Lorentzian curves. Peaks appear at 72, 70-71, 69.5, 68, and 66ppm. The assignment is achieved by the comparison between the observed spectra at various concentrations (O/Li) and on the basis of previous DSC[19] and X-ray[21] results. We found that peaks at 69.5 and 66ppm are due to the crystalline phase of PEO_3LiClO_4 and PEO_6LiClO_4 complexes, respectively. The high field shift of 4ppm of the 66ppm peak indicates that the PEO conformation in the crystalline phase changes from trans of CC-OC and/or CO-CC bonds to gauche. The ^{13}C spin-lattice relaxation (T_{1C}) curve of PEO_XLiClO_4 complexes show double-exponential. This suggests that the crystalline phase of PEO_XLiClO_4 complexes consists of two parts; mobile and rigid. The rigid PEO part interacts with Li^+-ions and the mobile PEO part does not. The ^7Li spin-lattice relaxation (^7Li-T_1) curve also shows double-exponential. This is attributed to mobile Li^+-ions in the amorphous phase and ridid Li^+-ions in the complex. The amount of mobile Li^+-ions obtained from the ^7Li-T_1 curve decreases with increasing $LiClO_4$. This is consistent with the results of conductivity. From the amounts of rigid PEO part and Li^+-ions, we found that the complex takes a structure in which $LiClO_4$s are surrounded by three PEO columns.

References

1. Paul,D.R.;Newman,S.,Eds. *Polymer Blends*; Academic Press: San Diego, California, 1978; Chapters 2-4.
2. (a)Bank,M.;Leffingwell,J.;Thies,C. *Macromolecules*, 1971, *4*, 43.
   (b)Shultz,A.R.;Gendron,B.M. *J. Appl. Polym. Sci.*, 1972, *16*, 461.
   (c)Chiou,J.S.;Barlow,J.W.;Paul,D.R. *J. Polym. Sci., Part B, Polym. Phys.*, 1987, *25*, 1459.
3. (a)Hashimoto,T.;Kumaki,J.;Kawai,H. *Macromolecules*, 1983, *16*, 641.
   (b)Saito,H.;Fufita,Y.;Inoue,T. *Polym. J.*, 1987, *19*, 405.
   (c)Saldanha,J.M.;Kyu,T. *Macromolecules*, 1987, *20*, 2840.
4. (a)Gells,R.;Frank,C.W. *Macromolecules*, 1982, *15*, 1486.
   (b)Halary,J.L.;Ubrich,J.M.;Nunzi,J.M.;Monnerie,L.;Stein,R.S. *Polymer*, 1984, *25*, 956.
   (c)Tsai,F.-J.;Torkelson,M. *Macromolecules*, 1988, *21*, 1026.
5. (a)Varnell,D.F.;Runt,J.P.;Coleman,M.M. *Macromolecules*, 1981,*14*, 1350.
   (b)Kim,H.-I.;Pearce,E.M.;Kwei,T.K. *Macromolecules*, 1989, *22*, 3374.
   (c)Alfredo,C.Q.;Pires,T.N.;Belfiore,L.A. *Macromolecules*, 1991, *24*, 666.

6. (a)Russell,T.P.;Lee,D.S.;Nishi,T.;Kim,S.C.
Macromolecules, 1993, *26*, 1922.
(b)Crevecoeur,G.;Groeninckx,G. *Macromolecules*,
1991, *24*, 1190.
(c)Nishio,Y.;Haratani,T.;Takahashi,T. *J. Polym. Sci.*,
Part B, Polym. Phys. 1990, *28*, 355.
7. (a)Yamanaka,K.;Takagi,Y.;Inoue,T. *Polymer*, 1989, *30*, 1839.
(b)Saleem,M.;Baker,W.E. *J. Appl. Polym. Sci.*, 1990, *39*, 655.
(c)Pomposo,J.A.;Calahorra,E.;Eguiazabal,I.;Cortazar,M.
Macromolecules, 1993, *26*, 2104.
8. Komoroski,R.A.,Ed. *High Resolution NMR Spectroscopy of*
Synthetic Polymers in Bulk; VCH: Deerfield Beach, 1986;
Chapters 2-5.
9. Abragam,A. *Principles of Nuclear Magnetism*; Clarendon:
Oxford, 1961, Chapter 5.
10. McBrierty,V.J.;Douglass,D.C. *J. Polym. Sci., Macromolecular*
Reviews, 1981, *16*, 295.
11. (a)Caravatti,P.;Neuenschwander,P.;Ernst,R.R. *Macromolecules*,
1985, *18*, 119.
(b)Caravatti,P.;Neuenschwander,P.;Ernst,R.R. *Macromolecules*,
1986, *19*, 1889.
12. VanderHart,D.L. *Makromol. Chem. Macromol. Symp.*,
1990, *34*, 125.
13. Schmidt-Rohr,K.;Clauss,J.;Blumich,B.;Spies,H.W.
Magn. Reson. Chem., 1990, *28*, S3.
14. (a)Pines,A.;Gibby,M.G.;Waugh,J.S. *J. Chem. Phys.*,
(b)Schaefer,J.;Stejskkal,E.O.;Buchdahl,R. *Macromolecules*,
1975, *8*, 291.

15. (a)Schaefer,J.;Sefcik,M.D.;Stejskal,E.O.;McKay,R.A.
Macromolecule, 1981, *14*, 188.
(b)Stejskal,E.O.;Schaefer,J.;Sefcik,M.D.;McKay,R.A.
Macromolecules, 1981, *14*, 275.
16. Zhang,X.;Takegoshi,K.;Hiichi,K. *Macromolecules*,
1992, *25*, 2336.
17. (a)Fenton,D.E.;Parker,J.M.;Wright,P.V.
Polymer, 1973, *14*, 589.
(b)Payne,D.R.;Wright,P.V. *Polymer*, 1982, *23*, 690.
(c)Bhattacharja,S.;Smoot,S.W.;Whitmore,D.H.
Solid State Ionics, 1986, *18&19*, 306.
18. Ferloni,P.;Chiodelli,G.;Magistris,A.;Sanesi,M.
Solid State Ionics, 1986, *18&19*, 265.
19. Gorecki,W.;Andreani,R.;Berthier,C.;Armand,M.;Mali,M.;Roos,J.;
Brinkmann,D. *Solid State Ionics*, 1986, *18&19*, 295.
20. (a)Watanabe,M.;Nagano,S.;Sanui,K.;Ogata,N.
Solid State Ionics, 1986, *18&19*, 338.
(b)Watanabe,M.;Nagano,S.;Sanui,K.;Ogata,N. *Polym. J.*,
1986, *18*, 809.
21. Robitaille,C.D.;Fauteux,D. *J. Electrochem. Soc.*
1986, *133*, 315.
22. O'Gara,J.F.;Nazri,G.;MacArthur,M. *Solid State Ionics*,
1991, *47*, 87.

Chapter 2 NMR Techniques for Studying the Heterogeneity of Polymers

2.1 Detection of Interaction in Solution

A ^{1}H Nuclear Overhauser Effect

The nuclear Overhauser effect (NOE) is a change of signal intensity of a nuclear spin when another spin is saturated.[1] The ^{1}H dipole-dipole interaction gives rise to the NOE between two ^{1}H spins. Since the strength of dipole-dipole interaction is proportional to the inverse sixth-power of the inter-proton distance, there occurs no appreciable NOE between protons separated by more than 5 Å.[1,2] NOE is, therefore, a sensitive tool to investigate whether component polymers are in close contact on a microscopic scale.

NOE is ordinarily observed in a form of difference spectra. In the case of steady-state NOE between ^{1}H spins, the observed signal intensity is positive and half of the original intensity when $\omega_H\tau_C \ll 1$. When $\omega_H\tau_C \gg 1$, it is negative. When $\omega_H\tau_C=\sqrt{5}/2$, the NOE signal is not observed.[1] However, the steady-state NOE is less specific and hence less useful because of spin-diffusion or spin-migration.[2] On the other hand, the initial buildup rates of truncated driven NOE difference spectra are simply related to the inverse sixth-power of the inter-proton distance.[2]

The initial build-up rate of NOE(cross-relaxation rate σ_{ij}) can be written[1,2]

$$\sigma_{ij}=(1/10)r_H^4\hbar^2 r_{ij}^{-6}\{-J_0(0)+6J_2(2\omega_H)\} \qquad (2\text{-}1)$$

where r_H is the ^{1}H magnetogyric ratio, $\hbar$ is Planck's constant divided by 2π, $\underline{r}_{ij}$ is the distance between proton i and proton j, $J_0(0)$ and $J_2(2\omega_H)$ are spectral densities of motion of the inter-proton distance r_{ij}, and ω_H is the ^{1}H Larmor frequency.

As can be seen in eq 2-1, $(\sigma_{ij}/\sigma_{ik})^{1/6}$ is equal to $(\underline{r}_{ik}/\underline{r}_{ij})$, if we assume that the spectral density is the same for all proton pairs. We can simply estimate the ratio of the distance between i-spin and k-spin and the distance between i-spin and j-spin.

B ^{13}C Spin-Lattice Relaxation

If a specific inter-polymer interaction exists between A and B polymers, the molecular motion of polymer chain in the mixture, in particular, of the interacting region is expected to be different from that of pure polymer. In solution, the fluctuation of ^{13}C-^{1}H dipole interaction determines the ^{13}C spin-lattice relaxation time(^{13}C-T_1). The molecular motion can be detected by observing ^{13}C-T_1.

The spin-lattice relaxation rate $1/(^{13}\text{C}\text{-}T_1)$ can be written

$$1/(^{13}\text{C}\text{-}T_1)=(1/20)K^2 r_{CH}^{-6}[J_0(\omega_H-\omega_C)+3J_1(\omega_C)+6J_2(\omega_H+\omega_C)] \qquad (2\text{-}2)$$

where K is $\hbar r_C r_H$. When the molecular reorientation can be described by means of a single rotational correlation time τ_C,[3] spectral density $J_m(\omega)$ becomes $2\tau_C/(1+\omega^2\tau_C^2)$ (m=0, 1, and 2).

In solution, the value of $1/(^{13}\text{C}\text{-}T_1)$ is governed mainly by the interaction with closer ^{1}H spin because of r_{CH}^{-6} term in eq 2-2.

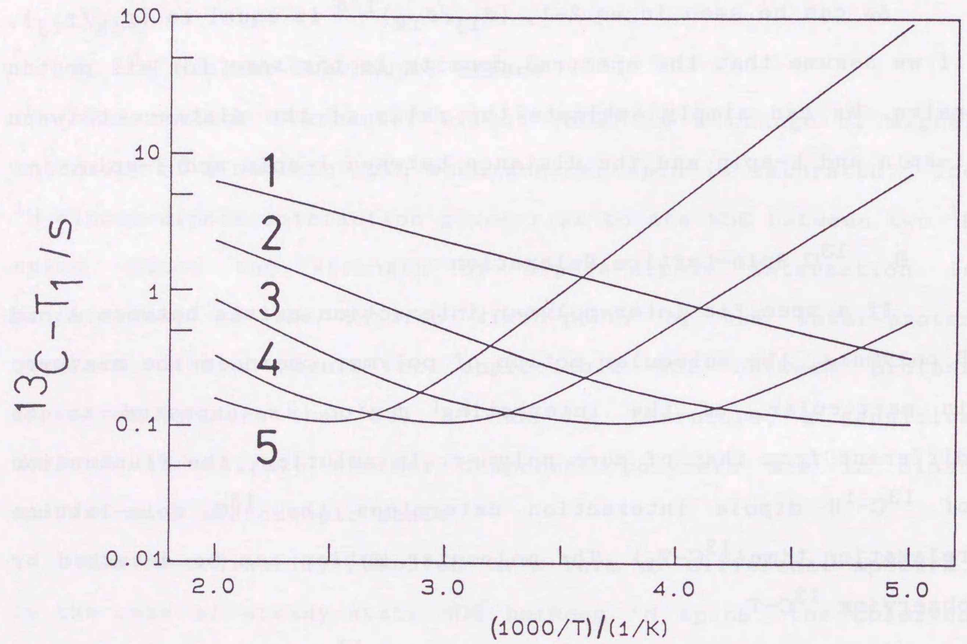

Figure 2-1. Simulated ^{13}C-T_1 curves of methine carbon. $\omega_C=2\pi\times67.5$MHz.

From the temperature dependence of ^{13}C-T_1, we can estimate an activation energy ΔE of motion contributing to ^{13}C-T_1 by the Arrhenius relation as follows[4]

$$\tau_C=\tau_0\exp(\Delta E/RT) \qquad (2\text{-}3)$$

where τ_0 is the correlation time at infinite temperature, R is the gas constant.

When $\omega_H\tau_C \ll 1$ or $\omega_H\tau_C \gg 1$, the plots of $\log(^{13}C$-$T_1)$ versus $1/T$ show linear relation because that $1/(^{13}C$-$T_1)$ is proportional to τ_C or τ_C^{-1}, the ΔE can be obtained from the slope.

Figure 2-1 shows the temperature dependence of ^{13}C-T_1 of a ^{13}C-^1H pair at various ΔEs. The value of τ_0 is 1.0×10^{-12}s and the bond-length of ^{13}C-^1H is 1.09 Å. Values of ΔE are 2.0Kcal/mol (1), 3.0Kcal/mol (2), 4.0Kcal/mol (3), 5.0Kcal/mol (4), and 6.0Kcal/mol (5). With increasing activation energy, T_1 minimum moves to higher temperatures and the minimum value remains unchanged. This indicates that if the temperature dependence of ^{13}C-T_1 moves to higher temperatures without change of the value of T_1 minimum, one can recognize that the activation energy becomes larger. For a ^{13}C-^1H dipole pair, a T_1 minimum appears at $\omega_C\tau_C\cong0.791$. When ω_C is $2\pi\times67.5$MHz, the value of ^{13}C-T_1 minimum becomes 0.106sec.

2.2 Characterization of Heterogeneity in Solid

A ^{1}H Spin-Diffusion

Spin-diffusion is a process of energy exchange (flip-flop) between interacting spins, resulting in a uniform energy distribution for whole spin system.[4] The spin-diffusion process via the ^{1}H dipole-dipole interaction homogenizes the heterogeneous magnetization. Since the dipole-dipole interaction depends on the inverse sixth-power of the inter-proton distance, the spin-diffusion provides information on the homogeneous domain size.

Figure 2-2 shows a schematic illustration of spin-diffusion between A- and B-domains. The flip-flop phenomena of inter- and intra-domains equalize energy levels of A- and B-domains. This is because the overall size of domain is smaller than the *maximum* diffusive path length of spin-diffusion.

We can estimate the diffusive path length from the given equation[5,6]

$$\partial M(r,t)/\partial t = D\,\nabla^2 M(r,t) - 1/T_1\{M(r,t) - M_{eq}\} \qquad (2\text{-}4)$$

where $M(r,t)$ is the magnetization at a position r and diffusion time t, M_{eq} is the equilibrium magnetization of $M(r,t)$, and D is the diffusion constant. In general, the contribution of the relaxation to the magnetization is not appreciable compared to that of spin-diffusion. Therefore, eq 2-4 can be rewritten

$$\partial M(r,t)/\partial t = D\,\nabla^2 M(r,t) \qquad (2\text{-}5)$$

The mean-square distance $\langle r^2 \rangle$ can be easily obtained with the initial magnetization of δ-function

$$\langle r^2 \rangle = 6Dt \qquad (2\text{-}6)$$

From eq (2-6), we can estimate the homogeneous domain size if one can obtain the value of D and the diffusion time t.

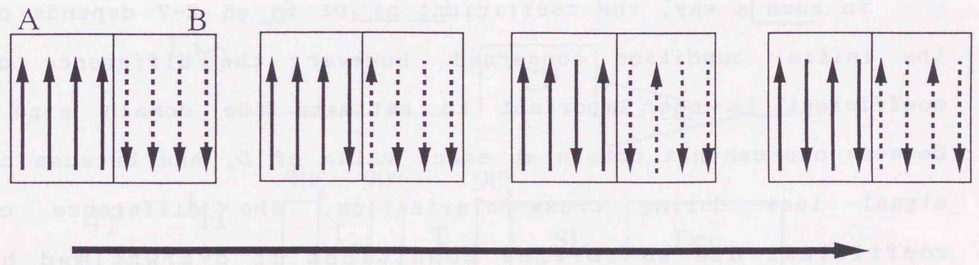

Figure 2-2. Schematic illustration of spin-diffusion behavior between A- and B-domains.

Various solutions can be obtained from various initial magnetizations. Havens and VanderHart assumed that the crystalline/amorphous phase of poly(ethylene terephthalate) corresponds to the one-dimensional (1D) lamellar model.[7] In order to simplify the model mathematically, the initial magnetization is assumed to be $M(x,0)=M_{eq}$ for all $x\leq 0$ and $M(x,0)=0$ for all $x>0$. Here, x is a 1D component of the 3D distance r. Under such conditions, the mean-square distance $\langle x^2\rangle$ is equal to

$$\langle x^2\rangle=(4/3)Dt \qquad (2\text{-}7)$$

In such a way, the coefficient of Dt in eq 2-7 depends on the initial condition concerned. However, the difference of coefficient is not important to estimate the domain size.[8] Because one can not obtain an exact value of D, and because of signal loss during cross-polarization, the difference of coefficient due to initial conditions is overwhelmed by experimental error.

However, in the case of Goldman-Shen[9] or analogous experiment (pulse sequence 4 in Figure 2-3), we directly observe the spin-diffusion process as a function of time; the initial conditions are important. For example, Tanaka, *et al.* obtained the signal change of spin-diffusion from the regular structured block copolymer sample, and determined whether the spatial dimension is 1D, 2D, or 3D.[6]

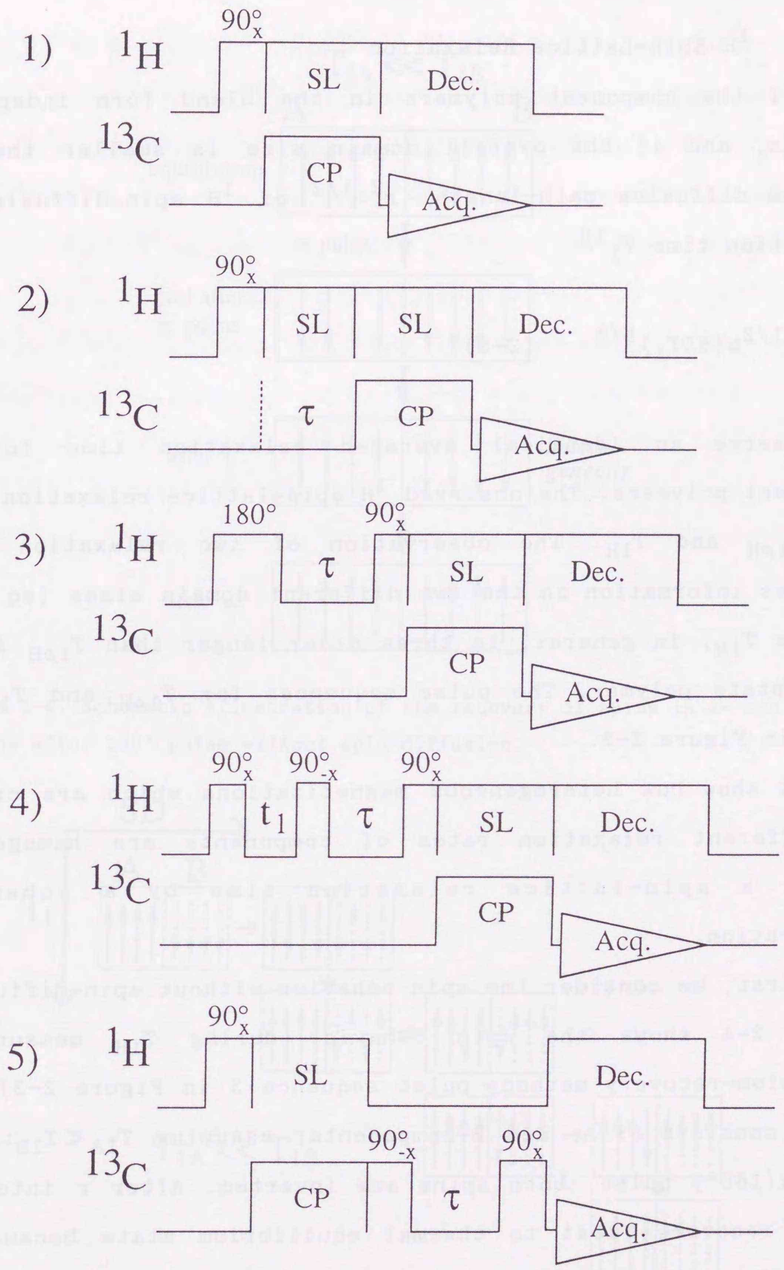

Figure 2-3. Pulse sequences with CP. 1) CP/MAS, 2) $T_{1\rho H}$, 3) T_{1H}, 4) Goldman-Shen, 5) Torchia (T_{1C}).

B ^{1}H Spin-Lattice Relaxation

If the component polymers in the blend form independent domains, and if the overall domain size is smaller than the *maximum* diffusive path-length $\langle r^2\rangle^{1/2}$ of ^{1}H spin-diffusion for relaxation time T_1[10]

$$\langle r^2\rangle^{1/2} \simeq (6DT_1)^{1/2} \qquad (2\text{-}8),$$

we observe an identical averaged relaxation time for all component polymers. The observed ^{1}H spin-lattice relaxation times are $T_{1\rho H}$ and T_{1H}. The observation of two relaxation times provides information on the two different domain sizes (eq 2-8), because T_{1H}, in general, is three order longer than $T_{1\rho H}$ in the solid state polymer. The pulse sequences for $T_{1\rho H}$ and T_{1H} are shown in Figure 2-3.

We show how heterogeneous magnetizations which are created by different relaxation rates of components are homogenized during a spin-lattice relaxation time by a schematic illustration.

First, we consider the spin behavior without spin-diffusion. Figure 2-4 shows the spin behavior during T_{1H} measurement (inversion-recovery method; pulse sequence 3 in Figure 2-3). The system consists of A- and B-components; assuming $T_{1A} \ll T_{1B}$. Just after $\pi(180°)$ pulse, both spins are inverted. After τ interval, A-spin recovers first to thermal equilibrium state because of fast relaxation rate compared to B-spin. The spin system is heterogeneous at that time.

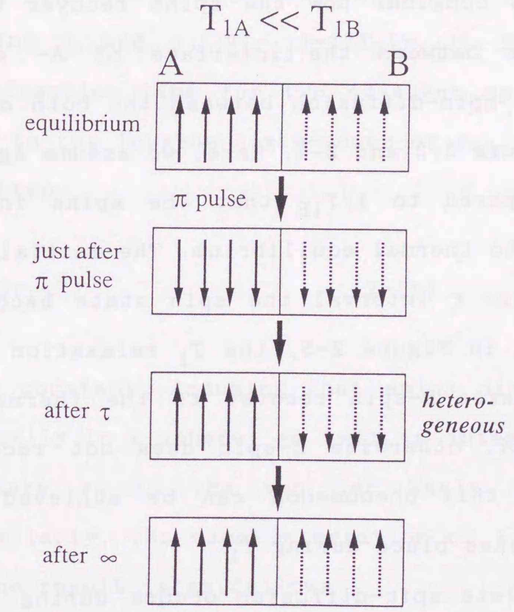

Figure 2-4. Schematic illustration of the recovery of spins in A- and B-domains after 180° pulse *without* spin-diffusion.

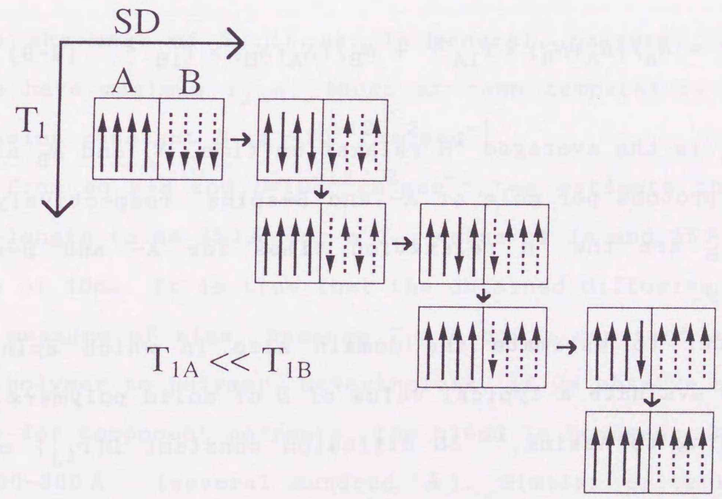

Figure 2-5. Schematic illustration of the recovery of spins in A- and B-domains after 180° pulse *with* spin-diffusion.

Next, let's consider how the spins recover when the spin-diffusion exists between the interface of A- and B-domains. Figure 2-2 shows spin-diffusion between the both domains. Figure 2-5 includes Figure 2-2 and 2-4. Here, we assume again that $1/T_{1A}$ is so large compared to $1/T_{1B}$ that the spins in A-domain can recover readily to thermal equilibrium. The initial state is left and top, and after τ interval the spin state becomes right and bottom. As shown in Figure 2-5, the T_1 relaxation combined with spin-diffusion makes B-spin recover to the thermal equilibrium within τ interval, otherwise B-spin does not recover in short time. Note that this phenomenon can be achieved only if the spin-diffusion takes place during T_1.

If the complete spin-diffusion occurs during a period less than the ^{1}H relaxation time among all protons of A- and B- spins, the ^{1}H relaxation rate is averaged as follows[10,11]

$$T_{1ave}^{-1} = N_A/(N_A+N_B) \times T_{1A}^{-1} + N_B/(N_A+N_B) \times T_{1B}^{-1} \qquad (2\text{-}9)$$

where T_{1ave} is the averaged ^{1}H relaxation time, N_A and N_B are the numbers of protons per mole of A- and B-spins, respectively, and T_{1A} and T_{1B} are the ^{1}H relaxation times for A- and B-spins, respectively.

In order to estimate the domain size in which spins can diffuse, we evaluate a typical value of D of solid polymers.

According to Assink,[12] 3D diffusion constant $D(r_{ij})$ can be written

$$D(r_{ij})=W(r_{ij})r_{ij}^2/6 \qquad (2\text{-}10)$$

where $W(r_{ij})$ is the probability of spin flip-flop for two adjacent spins i and j; $W(r_{ij})\sim 1/T_2(r_{ij})$, $T_2(r_{ij})$ is the ^{1}H spin-spin relaxation time for two adjacent spins. $1/T_2(r_{ij})$ is proportional to the inverse sixth-power of r_{ij}. Therefore, $D(r_{ij})$ can be rewritten

$$D(r_{ij})=C/(6r_{ij}^4) \qquad (2\text{-}11)$$

where C is a constant. Assuming that spins distribute uniformly and isotropically in a sphere, eq 2-11 is integrated from $2r_0$ to infinity, where r_0 is the van der Waals radius of proton (1.17 Å). Similarly, the same integration of $1/T_2(r_{ij})=Cr_{ij}^{-6}$ is performed. The result is as follows

$$D=2r_0^2/T_2=2.74\times10^{-10}/T_2 \ (cm^2sec^{-1}) \qquad (2\text{-}12)$$

where the unit of T_2 is μs. In general, polymers in the solid state have maximum T_2 of 100μs at room temperature. Hence, the diffusion constant D is $\sim10^{-12}cm^2sec^{-1}$.

From eq 2-8 and $D=10^{-12}cm^2sec^{-1}$, we estimate the diffusive path-length to be 250 Å for a T_{1H} value of 1s and 25 Å for a $T_{1\rho H}$ value of 10ms. It is true that the obtained diffusive path-length is a measure of size, because T_1 is not a constant and D varies from polymer to polymer. Nevertheless, if we observe a single T_{1H} value for component polymers, the blend is homogeneous on a scale of 200-300 Å (several hundred Å). Similar criteria hold for $T_{1\rho H}$ experiments; the blend is homogeneous on a scale of 20-30 Å (several ten Å).

Figure 2-6 shows the relation between the domain size and spin-diffusion in T_{1H} experiment. If the domain size is larger than 200-300 Å (Figure 2-6-b), heterogeneous spins can not be averaged for τ interval. On the other hand, if the domain size is less than 200-300 Å (Figure 2-6-a), spins of all domains are averaged after τ.

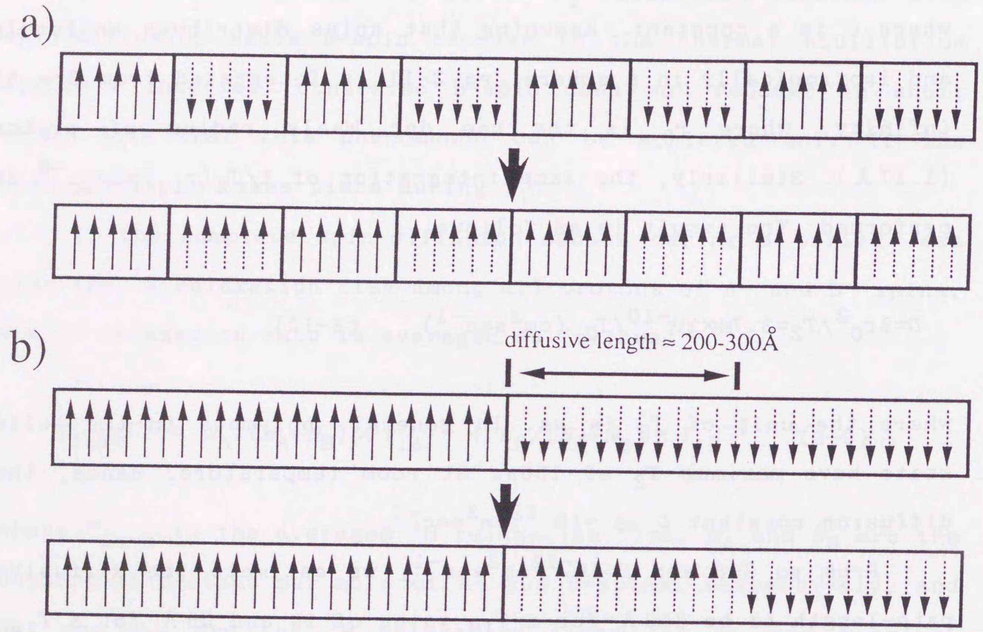

Figure 2-6. The relation between the domain size and spin-diffusion. a) the domain size is smaller than 200-300 Å . b) the domain size is larger than 200-300 Å .

C Phase-Separation

From the analysis of T_1 curve, we can detect the phase-separation process, in particular, the change in composition of polymer blend A/B. We assume that the phase-separated blend consists of two spatially separated domains: A-rich and B-rich domains. The T_1 curves for A and B are double-exponential: relaxation curves will appear in chapters 3 and 4. The spatial separation means that the spin-diffusion does not occur between the two domains. Within a domain, there is a sufficiently fast spin-diffusion between A and B to average each T_1. A similar view of the phase-separated domains can be found in fluorescence[13] and NMR studies.[14] Figure 2-7 shows a schematic drawing of domain structure of phase-separated blend. The above assumption suggests that A and B within a phase-separated domain have an identical T_1 value, but the two polymers in different domains have different T_1 values.

The normalized ^1H magnetization of A during relaxation process $M_A(\tau)$ is expressed by double exponential, reflecting the two relaxation rates of the two domains; A in the B-rich domain (B-domain) has $T_1^{B\text{-rich}}$ and that in the A-rich domain (A-domain) has $T_1^{A\text{-rich}}$. The $T_{1\rho}$ decay, for example, can be written

$$M_A(\tau)=\chi_A^{B\text{-rich}}\exp(-\tau/T_1^{B\text{-rich}}) + \chi_A^{A\text{-rich}}\exp(-\tau/T_1^{A\text{-rich}}) \qquad (2\text{-}13a)$$

Here, $\chi_A^{i\text{-rich}}$ denotes the fraction of A in the i-domain (i=B or A; $\chi_A^{B\text{-rich}}+\chi_A^{A\text{-rich}}=1$). A similar equation for B is given

$$M_B(\tau)=\chi_B^{\text{B-rich}}\exp(-\tau/T_1^{\text{B-rich}}) + \chi_B^{\text{A-rich}}\exp(-\tau/T_1^{\text{A-rich}}) \qquad (2\text{-}13b)$$

The composition in each domain can be determined by fitting the two decay curves observed for A and B to eq 2-13.

We can determine the weight fraction of the B-domain of the whole blend (r) and the coexistent composition ($\phi_A^{\text{B-rich}}$ and $\phi_A^{\text{A-rich}}$) of the phase-separated blend from $\chi_A^{\text{B-rich}}$ and $\chi_B^{\text{B-rich}}$ as follows

$$r = \chi_A^{\text{B-rich}}\,\phi_A^0 + \chi_B^{\text{B-rich}}\,(1-\phi_A^0) \qquad (2\text{-}14a)$$

$$\phi_A^{\text{B-rich}} = \chi_A^{\text{B-rich}}\,\phi_A^0/r \qquad (2\text{-}14b)$$

$$\phi_A^{\text{A-rich}} = (1-\chi_A^{\text{B-rich}})\phi_A^0/(1-r)$$

or

$$= 1 - (1-\chi_B^{\text{B-rich}})(1-\phi_A^0)/(1-r) \qquad (2\text{-}14c)$$

where ϕ_A^0 is the total weight fraction of A in blend (for the A/B=6:4 blend, ϕ_A^0 is 0.6), and $\phi_A^{\text{B-rich}}$ and $\phi_A^{\text{A-rich}}$ are weight fractions of A in the B- and A-domains, respectively. These equations are easily derived from the relation among ϕ_A^0, $\phi_A^{\text{B-rich}}$, $\phi_A^{\text{A-rich}}$, and r (Figure 2-7).

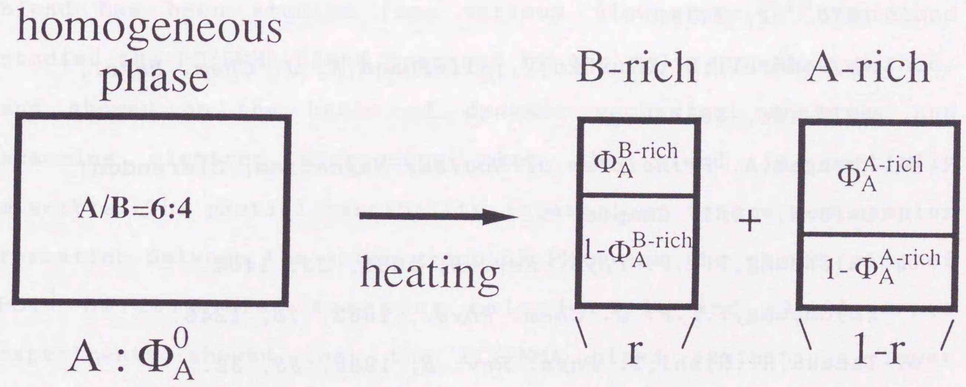

$$\Phi_A^{\text{B-rich}} \cdot r + \Phi_A^{\text{A-rich}} \cdot (1\text{-}r) = \Phi_A^0$$

Figure 2-7. Schematic illustration of phase-separation. The homogeneous blend (left, A/B=6:4) is phase-separated into two domains: the A-rich and the B-rich domains. $\phi_A^{\text{B-rich}}$ and $\phi_A^{\text{A-rich}}$ are the weight fraction of A in each domain. ϕ_A^0 is the total weight fraction of A and r is the fraction of the B-rich domain of the whole blend.

References

1. Noggle,J.H.;Schirmer,R.E.Eds., *The Nuclear Overharser Effect*; Academic Press: New York, 1971; Chapters 3 and 6.
2. Wagner,G.;Wuthrich,K. *J. Magn. Reson.*, 1979, *33*, 675.
3. (a)Kuhlmann,K.F.;Grant,D.M.;Harris,R.K. *J. Chem. Phys.*, 1970, *52*, 3439.
   (b)Doddrell,D.;Glushko,V.;Allerhand,A. *J. Chem. Phys.*, 1972, *56*, 3683.
4. Abragam,A. *Principles of Nuclear Magnetism*; Clarendon: Oxford, 1961, Chapter 5.
5. (a)Cheung,T.T.P. *Phys. Rev. B*, 1981, *23*, 1404.
   (b)Cheung,T.T.P. *J. Chem. Phys.*, 1982, *76*, 1248.
6. Tanaka,H.;Nishi,T. *Phys. Rev. B*, 1986, *33*, 32.
7. Havens,J.R.;VanderHart,D.L. *Macromolecules*, 1985, *18*, 1663.
8. Henrichs,P.M.;Tribone,J.;Massa,D.J.;Hewitt,J.M. *Macromolecules*, 1988, *21*, 1282.
9. Goldman,M.;Shen,L. *Phys. Rev.*, 1966, *144*, 321.
10. (a)McBrierty,V.J.;Douglass,D.C.;kwei,T.K. *Macromolecules*, 1978, *11*, 1265.
    (b)Albert,B.;Jerome,R.;Teyssie,P.;Smyth,G.;McBrierty,V.J. *Macromolecules*, 1984, *17*, 2552.
    (c)Albert,B.;Jerome,R.;Teyssie,P.;Smyth,G.;Boyle,N.G.; McBrierty,V.J. *Macromolecules*, 1985, *18*, 388.
11. Anderson,J.E.;Slichter,W.P. *J. Phys. Chem.*, 1965, *69*, 3099.
12. Assink,R.A. *Macromolecules*, 1978, *11*, 1233.
13. Gells,R.;Frank,C.W. *Macromolecules*, 1982, *15*, 1486.
14. Nishi,T.;Wang,T.T.;Kwei,T.K. *Macromolecules*, 1975, *8*, 227.

Chapter 3 Polycarbonate/Poly(methyl methacrylate) (PC/PMMA) Blend

3.1 Introduction

Bisphenol A polycarbonate/poly(methyl methacrylate)(PC/PMMA) blend has been studied from various viewpoints.[1-10] Gardlund studied the PC/PMMA blend prepared by the melt extruding method, and showed on the basis of dynamic mechanical analysis and scanning electron microscope that the blend is partially miscible. The partial miscibility is ascribed to the n-π complex formation between the ester group of PMMA and the phenyl ring of PC.[1] Differential scanning calorimetric and cloud point experiments showed that the PC/PMMA blend exhibits a lower critical solution temperature(LCST).[2-6] Kyu, *et al.*[4] investigated the phase-separation process of PC/PMMA blend cast from tetrahydrofuran(THF) solution using the time resolved light scattering method. Landry and Henrichs[6] investigated chain motion of deuterated PC/PMMA blend by the solid-state deuterium (^{2}H) NMR method and dynamic mechanical spectroscopy. The rheological properties,[7,8] polymer-polymer interaction parameter(χ),[3,9] glass transition temperature,[9] and solvent effects[4a] have been studied. The properties of chlorine-contained PC/PMMA[10] and PC-PMMA block copolymers[11] have been also examined.

In this chapter, we describe firstly the high-resolution NMR study on the inter-polymer interaction of PC/PMMA blend in solution. We describe next the miscibility and phase-separation of PC/PMMA blend in solid.

In section 3.3.1, ^{1}H NOE and ^{13}C-T_1 experiments in solution are described. It is true that the structure of blend in solution may not be identical to that in solids. Nevertheless, the interacting region is probably identical in both solution and solids. In fact, Crowther, *et al.*[12] and Mirau, *et al.*[13] carried out the ^{1}H NOE experiment to study PS/PVME blend. They showed that PS and PVME are in close contact in toluene, but not in chloroform. Zhang, *et al.*[14] investigated the hydrogen-bonding interaction of polymer blends in solution by examining NOE.

Evidence of the n-π interaction between the phenyl ring of PC and the methoxy group of PMMA is given. If such interaction exists, we expect that blending may alter molecular motion, which reflects ^{13}C-T_1. The temperature dependence of ^{13}C-T_1 is examined, and mixing effects on molecular motion of PC and PMMA are discussed.

In section 3.3.2, the ^{1}H spin-lattice relaxation behavior in both the laboratory (T_{1H}) and the rotating ($T_{1\rho H}$) frames are examined to study domain size and miscibility. We adopt the indirect method for obtaining T_{1H} and $T_{1\rho H}$ by observing the well-resolved ^{13}C signal, which can provide T_{1H} and $T_{1\rho H}$ for each polymer. The effect of magic-angle spinning to T_{1H} and $T_{1\rho H}$ is negligible in our experiments.[15]

We also investigate the thermally induced phase-separation behavior of PC/PMMA blend. The phase diagram of PC/PMMA blend is determined. Furthermore, the change of composition in the PC/PMMA blends during the phase-separation is determined, and the kinetics of phase-separation is discussed.

3.2 Experimental

A Materials

PC and PMMA were obtained from ALDRICH Chemical Co. Inc. The weight averaged molecular weight/number averaged molecular weight (Mw/Mn) is 33,800/13,400 for PC and 93,300/46,400 for PMMA. Atactic PMMA is used. The triad tacticity was determined from the intensity of signals of the α-methyl proton, and the ratio of mm:mr:rr is 13:40:47. PC and PMMA were dissolved in anhydrous THF at concentrations of 2-4wt/v%, and mixed at weight ratios of 3:7, 5:5, and 7:3. Very thin and optically transparent films were obtained by casting the solutions on a glass plate at 58℃.[6] The films were dried further under vacuum at 110°C for 5-6 days.

The transparent 5:5 film was dissolved again in deuterated THF(THF-d_8) at 5wt/v% for the ^{1}H NOE and ^{13}C-T_1 experiments.

The phase-separation was promoted for various time intervals in a furnace controlled at various temperatures. After heating, the films were quickly cooled in water at about 5°C to quench the phase-separation.

B NMR measurement

All NMR spectra were obtained on a JEOL JNM-GX270 spectrometer operating at 67.5MHz for ^{13}C and 270MHz for ^{1}H.

The ^{13}C-T_1 experiments in THF-d_8 solution at various temperatures were conducted by the conventional inversion recovery method. The free induction decays(FIDs) were stored in 8K data points. The number of accumulated FIDs was 48. The length of ^{13}C 90° pulse was 8μs, and acquisition time + pulse delay time was 40s. ^{1}H NOE difference spectra were obtained at -20°C by the truncated driven NOE technique.[3] The ^{1}H radio frequency intensity for irradiation was 15Hz. The FIDs were stored in 4K data points using ^{1}H 45° pulse of 8μs, and acquisition time + pulse delay time was 8s. The number of accumulated FIDs was 256.

High-resolution CP/MAS solid-state ^{13}C NMR experiments[16] were performed under conditions of a spinning rate of 6kHz and an rf intensity of 55kHz for both ^{13}C and ^{1}H; the magic-angle was set up by the KBr method.[17] The T_{1H} value was indirectly obtained by observing well-resolved ^{13}C resonances. After applying the sequence of 180°-τ-90° pulse to ^{1}H nucleus, the cross-polarization transfer from ^{1}H to ^{13}C was undertaken (pulse sequence 3 in Figure 2-3).[18] For the $T_{1\rho H}$ experiment the 90°-τ (spin-locking time) pulse sequence was applied before cross-polarization transfer (pulse sequence 2 in Figure 2-3).[19] The free induction decays(FIDs) were stored in 1k data points using ^{13}C 90° pulse of 4.5μs, cross-polarization contact time of 2ms, and repetition time of 4s. The number of accumulated FIDs was 640. All T_{1H} and $T_{1\rho H}$ experiments were done at 38°C.

3.3 Results and Discussion

3.3.1 Solution Study

A ^{1}H Nuclear Overhauser Effect

Figure 3-1 shows the ^{1}H NOE difference spectra at -20°C. The methoxy(OCH_3) protons of PMMA at 3.4ppm were irradiated. The irradiation time is indicated on the right-hand side in the figure. Both the intramolecular(☆) and inter-polymer(＊) NOE are observed, which are all negative NOEs. Observation of the inter-polymer NOE indicates that the closest distance between PC and PMMA is less than 5 Å.

The relative intensity of NOE was estimated by the Lorentzian curve fitting. The NOE intensity is plotted against irradiation time in Figure 3-2. It is worthy of noting that the build-up rate is much faster for the phenyl protons than for the methyl protons of PC.

From the initial build-up rate of NOE (eq 2-1 in chapter 2), $(\sigma_{ij}/\sigma_{ik})^{1/6}$ is equal to (r_{ik}/r_{ij}), if we assume that the spectral density is the same for all proton pairs. We can estimate the ratio of the distance between the methoxy group of PMMA (i-spin) and phenyl group of PC (k-spin) and the distance between the methoxy group of PMMA and methyl group of PC (j-spin). The initial rate of the phenyl ring protons of PC is four times greater than that of the methyl protons of PC. Thus, the distance between the methoxy group of PMMA and the phenyl ring of PC is about 20% shorter than the distance between the methoxy group and the methyl group. This provides evidence of intimate

closeness between the methoxy group of PMMA and the phenyl group of PC.

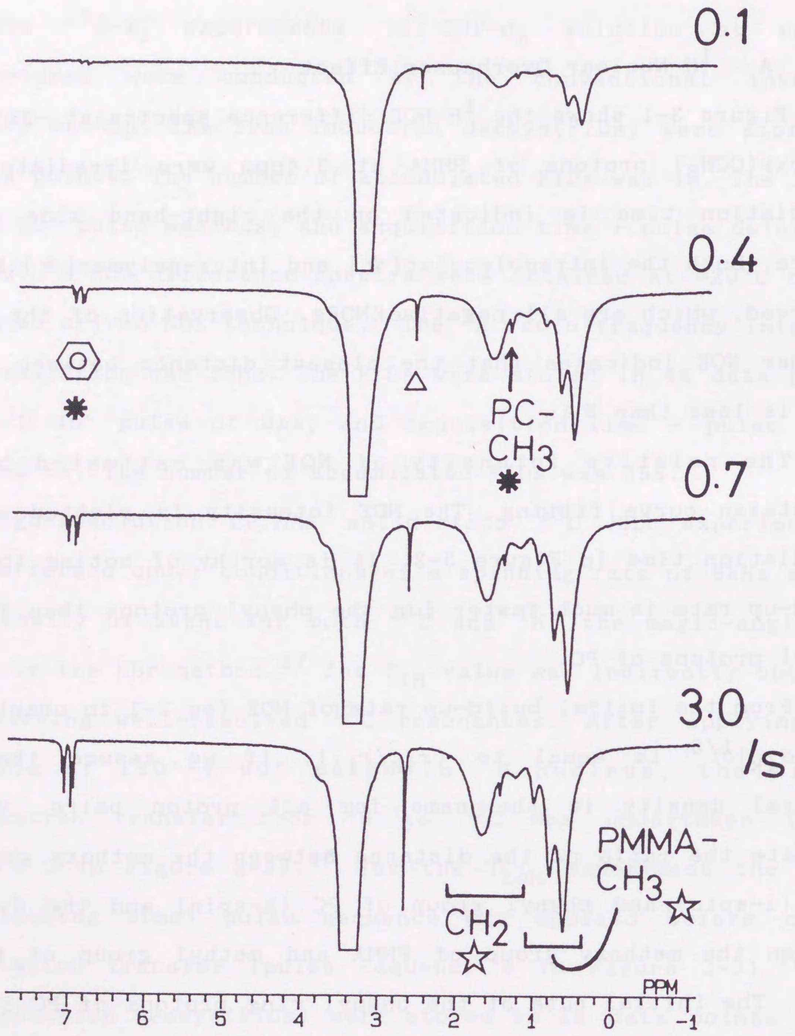

Figure 3-1. ^{1}H NOE difference spectra of PC/PMMA=5:5 mixture in THF-d_8 at -20°C. The methoxy protons of PMMA are irradiated for the period shown in each spectrum. A symbol △ denotes the residual water peak in THF-d_8 solution.

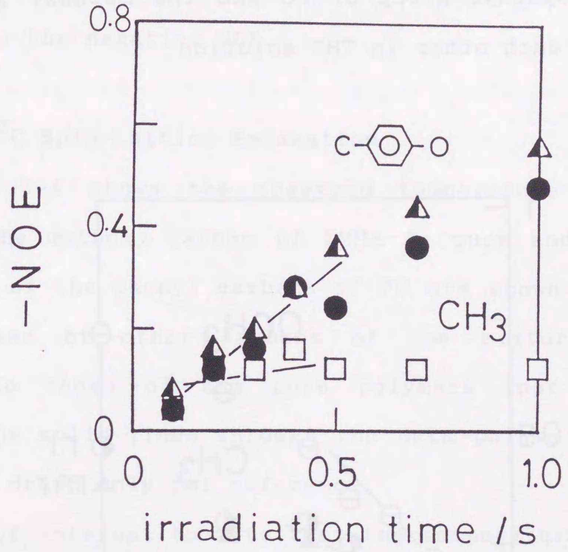

Figure 3-2. Irradiation time dependence of the inter-polymer ^{1}H NOE at -20°C when the methoxy protons of PMMA are irradiated. Relative NOE is plotted: the phenyl ring protons at carbon side (●) and oxygen side (▲), and the methyl protons of PC (□). The solid lines show the initial slope from which relative distances are deduced. The ordinate is in arbitrary units.

The NOE difference spectra of the phenyl protons of PC irradiated were also examined. The irradiation time dependence of the relative intensity of the inter-polymer NOE is shown in Figure 3-3. The build-up rate of NOE is larger for the methoxy peak of PMMA than for the *mr* triad and *rr* triad α-methyl peaks of PMMA. NOE is not remarkable for the *mm* triad α-methyl and the methylene peaks (not shown in the figure). Accurate estimation for the former peak may not be possible because of the small peak intensity. This NOE result also gives proof of the proximity of

the methoxy group of PMMA and the phenyl ring group of PC. To conclude, the phenyl group of PC and the methoxy group of PMMA interact with each other in THF solution.

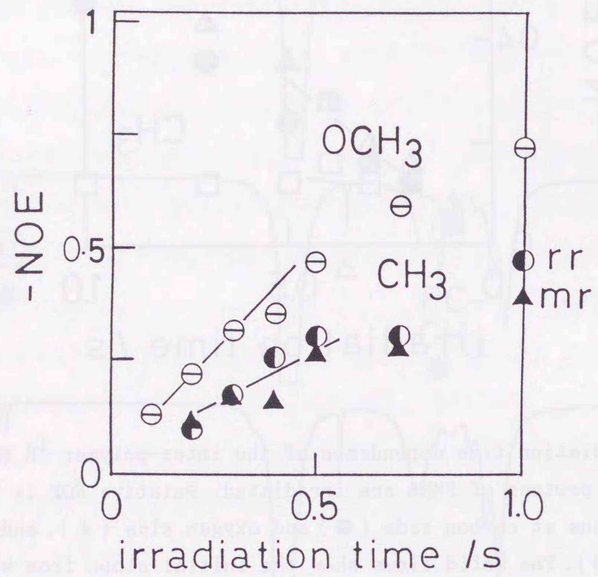

Figure 3-3. Irradiation time dependence of the inter-polymer ^{1}H NOE at -20°C when the phenyl ring protons of PC are irradiated: the protons of methoxy protons (⊖), *rr* (◐), and *mr* (▲) triad α-methyl protons of PMMA. The solid lines show the initial slope from which relative distances are deduced. The ordinate is in arbitrary units.

It was found that the inter-polymer NOE can be observed only below -20°C. At higher temperatures above -20°C, the correlation time is presumably in a region where NOE is ineffective.[20] A sharp peak showing negative NOE near 2.7ppm in Figure 3-1 is due to residual water in THF-d_8. NOE was not observed for the water

peak, when the phenyl protons of PC were irradiated. The interaction between the methoxy group and the water molecule may give rise to the negative NOE.

B ^{13}C Spin-Lattice Relaxation

Figure 3-4 shows the observed temperature dependence of ^{13}C-T_1 of the methoxy carbon of PMMA in pure and mixed states. The results of the phenyl carbons of PC are shown in Figure 3-5. ^{13}C-T_1 values of other carbons of the mixtures are almost identical to those of the pure polymers (not shown in the figures). The solid lines through the data points in Figures 3-4 and 3-5 are drawn only for reference.

It is of interest to note that the temperature of T_1 minimum of the methoxy carbon of PMMA is about 25°C higher for the mixture than for pure PMMA (Figure 3-4). This indicates that the correlation time of motion τ_C is larger in the mixture than in the pure polymer. The molecular motion becomes slower by mixing.

The T_1 curve of the phenyl carbons of PC in the mixture shifts to high temperatures compared to that of pure PC (Figure 3-5), indicating that the motion of the phenyl rings of PC is restricted by mixing. ^{13}C-T_1s of other carbons are not influenced by mixing. Since the molecular motion of only interacting region is affected, it is evident that change of ^{13}C-T_1 curve proves the presence of interaction between the methoxy group of PMMA and phenyl group of PC.

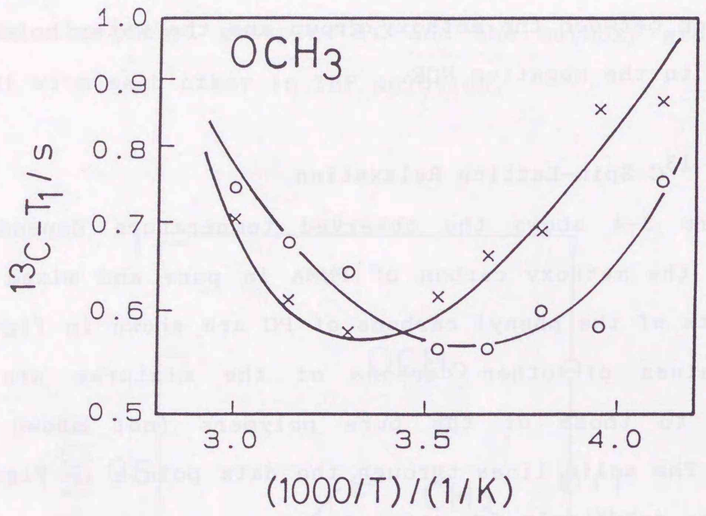

Figure 3-4. ^{13}C-T_1 curves of the methoxy carbon of pure PMMA (○) and PC/PMMA=5:5 mixture (×) in THF-d_8. The solid lines are written to guide reader's eyes.

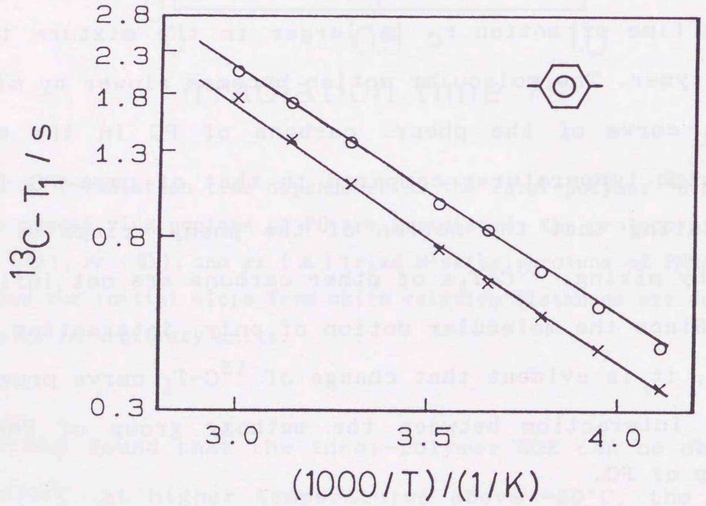

Figure 3-5. ^{13}C-T_1 curves of the phenyl carbons of pure PC (○) and PC/PMMA=5:5 mixture (×) in THF-d_8. The solid lines are written to guide reader's eyes.

3.3.2 Solid State Study

Figure 3-6 shows the ^{13}C CP/MAS spectra of pure PC, pure PMMA, and the PC/PMMA=5:5 blend at room temperature. The chemical sift change affected by blend can be not observed, but the peaks of phenyl ring carbon slightly broaden after blending. This indicates the n-π interaction between the methoxy group of PMMA and the phenyl group of PC.

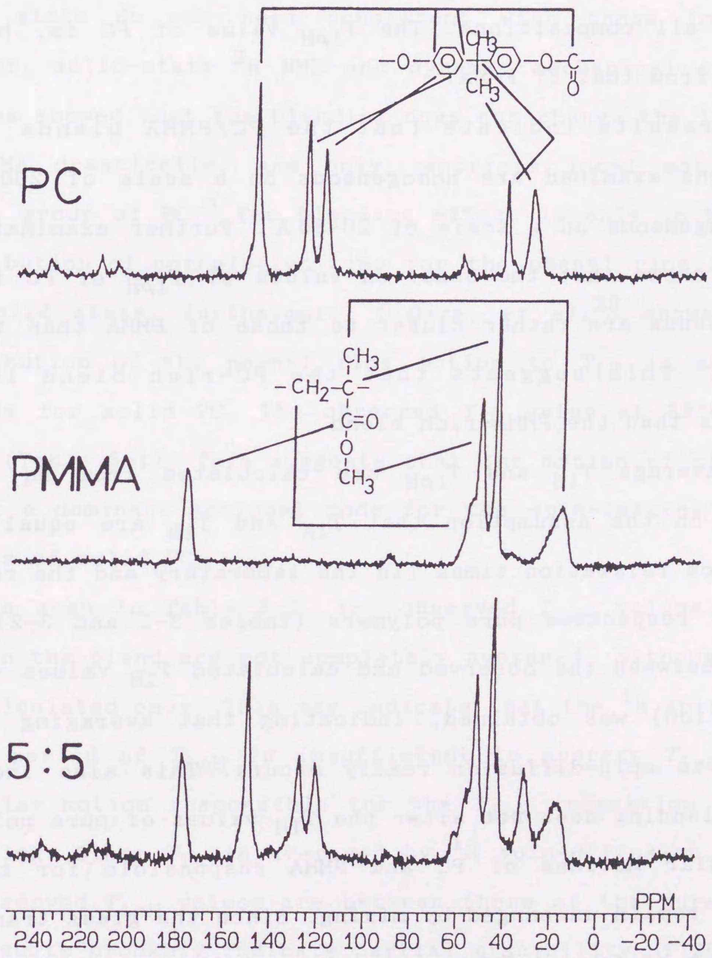

Figure 3-6. ^{13}C CP/MAS spectra of PC, PMMA, and PC/PMMA=5:5 blend.

A Miscibility

Tables 3-1 and 3-2 list observed T_{1H} and $T_{1\rho H}$ for blends at 3:7, 5:5, and 7:3 compositions. The observed T_{1H} and $T_{1\rho H}$ values of the single pure polymers are consistent with those reported for PMMA[21] and PC,[22] provided the difference in resonance frequency is taken into account. The observed T_{1H} values of PC are in good agreement with those of PMMA within experimental error for all compositions. The $T_{1\rho H}$ value of PC is, however, different from that of PMMA.

The results indicate that the PC/PMMA blends at all compositions examined are homogeneous on a scale of 200-300 Å, but heterogeneous on a scale of 20-30 Å. Further examination of Table 3-2 shows that the observed values of $T_{1\rho H}$ of PC for 5:5 and 7:3 blends are rather closer to those of PMMA than that of 3:7 blend. This suggests that the PC-rich blend is more homogeneous than the PMMA-rich blend.

The average T_{1H} and $T_{1\rho H}$ are calculated from eq 2-9 in chapter 2 on the assumption that T_{1A} and T_{1B} are equal to ^1H spin-lattice relaxation times (in the laboratory and the rotating frames) of respective pure polymers (Tables 3-1 and 3-2). Good agreement between the observed and calculated T_{1H} values (within 10% deviation) was obtained, indicating that averaging of T_{1H} rates due to spin-diffusion really occurs. This also indicates that the blending does not alter the T_{1H} values of pure polymers; the molecular motions of PC and PMMA responsible for the T_{1H} relaxation remain unchanged by mixing. Since the glass transition temperatures of PC and PMMA are rather similar and sufficiently higher than the experimental temperature (38℃) (T_g of PC is

about 150℃ and that of PMMA is about 110℃), the blending does not significantly alter the overall chain motion.

If the inter-polymer interaction exists between PC and PMMA, we expect that the blending may alter molecular motion. We found that mixing in solution hinders the local motion of the phenyl group of PC and the methoxy group of PMMA.

The results for the molecular motion of the blend in the solid state do not seem consistent with those in solution. However, solid-state ^2H NMR and dynamic mechanical spectroscopy studies showed that the blending does not change the local motion of PMMA drastically, and only restricts local motion of the phenyl group of PC.[6] The blending effect is only to broaden the distribution of correlation time for the phenyl ring flipping in the solid state. Furthermore, O'Gara, *et al.*[23] showed that the contribution of the phenyl ring motion to T_{1H} is about a few seconds for solid PC. The observed T_{1H} value at 38°C is about 270ms (Table 3-1). This suggests that the motion of phenyl group is not a dominant motional mode for the spin-lattice relaxation process of solid PC.

As seen in Table 3-2, the observed $T_{1\rho H}$ values of PC and PMMA in the blend are not completely averaged, although close to the calculated ones. This may indicate that the ^1H spin-diffusion for a period of $T_{1\rho H}$ is insufficient to average $T_{1\rho H}$, or that molecular motion responsible for the $T_{1\rho H}$ relaxation is altered by mixing. Since T_{1H} is averaged by ^1H spin-diffusion, and since the observed $T_{1\rho H}$ values are between those of the pure polymers, the results probably indicate partial miscibility of 20-30 Å.

Table 3-1 Observed and calculated values of T_{1H} of PC/PMMA 3:7, 5:5, and 7:3 blends

Compositions		Obs/ms	Calc/ms
pure PC		268±13	
pure PMMA		395±29	
	PC	362±15	
3:7			357±23
	PMMA	384± 7	
	PC	339± 8	
5:5			331±20
	PMMA	351±11	
	PC	304±13	
7:3			306±17
	PMMA	313±20	

Error is σ

The homogeneity of PC/PMMA blends determined by the NMR methods is summarized in Table 3-3. If the complete inter-polymer spin-diffusion occurs, the T_1s of PC and PMMA have the same value. The values in Table 3-3 shows how much the T_1s are in agreement with each other. We can recognize again visually that the PC-rich blend is more homogeneous than the PMMA-rich blend.

Table 3-2 Observed and calculated values of $T_{1\rho H}$ of PC/PMMA 3:7, 5:5, and 7:3 blends

Compositions		Obs/ms	Calc/ms
pure PC		5.4±0.3	
pure PMMA		15.7±0.6	
	PC	9.1±0.8	
3:7			10.9±0.5
	PMMA	13.3±0.5	
	PC	6.3±0.3	
5:5			8.8±0.4
	PMMA	9.2±0.3	
	PC	5.7±0.1	
7:3			7.2±0.3
	PMMA	7.5±0.5	

Error is σ

Table 3-3 Miscibility of PC/PMMA blends determined by ^1H spin-lattice relaxation time

Compositions	T_{1H} * 200-300Å	$T_{1\rho H}$ * 20-30Å
3:7	83%	59%
5:5	91%	72%
7:3	93%	83%

$$* \left(1-\frac{(T_{1PMMA}-T_{1PC})_{blend}}{(T_{1PMMA}-T_{1PC})_{pure}}\right)\times 100\%$$

B Determination of Phase Diagram

When the PC/PMMA blend is heated above its binodal curve, phase-separation occurs and the two coexistent phases appear: PC-rich and PMMA-rich phases.[2-5]

Initially, we approximately estimate the phase-separation temperature for the 3:7, 5:5, and 7:3 blends. We observe the T_{1H} recovery curves at room temperature after the 30min-heating at various temperatures. Although the observed T_{1H} recovery curves after heating above 150°C are slightly non-single exponential, we analyze the curves approximately as a single exponential to obtain the *apparent* T_{1H}. Detailed analysis of non-single exponential behavior will be given later.

Figure 3-7 shows *apparent* T_{1H} values of PC and PMMA of the 5:5 blend as a function of heating temperature. The *apparent* T_{1H} values of PC and PMMA are approximately the same at heating temperatures not higher than 140°C, indicating that heating below 140°C does not initiate phase-separation. The values of PC and PMMA become different at a heating temperature of 150°C, and approach the respective values of pure polymers as the heating temperature increases. This indicates that phase-separation occurs.

The two curves in Figure 3-7 diverge at about 145℃. We define the phase-separation temperature as the divergent temperature of found 145℃ for the 5:5 blend, 145℃ for 7:3 blend, and 140℃ for the 3:7 blend. These temperatures are plotted in Figure 3-8 against composition as ●. The phase-separation temperature is slightly higher than the glass transition temperature for each blend: 115°C, 120°C, and 130°C

for 3:7, 5:5, and 7:3 blends, respectively.[2,5]

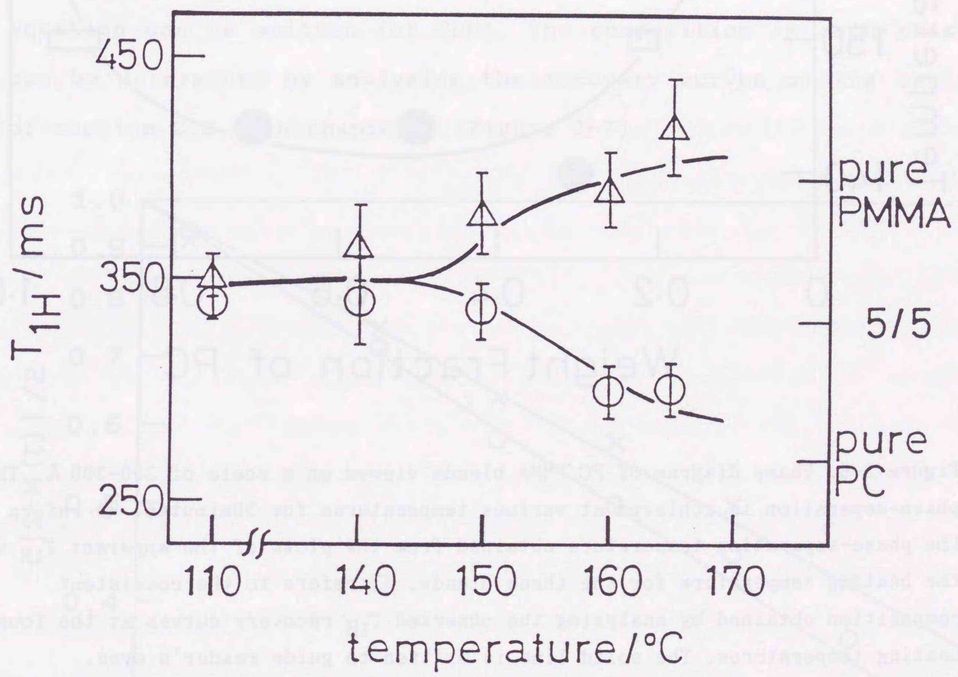

Figure 3-7. *Apparent* T_{1H} values for PC (○) and PMMA (△) vs. heating temperature for PC/PMMA=5:5 blend. A symbol "5/5" of the right ordinate indicates the value calculated from eq 2-9 for PC/PMMA=5:5 blend (see Table 3-1).

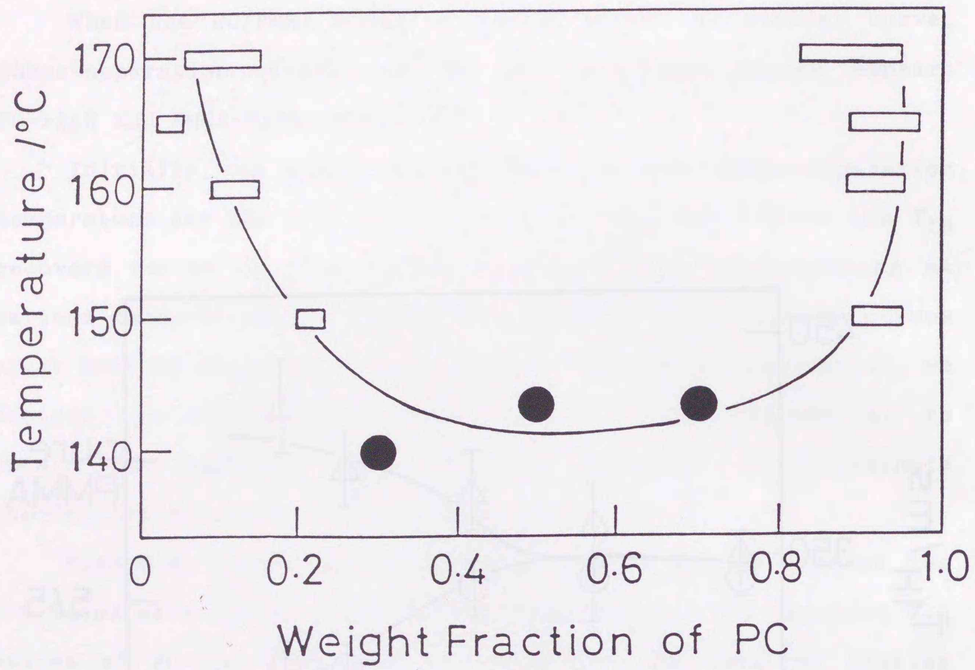

Figure 3-8. Phase diagram of PC/PMMA blends viewed on a scale of 200-300 Å . The phase-separation is achieved at various temperatures for 30minutes. ● refers to the phase-separation temperature obtained from the plots of the *apparent* T_{1H} vs. the heating temperature for the three blends. □ refers to the coexistent composition obtained by analyzing the observed T_{1H} recovery curves at the four heating temperatures. The solid line is written to guide reader's eyes.

We analyzed the non-single exponential behavior of the ^1H relaxation rate in more detail. A normalized ^1H magnetization of PC $M_{PC}(\tau)$ is expressed by two exponentials corresponding to the relaxations in the two phases: the PC-rich phase (C-phase) and the PMMA-rich phase (M-phase). For the inversion-recovery

experiment, it can be written by:

$$M_{PC}(\tau)=\chi^{M}_{PC}\{1-2\exp(-\tau/T^{M})\}+\chi^{C}_{PC}\{1-2\exp(-\tau/T^{C})\} \quad (3-1)$$

where χ^{M}_{PC} and χ^{C}_{PC} denote fractions of PC in M- and C-phases, respectively ($\chi^{M}_{PC} + \chi^{C}_{PC} = 1$). T^{M} and T^{C} are ^1H relaxation times of PC (and PMMA) in M- and C-phases, respectively. A similar equation can be written for PMMA. The composition in each phase can be determined by analyzing the recovery curves on the basis of section 2.2.B in chapter 2 (Figure 2-7).

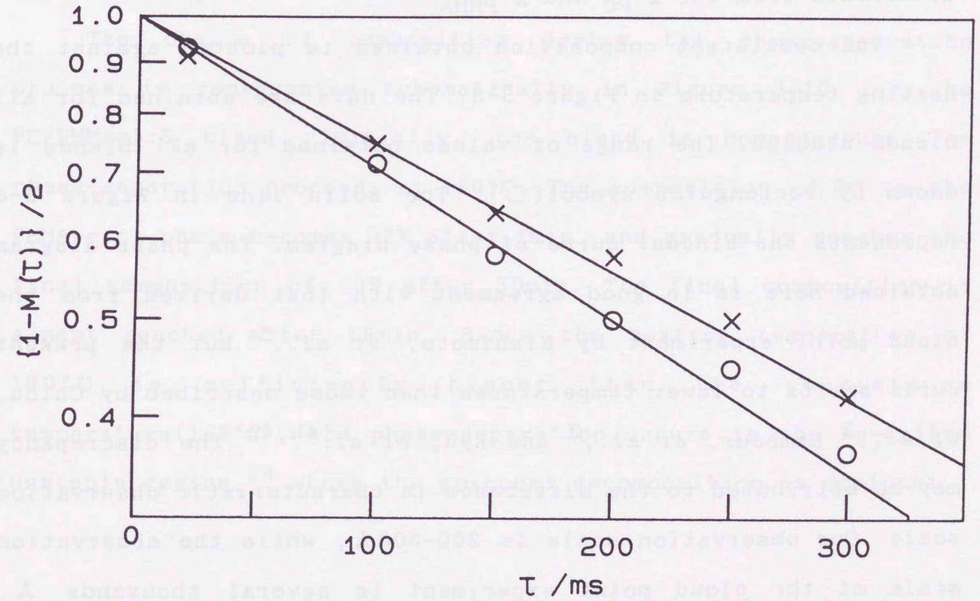

Figure 3-9. Observed T_{1H} recovery curves of PC (○) and PMMA (×) of PC/PMMA=7:3 blend after 30min heating at 160°C. The solid lines are the "best fitted" ones to eq 3-1.

There are four parameters to be deduced from experimental recovery curves, namely, χ^{M}_{PC}, χ^{M}_{PMMA}, T^{M}, and T^{C}. We make an assumption that the spin-diffusion in each phase is completely occurred to reduce the number of parameters to only two. On the assumption, adjustable parameters are only χ^{M}_{PC} and χ^{M}_{PMMA}, because the values of the relaxation time T^{M} and T^{C} can be determined through eq 2-9 in chapter 2 from χ^{M}_{PC} and χ^{M}_{PMMA}.

The observed T_{1H} recovery curves were least-square fitted to eq 3-1 by adjusting χ^{M}_{PC} and χ^{M}_{PMMA} as shown in Figure 3-9. The coexistent composition of the phase-separated blend is thus determined from the χ^{M}_{PC} and χ^{M}_{PMMA}.

The coexistent composition obtained is plotted against the heating temperature in Figure 3-8. The data are obtained for all blends studied. The range of values obtained for all blends is shown by rectangular symbol(□). The solid line in Figure 3-8 represents the binodal curve of phase diagram. The phase diagram obtained here is in good agreement with that derived from the cloud point experiment by Nishimoto, *et al.*,[5] but the present curve shifts to lower temperatures than those described by Chiou, *et al.*,[2] Kambour, *et al.*,[3] and Kyu, *et al.*[4b,4c] The discrepancy may be attributed to the difference in characteristic observation scale. Our observation scale is 200-300 Å, while the observation scale of the cloud point experiment is several thousands Å. Domains of 200-300 Å are attained in a rather short heating time, but domains of several thousands Å are attained in a much longer heating time. If the heating is not long enough to establish equilibrium, the phase-separation temperature will be estimated somewhat higher. In fact, Nishimoto, *et al.*'s cloud point

experiment was carried out for several days.[5]

C Compositional Change during Phase-Separation

The phase-separation on a scale of 200-300 Å is found to occur for several tens min. It is possible to examine the compositional change during phase-separation by monitoring the ^{1}H relaxation curves at various heating times. The observed T_{1H} recovery curves after heating for 1, 5, 10, and 15min at 160°C were least-squares fitted to eq 3-1 to obtain the composition.

The change of composition during the phase-separation process is represented schematically in Figure 3-10 for the PC/PMMA=5:5 blend. Initially, the blend is homogeneous. The phase-separation proceeds at 160°C. The composition of PC in the PMMA-rich phase becomes 32% after 1min, and gradually reaches the final composition of 10% after 30min. The final composition is almost reached after 15min. Since the heating temperature of 160°C is sufficiently higher than the coexistence temperature(145°C), the phase-separation occurs in the so-called unstable region,[24] where the spinodal decomposition is dominant.

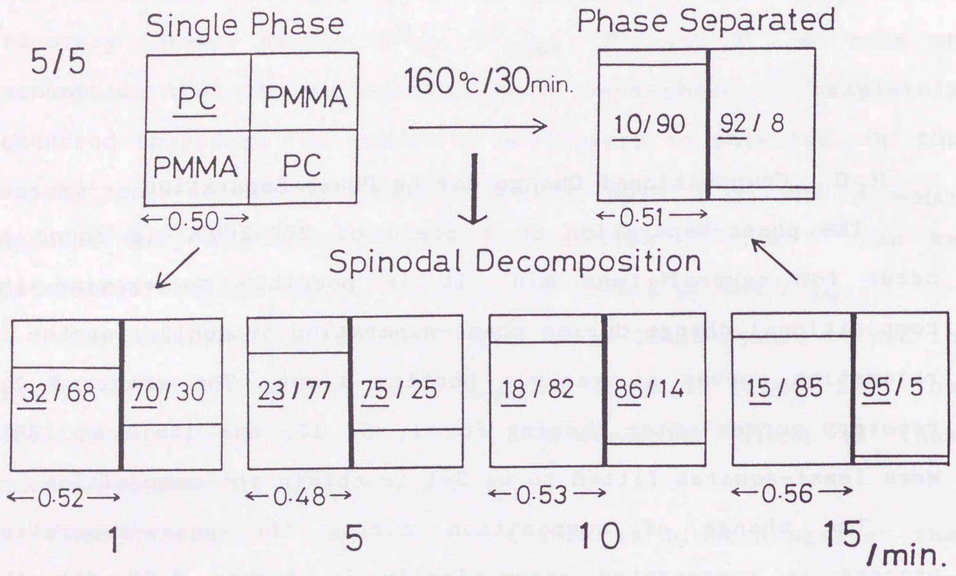

Figure 3-10. Schematic illustration of the compositional change during heat-treatment of PC/PMMA=5:5 blend. The composition of PC is indicated by underlined numbers.

D Kinetics of Phase-Separation

On the basis of Cahn theory,[25] Nishi, *et al.*[26] derived the following equation for the total reduction Q ($Q=\phi^{0}_{PC}-\phi^{M}_{PC}$) of the composition of a minor component in a given phase:

$$\ln(Q)=\text{constant}+3Rt \qquad (3\text{-}2)$$

where R expresses the growth rate of compositional change in phase-separation process and t is the phase-separation time

(heating time). We found R in the PMMA-rich phase to be about $+6.0\times10^{-4}s^{-1}$ ($3.6\times10^{-2}min^{-1}$) for all samples (Figure 3-11). This value is in good agreement with that obtained for PS/PVME by Nishi, *et al.*[26] In particular, the plus sign of R is consistent with the spinodal decomposition.

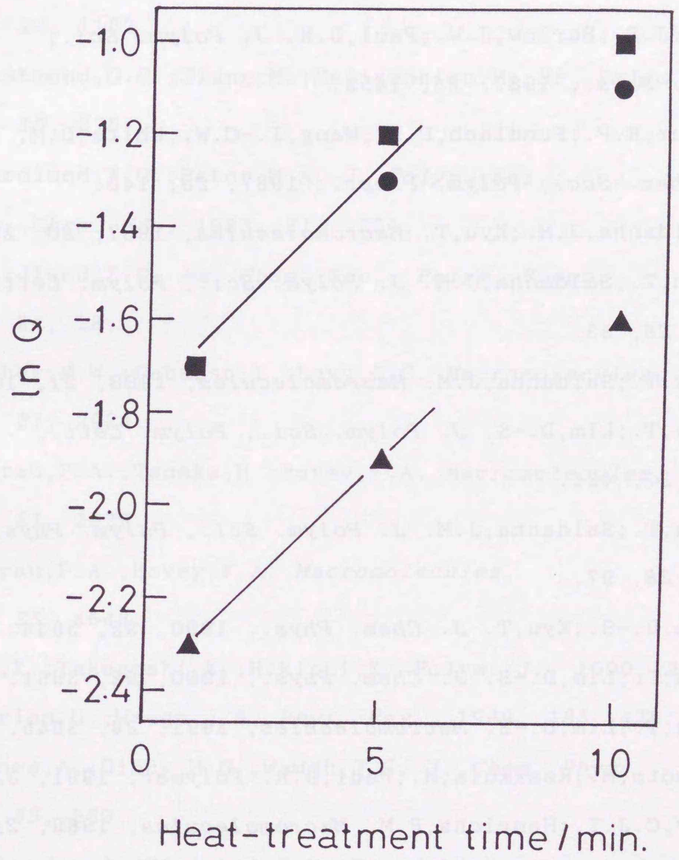

Figure 3-11. Plot of $\ln(Q)$ vs. phase-separation time. Q is the total reduction of the composition. The slope corresponds to growth rate of compositional change in phase-separation (phase-separation rate). Symbols of '▲','●',and '■' are 3:7, 5:5, and 7:3 blends, respectively.

References

1. (a)Gardlund,Z.G. *Am. Chem. Soc., Polym. Prepr.* 1982, *23*, 258.
(b)Han,C.D.,Ed., *Polymer Blends and Composites in Multiphase Systems*; Advances in Chemistry, Am. Chem. Soc.: Washington,D.C., 1984; Chapter 9.
2. Chiou,J.S.;Barlow,J.W.;Paul,D.R. *J. Polym. Sci., Polym. Phys.*, 1987, *25*, 1459.
3. Kambour,R.P.;Fundlach,P.E.;Wang,I.-C.W.;White,D.M. *Am. Chem. Soc., Polym. Prepr.*, 1987, *28*, 140.
4. (a)Saldanha,J.M.;Kyu,T. *Macromolecules*, 1987, *20*, 2840.
(b)Kyu,T.;Saldanha,J.M. *J. Polym. Sci., Polym. Lett.*, 1988, *26*, 33.
(c)Kyu,T.;Saldanha,J.M. *Macromolecules*, 1988, *21*, 1021.
(d)Kyu,T.;Lim,D.-S. *J. Polym. Sci., Polym. Lett.*, 1989, *27*, 421.
(e)Kyu,T.;Saldanha,J.M. *J. Polym. Sci., Polym. Phys.*, 1990, *28*, 97.
(f)Lim,D.-S.;Kyu,T. *J. Chem. Phys.*, 1990, *92*, 3944.
(g)Kyu,T.;Lim,D.-S. *J. Chem. Phys.*, 1990, *92*, 3951.
(h)Kyu,T.;Lim,D.-S. *Macromolecules*, 1991, *24*, 3645.
5. Nishimoto,M.;Keskkula,H.;Paul,D.R. *Polymer*, 1991, *32*, 272.
6. Landry,C.J.T.;Henrichs,P.M. *Macromolecules*, 1989, *22*, 2157.
7. Koo,K.-K.;Inoue,T.;Miyasaka,K. *Polym. Eng. Sci.*, 1985, *25*, 741.

8. Razinskaya,I.N.;Galle,B.S.;Ott,L.I.;Bubnova,L.P.; Batuyeva,L.I.;Pupukina,N.I.;Adamova,L.V.;Shtarkman,B.P., *Polym. Sci., U.S.S.R.*, 1985, *27*, 204.
9. (a)Kim,W.N.;Burns,C.M. *Macromolecules*, 1987, *20*, 1876.
(b)Kim,W.N.;Burns,C.M. *J. Appl. Polym. Sci.*, 1990, *41*, 1575.
10. (a)Eastmond,G.C.;Jiang,M.;Malinconico,M. *Polymer*, 1983, *24*, 1162.
(b)Eastmond,G.C.;Jiang,M.;Malinconico,M. *Br. Polym. J.*, 1987, *19*, 275.
11. (a)Gardlund,Z.G.;Bator,M.A. *J. Polym. Sci., Polym. Chem. Ed.*, 1983, *21*, 1251.
(b)Gardlund,Z.G. *Am. Chem. Soc., Polym. Prepr.* 1983, 24, 18.
12. Crowther,M.W.;Cabasso,I.;Levy,G.C. *Macromolecules*, 1988, *21*, 2924.
13. (a)Mirau,P.A.;Tanaka,H.;Bovey,F.A. *Macromolecules*, 1988, *21*, 2929.
(b)Mirau,P.A.;Bovey,F.A. *Macromolecules*, 1990, *23*, 4548.
14. Zhang,X.;Takegoshi,K.;Hikichi,K. *Polym. J.*, 1990, *23*, 79.
15. Haeberlen,U.;Waugh,J.S. *Phys. Rev.*, 1969, *185*, 420.
16. (a)Pines,A.;Gibby,M.G.;Waugh,J.S. *J. Chem. Phys.*, 1973, *59*, 569.
(b)Schaefer,J.;Stejskal,E.O.;Buchdahl,R. *Macromolecules*, 1975, *8*, 291.
17. Frye,J.S.;Maciel,G.E. *J. Magn. Reson.*, 1982, *48*, 125.

18. Zumbulyadis,N. *J. Magn. Reson.*, 1983, *53*, 486.

19. Alla,M.;Lippmaa,E. *Chem. Phys. Lett.*, 1976, *37*, 260.

20. (a)Noggle,J.H.;Schirmer,R.E. *The Nuclear Overhauser Effect*; Academic Press: New York, 1971; Chapters 3 and 6.
(b)Doddrell,D.;Glushko,V.;Allerhand,A. *J. Chem. Phys.*, 1972, *56*, 3683.

21. Douglass,D.C.;McBrierty,V.J. *Macromolecules*, 1978, *11*, 766.

22. Henrichs,P.M.;Tribone,J.;Massa,D.J.;Hewitt,J.M. *Macromolecules*, 1988, *21*, 1282.

23. O'Gara,J.F.;Jones,A.A.;Hung,C.-C.;Inglefield,P.T. *Macromolecules*, 1985, *18*, 1117.

24. Paul,D.R.;Newman,S.,Ed., *Polymer Blends*; Academic Press: San Diego, California, 1978; Chapter 4.

25. Cahn,J.W. *J. Chem. Phys.*, 1965, *42*, 93.

26. Nishi,T.;Wang,T.T.;Kwei,T.K. *Macromolecules*, 1975, *8*, 227.

Chapter 4 Polystyrene/Poly(vinyl methyl ether) (PS/PVME) Blend

4.1 Introduction

The differential scanning calorimetry and dielectric relaxation studies of PS/PVME blend cast from toluene (or benzene) solution indicated that the two polymers are microscopically mixed, because the blend behaves as a single-phase system.[1]

NMR studies have, however, presented diverse views on the miscibility. Caravatti, *et al* examined the inter-polymer ^1H spin-diffusion for PS/PVME blends by the two-dimensional (2D) ^1H exchange NMR spectroscopy[2a] and by 1D ^1H saturation transfer NMR experiments.[2b] They interpreted the results in terms of a three-phase model consisting of mixed, pure PS, and pure PVME domains. Chu, *et al*. examined $T_{1\rho H}$ at -5℃. They showed that PS-rich blends are homogeneous but PVME-rich blends are microscopically heterogeneous.[3]

Kaplan concluded from $T_{1\rho H}$ and Goldman-Shen[4] experiments that the blends are homogeneous on a scale of 6-20 Å.[5] Gobbi, *et al*. examined at -33℃ the cross-polarization transfer from PVME protons to ^{13}C nuclei of deuterated PS (d-PS) in d-PS/PVME=5:5 blend which was prepared by mechanical mixing.[6] The results suggested that d-PS/PVME=5:5 is homogeneous on a scale less than 20 Å.[6] More recently, the specific intermolecular interaction between the phenyl group of PS and the methoxy group of PVME has been revealed by examining nuclear Overhauser effect (NOE) in the solid state at -60℃.[7]

In toluene solution, NOE was observed between the aromatic protons of PS and the methoxy protons of PVME.[8] The results indicate that the distance between the phenyl ring of PS and the ether group of PVME is less than 5 Å.[8]

Kwei, *et al.* found a long T_2 component above 25℃ for PS/PVME blends prepared by solvent casting. They suggested the micro-heterogeneity on a segmental scale.[9] An electron spin resonance study of poly(styrene-*co*-(maleic anhydride))/PVME blend prepared by solvent casting indicated that the blend is inhomogeneous in concentration on a molecular scale (≤50 Å).[10] ^{13}C linewidth studies revealed that molecular motions of PS and PVME in the blend are not cooperative,[11,12] indicating *motional* heterogeneity.

These confusing results on the miscibility of PS/PVME blend prompt us to re-examine the ^1H spin-relaxation. In view of the fast motion of PS/PVME blend, we think that the apparent heterogeneity reported by several groups is a consequence of ineffective spin-diffusion due to motional averaging of the ^1H dipole interaction.

The phase-separation behavior is also studied. The phase-separation of PS/PVME blend has been studied by light scattering[13] and fluorescence emission.[14,15] Nishi, *et al.* analyzed the ^1H relaxation curve of the phase-separated PS/PVME blends observed directly from ^1H NMR signal.[16] They elucidated the compositional change of PVME in the PS-rich domain. The authors pointed out that the direct observation of ^1H spins has some difficulty in detecting the minor domain. In this work, we observe the ^1H spin-relaxation curves for PS and PVME through

well-resolved ^{13}C signal. This enables us to detect not only the major domain but also the minor domain.

Firstly, we describe the ^1H spin-lattice relaxation experiments (T_{1H} and $T_{1\rho H}$) for studying the domain size and the miscibility of PS/PVME=5:5 blend. Secondly, we examine the effect of molecular motion on the ^1H spin-diffusion. ^1H cross-relaxation rates among protons of PS, methoxy, and methine protons of PVME in PS/PVME=5:5 blend are obtained. Thirdly, we describe the thermally induced phase-separation behavior of PS/PVME=5:5 blend. The composition of each domain in the blend during phase-separation is determined and the kinetics of phase-separation is discussed.

4.2 Experimental Section

A Materials

PS is a commercial PS-666 from Dow Chemical Co., and the average molecular weight (*Mv*) is 93000. PVME (*Mv*=87000) was obtained from Aldrich Chemical Co. Inc. The average molecular weight was determined by the conventional intrinsic viscosity method. A transparent and tough PS/PVME film was prepared at room temperature by casting the benzene solution of both polymers mixed at a weight ratio of 5:5 (PS/PVME=5:5). The film was further dried under vacuum at 60℃ at least for a week. Phase-separated samples were obtained by heat-treating the single phase film. The phase-separation was promoted for various times in a

furnace controlled at 140℃. After heating, the film was quickly cooled in liquid nitrogen to quench the phase-separation process.

B NMR Measurements

^{13}C NMR measurements were made using a JEOL JNM-GX270 spectrometer operating at 67MHz. The high-resolution solid-state ^{13}C NMR spectra were obtained by the combined use of cross-polarization (CP) and magic-angle-spinning (MAS).[17] The radio frequency field strength for both ^{1}H and ^{13}C was 55kHz. The spinning frequency was about 5.5kHz. T_{1H} was measured by well-resolved ^{13}C signals enhanced by CP after applying 180° pulse to ^{1}H nuclei (pulse sequence 3 of Figure 2-3 in chapter 2). $T_{1\rho H}$ was obtained by the ^{13}C signals with combined use of CP and the spin-locking to ^{1}H nuclei. (pulse sequence 2 of Figure 2-3 in chapter 2). The contact time for the CP signal enhancement was 500μs for the $T_{1\rho H}$ measurement and 2ms for the T_{1H} measurement. The temperature calibration was done by using proton signals of methanol under spinning at 5.5kHz.[11,18]

4.3 Results and Discussion

A Miscibility

Figure 4-1 shows solid-state ^{13}C NMR spectra of PS, PVME, and PS/PVME=5:5 blend at 38℃(a) and -45℃(b). The methine carbon peak of PVME of the blend is broadens noticeably at 38℃. This is ascribed to molecular motion.[11]

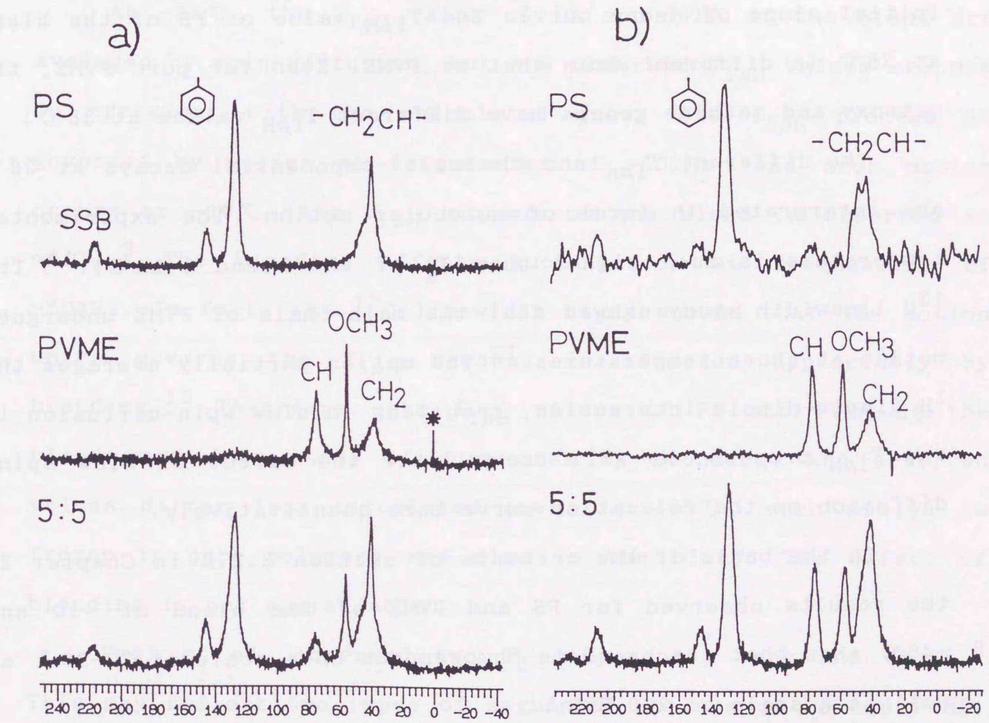

Figure 4-1. ^{13}C CP/MAS spectra of pure PS, pure PVME, and PS/PVME=5:5 blend at 38℃ (a) and -45℃ (b), respectively. Peak assignments are also depicted. Symbol '*' in (a) is ascribed to silicon rubber of the stopper of sample tube. SSB denotes the spinning side band. Chemical shift is from TMS.

Tables 4-1 and 4-2 list the observed ^1H relaxation times T_{1H} and $T_{1\rho H}$, respectively, for pure PS, pure PVME, and PS/PVME=5:5 blend at -45, -10, and 38℃. The observed T_{1H} of PS of the blend at -45℃ is in good agreement with that of PVME. The agreement is also found at 38℃. The $T_{1\rho H}$ values of PS of the blend at -45 and -10℃ are in good agreement with those of PVME.

At 38℃, $T_{1\rho H}$ decay curves of PS and PVME are multi-exponential (Figure 4-2). The $T_{1\rho H}$ value was estimated from the initial slope of decay curve. The $T_{1\rho H}$ value of PS of the blend at 38℃ is different from that of PVME. Even for pure PVME, the methoxy and methine groups have different $T_{1\rho H}$ values at 38℃.

The different $T_{1\rho H}$ and the multi-exponential decays at 38℃ are interpreted in terms of molecular motion. The experimental temperature is much higher than T_g of the blend (-14℃).[1a] The ^{13}C linewidth study showed that the main-chain of PVME undergoes motion at those temperatures.[11] The motion partially averages the ^1H dipole-dipole interaction, resulting in slow spin-diffusion in the $T_{1\rho H}$ process. We will treat later the effect of slow spin-diffusion on the relaxation curve more quantitatively.

On the basis of the criteria of section 2.2.B in Chapter 2, the results observed for PS and PVME of the blend at -10 and -45℃ show that the blend is homogeneous on a scale of 20-30 Å as well as a scale of 200-300 Å.

If the spin-diffusion is completed between PS and PVME in blend, the ^1H relaxation rates of PS and PVME are averaged to a single value. The average T_{1H} and $T_{1\rho H}$ can be calculated on the assumption that the intrinsic relaxation times of PS and PVME of the blend are equal to the relaxation times of the respective

pure polymer (eq 2-9, in section 2.2.B). This assumption implies that the molecular motion of component polymers is not affected by blending.

At -45℃, the observed T_{1H} and $T_{1\rho H}$ values are in good agreement with calculated ones (Table 4-1 and 4-2). This indicates that averaging of the ^1H relaxation rates by spin-diffusion occurs, and that the molecular motion is not affected by blending.

At -10℃, the $T_{1\rho H}$ rates of PS and PVME of the blend are averaged by spin-diffusion, but the observed $T_{1\rho H}$ values are not in agreement with the calculated ones. The $T_{1\rho H}$ process is governed by motion at frequencies of ~50kHz, and such motion occurs at -10℃ (the $T_{1\rho H}$ minimum of the blend is observed at ~0℃).[3] The blending affects such motion at frequencies of ~50kHz. In fact, the ^{13}C linewidth study showed that the motion which governs the $T_{1\rho H}$ process is affected appreciably by blending.[11] Therefore, the $T_{1\rho H}$ values of PS and PVME of the blend vary from those of pure ones by blending; the observed values differ from calculated ones. At -45℃, such motion is frozen in pure polymers and also in the blend. The effect of blending is not appreciable.

Kwei *et al.* observed two T_2 components, long and short.[9] This may reflect two types of segmental motions of PS and PVME, respectively, of the blend above T_g. The different segmental motions of PS and PVME have been revealed by our group[11] and Menestrel, *et al.*[12]

The micro-heterogeneity of PS/PVME blend has been suggested by several groups.[2,3,9,10] These groups analyzed the blend at

higher temperatures than T_g. The micro-heterogeneity may be misled by the ineffective spin-diffusion due to fast motion above T_g.

Table 4-1 Observed and calculated (average) T_{1H} values(s) of PS/PVME=5:5 blend at -45 and 38 ℃

T_{1H} (s)		38°C	-45°C
Pure	PS	1.70±0.01	16.2±0.5
	PVME	1.42±0.03	1.64±0.03
Blend	PS	2.2±0.1	2.8±0.1
	PVME	2.1±0.1	2.7±0.1
Calc.		1.5	2.7

Error is σ

Table 4-2 Observed and calculated (average) $T_{1\rho H}$ values(ms) of PS/PVME=5:5 blend at -45, -10, and 38 ℃

$T_{1\rho H}$ (ms)		-45°C	-10°C	38°C
Pure	PS	24±1	11.8±0.2	5.35±0.03
	PVME (OCH_3)	28±1	2.8±0.1	1.05±0.02*
	(CH)	29±1	2.9±0.1	0.44±0.01*
Blend	PS	25±1	12.3±0.3	1.91±0.06*
	PVME (OCH_3)	26±1	11.2±0.9	0.91±0.03*
	(CH)	26±1	12.5±0.4	0.56±0.03*
Calc.		26	4.2	—

Error is σ * : **initial relaxation time obtained by initial several data points.**

B Effects of Molecular Motion on ^1H Relaxation Curves

Figure 4-2 shows the $T_{1\rho H}$ decay curves of PS and PVME of the blend at 38 ℃. Observed $T_{1\rho H}$ decays are depicted by '○', '△', and '×' for the aromatic carbons of PS, the methoxy carbon (OCH_3) of PVME, and the methine carbon (CH) of PVME, respectively. All $T_{1\rho H}$ decay curves are multi-exponential.

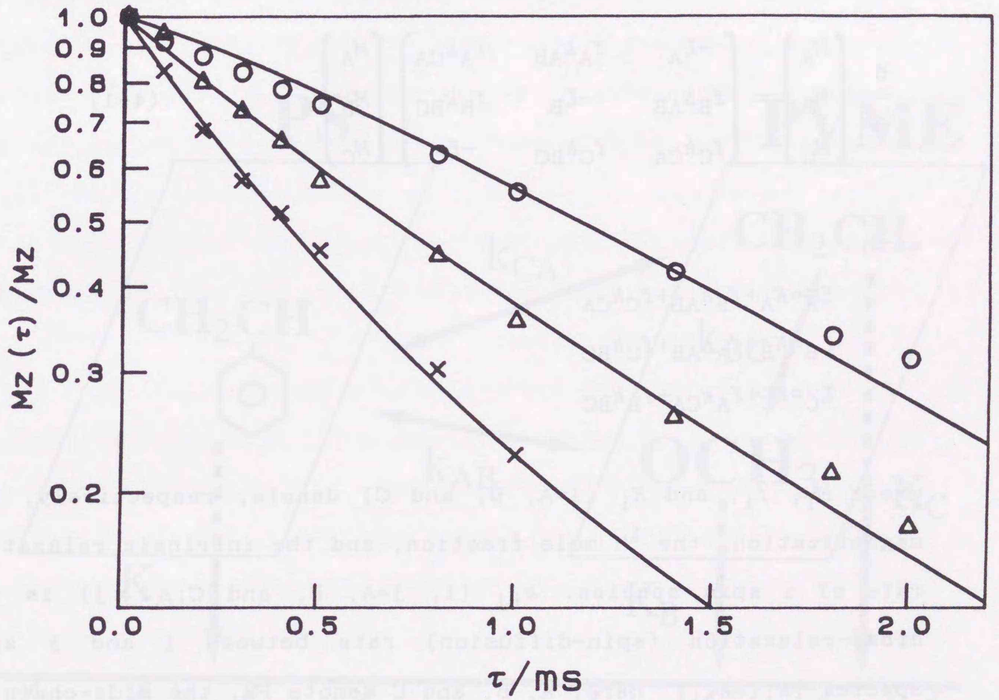

Figure 4-2. $T_{1\rho H}$ decay curves of PS/PVME=5:5 blend at 38 ℃. ○, △, and × are referred to protonated phenyl ring of PS, OCH_3 and CH of PVME in the blend, respectively. The solid lines are simulated curves by eq 4-1 to fit the observed ones.

In order to estimate the efficiency of spin-diffusion of the blend, we examine the $T_{1\rho H}$ decay curves quantitatively. We assume that the ^1H spin system of the blend consists of three ^1H spin species: protons of PS, the side-chain protons of PVME, and the main-chain protons of PVME. The three proton species exchange the magnetization via spin-diffusion as depicted schematically in Figure 4-3. The equation of the spin system can be given as:

$$\frac{d}{dt}\begin{bmatrix} M_A \\ M_B \\ M_C \end{bmatrix} = \begin{bmatrix} -\xi_A & f_A k_{AB} & f_A k_{CA} \\ f_B k_{AB} & -\xi_B & f_B k_{BC} \\ f_C k_{CA} & f_C k_{BC} & -\xi_C \end{bmatrix} \begin{bmatrix} M_A \\ M_B \\ M_C \end{bmatrix} \qquad (4\text{-}1)$$

with

$$\xi_A = K_A + f_B k_{AB} + f_C k_{CA}$$
$$\xi_B = K_B + f_A k_{AB} + f_C k_{BC}$$
$$\xi_C = K_C + f_A k_{CA} + f_B k_{BC}$$

where M_i, f_i, and K_i (i=A, B, and C) denote, respectively, the magnetization, the ^1H mole fraction, and the intrinsic relaxation rate of i spin species. k_{ij} (i, j=A, B, and C; $i \neq j$) is the cross-relaxation (spin-diffusion) rate between i and j spin species ($k_{ij}=k_{ji}$). Here, A, B, and C denote PS, the side-chain of PVME (OCH_3), and the main-chain of PVME (CH and CH_2), respectively.

A general solution of magnetization M_A can be written as follows;

$$M_A = \lambda_{A1}\exp(\varepsilon_1 t) + \lambda_{A2}\exp(\varepsilon_2 t) + \lambda_{A3}\exp(\varepsilon_3 t) \qquad (4\text{-}2)$$

where λ_{Ai} and ε_i (i = 1, 2, and 3) are elements of the transform matrix (λ_{Ai}, λ_{Bi}, λ_{Ci}) and the eigenvalue of the matrix in eq 1. We numerically solve this equation with initial magnetizations $M_A^0 : M_B^0 : M_C^0 = f_A : f_B : f_C$. The "best fitted" lines in Figure 4-2 are calculated using the relaxation rates of $K_A=0.40\times10^3 s^{-1}$, $K_B=1.06\times10^3 s^{-1}$, $K_C=1.85\times10^3 s^{-1}$, $k_{AB}=1.0\times10^3 s^{-1}$, $k_{CA}=1.1\times10^3 s^{-1}$, and $k_{BC}\leq100 s^{-1}$. The K_i values are in good agreement with the observed initial rates (Table 4-2).

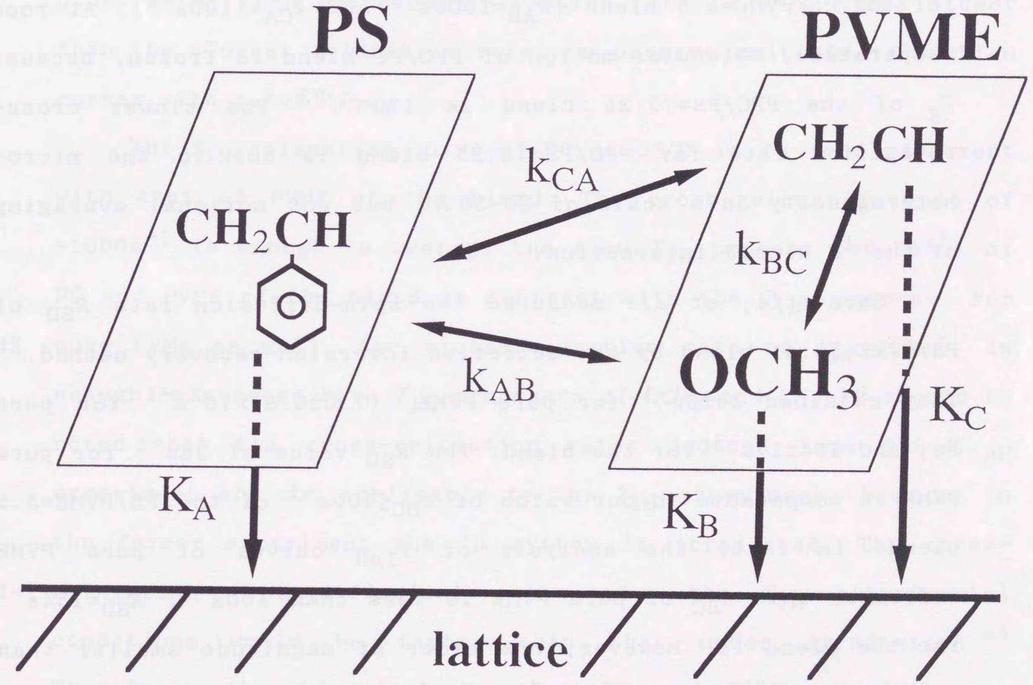

Figure 4-3. A model of three ^1H spin species for relaxation process for PS/PVME blends. The cross-relaxation rate is denoted by k_{ij}; i and j are species of spin. K_i is the intrinsic relaxation rate of i-spin species to the lattice.

k_{AB} and k_{CA} are larger than k_{BC}, indicating that the ^1H spin-diffusion operates effectively between PS and PVME as compared to intra-PVME. The combination of fast overall motion of the main-chain and the internal rotation of OCH_3 of PVME average the intramolecular dipole interaction more effectively, resulting in smaller k_{BC} value.

A similar analysis has been reported for poly(2,6-dimethyl-p-phenylene oxide)(PPO)/PS=75:25 blend; the ^1H cross-relaxation rate between PPO and PS is $135s^{-1}$,[22] about 1/8 of those obtained for the PS/PVME=5:5 blend (k_{AB}=1000s^{-1} and k_{CA}=1100s^{-1}). At room temperature, molecular motion of PPO/PS blend is frozen, because T_g of the PPO/PS=75:25 blend is 170℃.[23] The slower cross-relaxation rate for PPO/PS=75:25 blend is due to the micro-heterogeneity on a scale of 20-30 Å, but not motional averaging of the ^1H dipole interaction.

Caravatti, *et al.* measured the spin-diffusion rate R_{SD} of PS/PVME=59:41 blend by the selective inversion-recovery method.[2b] They obtained 38±6s^{-1} for pure PVME, (7.0±0.8)×10^3s^{-1} for pure PS, and 154±17s^{-1} for the blend. The R_{SD} value of 38s^{-1} for pure PVME is comparable to our value of k_{BC}≤100s^{-1} of the PS/PVME=5:5 blend. In fact, the analysis of $T_{1\rho H}$ curves of pure PVME indicates that k_{BC} of pure PVME is less than 100s^{-1}. R_{SD}=154s^{-1} for the blend is, however, one order of magnitude smaller than our value of $k_{AB}=k_{CA}$=~1000s^{-1}. This is ascribed to averaging of the ^1H dipole interaction by faster molecular motion at a high experiment temperature of 67℃ compared to our 38℃. In addition, the difference in sample preparation may bring about the different result.

The cross-relaxation rate between PS and PVME (k_{AB} and k_{CA}) of ~1000s^{-1} is not enough to average the fast $T_{1\rho H}$ process of the blend. In order to realize the single average relaxation rate, the cross-relaxation rate must be much higher than the fastest intrinsic relaxation rate. Equation 4-1 indicates that K_{ij} of the PS/PVME=5:5 blend at 38℃ must be greater than 2×10^4s^{-1} in order to realize a single average decay curve. When the cross-relaxation rate is 10-100 times faster than the fastest relaxation rate, we can observe a single relaxation curve. On the other hand, when the cross-relaxation rate is 4-10 times slower than the slowest relaxation rate, we observe multiple relaxation curves with rates of K_i.

The T_{1H} relaxation curve of PS at 38℃ is in good agreement with that of PVME of the blend. The cross-relaxation rate of ~1000s^{-1} is enough to average the slow T_{1H} process (~0.5s^{-1}) of PS and PVME of the blend in contrast with the $T_{1\rho H}$ process. For pure PVME as well, the cross-relaxation rate of k_{BC}=100s^{-1} is enough to average both T_{1H} processes of OCH_3 and CH. It should be noted that the cross-relaxation rates deduced from the $T_{1\rho H}$ experiment are not applicable to the T_{1H} experiment, because in the former experiment the ^1H system is irradiated. The cross-relaxation (spin-diffusion) rate under the T_{1H} experimental conditions would be faster than that under irradiation.[24] Therefore, the identical T_{1H} for PS and PVME at 38℃ are rationalized.

C Compositional Change during Phase-Separation

In the previous sections, we showed that the blend is homogeneous on a scale of 20-30 Å. Since the PS/PVME blend exhibits an LCST phase diagram, the blend becomes inhomogeneous when heated above 100-120 ℃: the binodal point of 5:5 composition.[1b,16] The heterogeneity of phase-separated blend will affect the relaxation process. To investigate the phase-separation of PS/PVME=5:5 blend, we examine the compositional change during phase-separation by analyzing the $T_{1\rho H}$ decay curve.

Figures 4-4 and 4-5 show the observed $T_{1\rho H}$ decay curves of the blend after heat-treatment for 1min and 2min, respectively, at 140 ℃ (PS; ○ and PVME; ×). In order to neglect the effects of molecular motions on $T_{1\rho H}$ decay curves, these decay curves are observed at -10 ℃. After heat-treatment, the $T_{1\rho H}$ curves of PS and PVME show double-exponential behavior. At -45 ℃, single-exponential decays are observed. This is because the $T_{1\rho H}$ value of pure PS happens to be close to that of pure PVME at -45 ℃.

The decay curves of PS in Figures 4-4 and 4-5 are different from those of PVME. The difference in decay curve is more significant as the heat-treatment time is longer. This difference is clearly brought about by the phase-separation, because the decay curves are almost identical before heat-treatment.

To analyze the $T_{1\rho H}$ curve of phase-separated blend, we assume that the phase-separated blend consists of two spatially separated domains (Figure 2-7 of section 2.2.B).

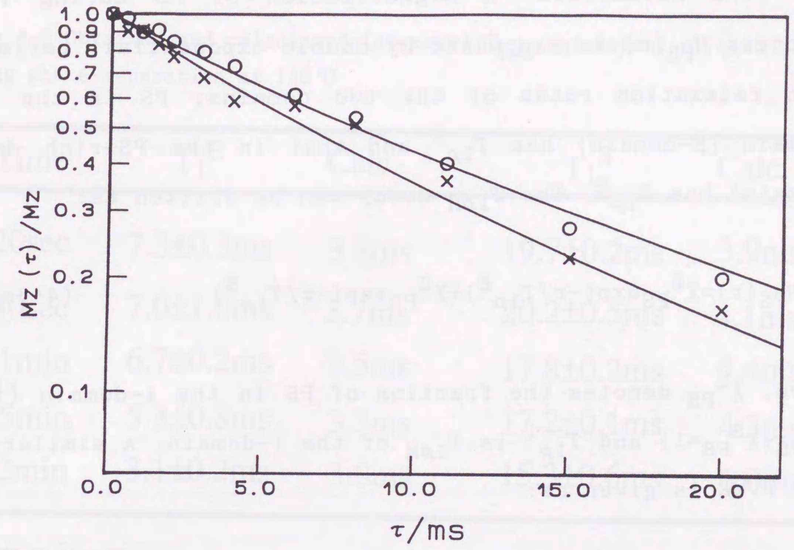

Figure 4-4. Observed $T_{1\rho H}$ decay curves of PS (○) and PVME (×) of PS/PVME=5:5 blend after 1min heating at 140 ℃. These decay curves were obtained at -10 ℃. The solid lines are the "best fitted" ones to eq 4-3.

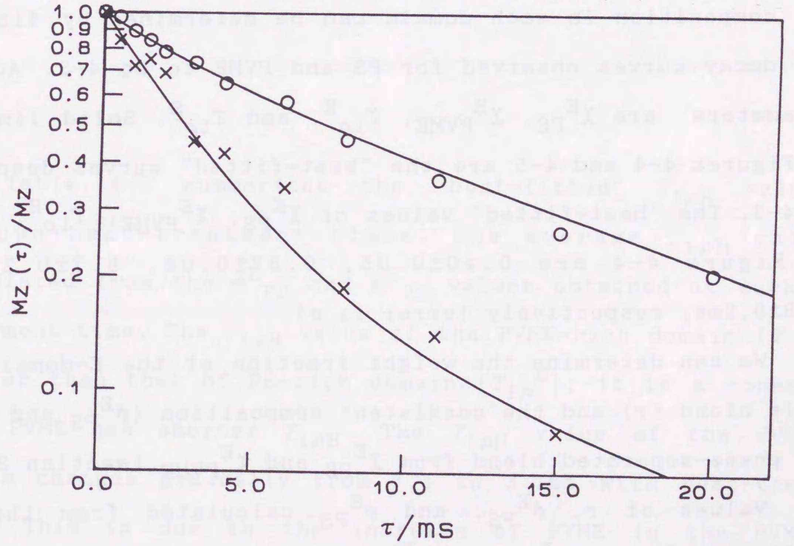

Figure 4-5. Observed $T_{1\rho H}$ decay curves of PS (○) and PVME (×) of PS/PVME=5:5 blend after 2min heating at 140 ℃. These decay curves were obtained at -10 ℃. The solid lines are the "best fitted" ones to eq 4-3.

The normalized ^1H magnetization of PS during relaxation process $M_{PS}(\tau)$ is expressed by double exponential, reflecting the two relaxation rates of the two domains; PS in the PVME-rich domain (E-domain) has $T_{1\rho}{}^{E}$ and that in the PS-rich domain (S-domain) has $T_{1\rho}{}^{S}$. The $T_{1\rho H}$ decay can be written as:

$$M_{PS}(\tau)=\chi^{E}{}_{PS}\exp(-\tau/T_{1\rho}{}^{E})+\chi^{S}{}_{PS}\exp(-\tau/T_{1\rho}{}^{S}) \qquad (4\text{-}3a)$$

Here, $\chi^{i}{}_{PS}$ denotes the fraction of PS in the i-domain (i=E or S; $\chi^{E}{}_{PS}+\chi^{S}{}_{PS}=1$) and $T_{1\rho}{}^{i}$ is $T_{1\rho H}$ of the i-domain. A similar equation for PVME is given as:

$$M_{PVME}(\tau)=\chi^{E}{}_{PVME}\exp(-\tau/T_{1\rho}{}^{E})+\chi^{S}{}_{PVME}\exp(-\tau/T_{1\rho}{}^{S}) \qquad (4\text{-}3b)$$

The composition in each domain can be determined by fitting the two decay curves observed for PS and PVME to eq 4-3. Adjustable parameters are $\chi^{E}{}_{PS}$, $\chi^{E}{}_{PVME}$, $T_{1\rho}{}^{E}$, and $T_{1\rho}{}^{S}$. Solid lines shown in Figures 4-4 and 4-5 are the "best-fitted" curves described by eq 4-3. The "best-fitted" values of $\chi^{E}{}_{PS}$, $\chi^{E}{}_{PVME}$, $T_{1\rho}{}^{E}$, and $T_{1\rho}{}^{S}$ in Figure 4-4 are 0.40±0.05, 0.62±0.06, 6.7±0.2ms, and 17.8±0.2ms, respectively (error is σ).

We can determine the weight fraction of the E-domain of the whole blend (r) and the coexistent composition ($\phi^{E}{}_{PS}$ and $\phi^{S}{}_{PS}$) of the phase-separated blend from $\chi^{E}{}_{PS}$ and $\chi^{E}{}_{PVME}$ (section 2.2.B).

Values of r, $\phi^{E}{}_{PS}$, and $\phi^{S}{}_{PS}$ calculated from the "best-fitted" values of $\chi^{E}{}_{PS}$ and $\chi^{E}{}_{PVME}$ in Figure 4-4 are 0.51±0.05, 0.39±0.05, and 0.62±0.05, respectively, (error is σ). The values of $\phi^{E}{}_{PS}$ and $\phi^{S}{}_{PS}$ are summarized in Figure 4-6.

Table 4-3 Obtained and calculated (average) $T_{1\rho H}$ values(ms) of each domain during phase-separation at 140℃

Time	$T_1{}^{E}$	Calc.	$T_1{}^{S}$	Calc.
20sec	7.3±0.3ms	3.8ms	19.7±0.2ms	3.9ms
40sec	7.0±1.0ms	3.7ms	20.2±0.5ms	4.1ms
1min	6.7±0.2ms	3.5ms	17.8±0.2ms	4.4ms
1.5min	5.3±0.8ms	3.3ms	17.2±0.1ms	4.3ms
2min	3.1±0.2ms	3.0ms	15.3±0.6ms	6.0ms

Error is σ

Table 4-3 summarizes the "best-fitted" $T_{1\rho H}$ values at various heat-treatment times. The average $T_{1\rho H}$ value is calculated from the $\phi^{E}{}_{PS}$ and $\phi^{S}{}_{PS}$ values obtained at each heat-treatment time. The $T_{1\rho H}$ value of the PVME-rich domain ($T_{1\rho}{}^{E}$) is shorter than that of PS-rich domain ($T_{1\rho}{}^{S}$); it is a consequence that PVME has shorter $T_{1\rho H}$. The $T_{1\rho H}$ value of the PVME-rich domain changes gradually from 7.3 to 3.1ms with heat-treatment time. This is due to the increase of PVME in the PVME-rich domain. In the PS-rich domain, $T_{1\rho H}$ is less sensible to the decrease of PVME. This phenomenon was observed also by Chu et

al.[3] At present, we do not have any concrete idea for explaining this. The calculated values are different from the observed ones, as is the case of the homogeneous blend (Table 4-2). This suggests that molecular motion of PS and PVME in phase-separated domains are affected by blending.

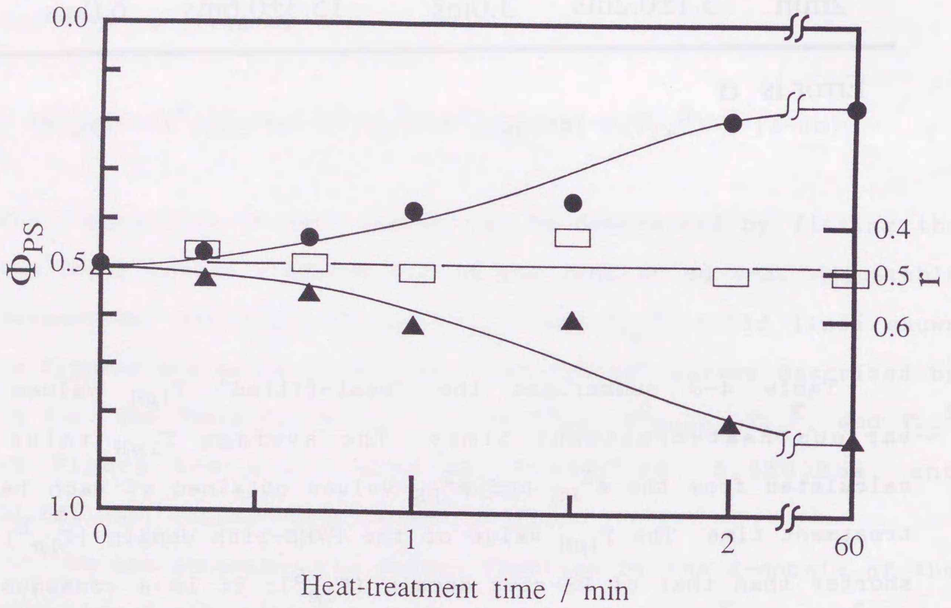

Figure 4-6. Compositional change during phase-separation of PS/PVME=5:5 blend. The compositional changes of PS in the PVME-rich domain and in the PS-rich domain are depicted by ● and ▲, respectively. The fraction of the PVME-rich domain r is depicted by □. The solid lines are written for the guidance of reader's eyes.

Here, we briefly touch upon the effects of motions on the $T_{1\rho H}$ decay curve (eq 4-3). Figure 4-7 shows the $T_{1\rho H}$ decay curves of the PS/PVME=5:5 blend observed at 38℃. The fast molecular motion of PVME in the blend averages the ^1H dipole-dipole interaction between PS and PVME; the spin-diffusion within each domain is slow at 38℃. Even in the same domain, the $T_{1\rho H}$ value of PS is different from that of PVME. Eq 4-3 should be rewritten as:

$$M_{PS}(\tau)=\chi^{E}_{PS}\exp(-\tau/{T_1}^{E}_{PS})+(1-\chi^{E}_{PS})\exp(-\tau/{T_1}^{S}_{PS}) \quad (4\text{-}4a)$$

$$M_{PVME}(\tau)=\chi^{E}_{PVME}\exp(-\tau/{T_1}^{E}_{PVME})+(1-\chi^{E}_{PVME})\exp(-\tau/{T_1}^{S}_{PVME}) \quad (4\text{-}4b)$$

We assume that the relaxation curve of each component is single exponential. We adopt six parameters χ^{E}_{PS}, ${T_1}^{E}_{PS}$, and ${T_1}^{S}_{PS}$ for PS, and χ^{E}_{PVME}, ${T_1}^{E}_{PVME}$, and ${T_1}^{S}_{PVME}$ for PVME to fit the two observed $T_{1\rho H}$ curves to eq 5. In Figure 4-7 the "best-fitted" curves are shown by solid lines. It is shown that the "best-fitted" χ values at 38℃ (χ^{E}_{PS}=0.31±0.08 and χ^{E}_{PVME}=0.6±0.1 in Figure 4-7) are in agreement with the values obtained at −10℃ (χ^{E}_{PS}= 0.40±0.05 and χ^{S}_{PVME}=0.62±0.06 in Figure 4-4) within experimental error. The observed decay curves at various heat-treatment times can be described by eq 4-4 with χ values obtained at −10℃. This indicates that even if the insufficient spin-diffusion occurs within each domain, we can deduce the composition in each phase-separated domain. In some case more rigorous treatment like eq 4-1 is required. It is recommended to conduct the experiment at lower temperatures than T_g.

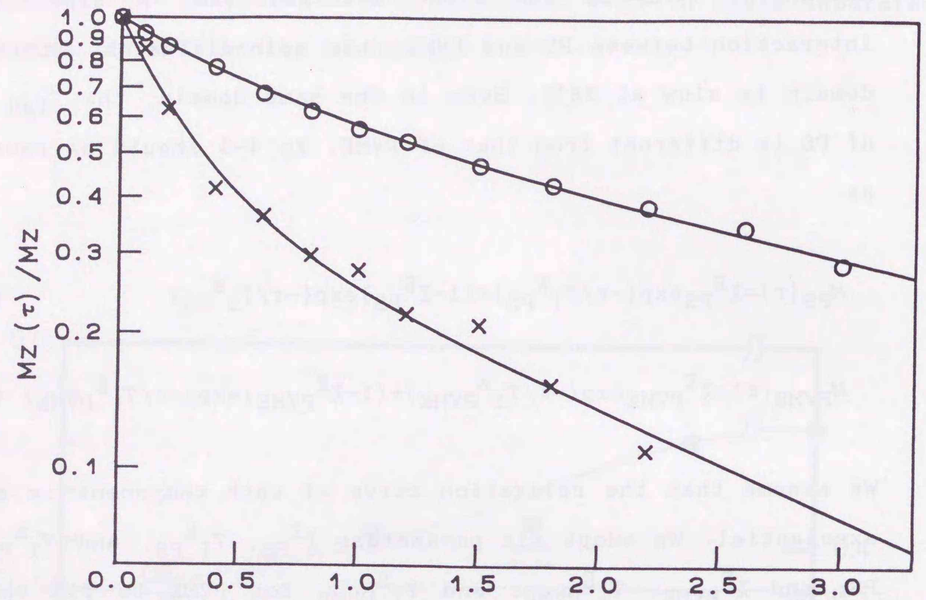

Figure 4-7. Observed $T_{1\rho H}$ decay curves of PS (○) and PVME (×) of PS/PVME=5:5 blend after 1min heating at 140 ℃. These decay curves were obtained at 38 ℃. The solid lines are the "best fitted" ones to eq 4-4.

The change in composition during the phase-separation process at 140 ℃ is summarized in Figure 4-6 for the PS/PVME=5:5 blend. Further heat-treatment for more than 2min does not cause any appreciable change in $T_{1\rho H}$. In the $T_{1\rho H}$ experiments, we detect the phase-separation process on a scale of 20-30 Å. Heat-

treatment for more than 2min would cause a morphological change on a scale larger than 20-30 Å. The morphological change would proceed more slowly; it is not reflected in $T_{1\rho H}$. From the analysis of T_{1H} curve, it is possible to detect morphological change on a large scale of 200-300 Å. We do not show the T_{1H} results, because the T_1^E and T_1^S values are similar at these temperatures; the effect of the phase-separation can not be appreciated.

D Kinetics of Phase-Separation

It is an important problem whether the phase-separation is governed by the spinodal decomposition or the nucleation and growth process. In the early stage of the spinodal decomposition process, the composition of each domain changes continuously with time.[13b,16,25] In addition, the fraction of the two domains remains unchanged during the early stage of phase-separation. In the nucleation and growth process,[16,26] an amount of nuclei with a composition close to the binodal increases remarkably with time. The composition of nucleus remains approximately constant and the fraction of the nucleus increases during phase-separation.

Figure 4-6 shows that the ratio of the PVME-rich domain to the PS-rich domain r remains at ~0.5 during phase-separation. The composition of PS of the PVME-rich domain (ϕ^E_{PS}) decreases gradually from 50% to 20% for the first 2min; the composition of PS of the PS-rich domain ϕ^S_{PS} increases from 50% to 81%. These results clearly indicate that the phase-separation is not

proceeded by the nucleation and growth, but initiated by the spinodal decomposition. The compositions at 60min, 17:83 for the PVME-rich domain and 85:15 for the PS-rich domain, should be close to the binodal composition. Therefore, this approach can also be applied to determine the phase diagram (binodal curve) of blend.[27]

Even though the phase-separation starts from the 5:5 composition, the *r* value is not always 0.5. In fact, Nishi, *et al.* obtained an *r* values of 0.35-0.40 from the direct ^1H observation.[16] The *r* value reflects the shape of binodal curve. Our *r* value of ~0.5 implies that the binodal curve is approximately symmetrical.

On the basis of Cahn theory,[25] Nishi, *et al.* derived an equation for the total reduction *Q* of composition of a minor component in a given phase ($\phi^0_{PS}-\phi^E_{PS}$ or $\phi^0_{PVME}-\phi^S_{PVME}$) as follows (the same equation is shown in section 3.3.2.D in chapter 3):[16]

$$\ln(Q)=\text{constant}+3Rt \qquad (4\text{-}5)$$

where *R* expresses the growth rate of compositional change in phase-separation process (phase-separation rate) and *t* is the heat-treatment time. If the phase-separation process is initiated by the spinodal decomposition, *R* should be positive because the compositional change always proceeds with time. Negative *R* is expected for the nucleation and growth, because the composition of nucleus does not change significantly.[16]

From the compositional change of ϕ^E_{PS} (Figure 4-6), we found

the *R* value of the PVME-rich domain to be $+8.3\times10^{-3}s^{-1}$ ($\sim0.5min^{-1}$) at 140℃. Similarly from ϕ^S_{PVME}, we found that *R* in the PS-rich domain to be $+7.7\times10^{-3}s^{-1}$ ($\sim0.5min^{-1}$). The two values are close together. The plus sign of *R* is consistent with the spinodal decomposition. These values are one order of magnitude larger than the value obtained by Nishi, *et al.* for PVME in the PS-rich domain ($3.82\times10^{-4}s^{-1}$ ($2.3\times10^{-2}min^{-1}$)) at 130℃.[16] This difference is attributed mainly to the different heat-treatment temperature, and indicates that the phase-separation rate at 140℃ is 10-times faster than that at 130℃. Gelles and Frank analyzed the results of the excimer fluorescence experiment for phase-separated PS/PVME=1:9 blend at 150℃ by assuming the spinodal decomposition.[14] They obtained an *R* value of $0.9min^{-1}$ for the PS-rich domain. This value is a slightly larger than the present value, again reflecting the different temperature. The correlation between temperature and phase-separation rate has also been shown by Larbi, et al.[26]

References

1. (a)Bank,M.;Leffingwell,J.;Thies,C. *Macromolecules*, 1971, *4*, 43.
   (b)Bank,M.;Leffingwell,J.;Thies,C. *J. Polym. Sci., Part A-2*, 1972, *10*, 1097.
2. (a)Caravatti,P.;Neuenschwander,P.;Ernst,R.R.*Macromolecules*, 1985, *18*, 119.
   (b)Caravatti,P.;Neuenschwander,P.;Ernst,R.R. *Macromolecules*, 1986, *19*, 1889.
3. Chu,C.W.;Dickinson,L.C.;Chien,J.C.W. *J. Appl. Polym. Sci.*, 1990, *41*, 2311.
4. Goldman,M.;Shen,L. *Phys. Rev.*, 1966, *144*, 321.
5. Kaplan,S. *Am. Chem. Soc., Polym. Prep.* 1984, *25*, 356.
6. (a)Gobbi,G.C.;Silvestri,R.;Russell,T.P.;Lyerla,J.R.; Fleming,W.W. *J. Polym. Sci., Part C: Polym. Lett.*, 1987, *25*, 61.
   (b)Parmer,J.F.; Dickinson,L.C.;Chien,J.C.W.;Porter,R.S. *Macromolecules*, 1987, *20*, 2308.
7. White,J.L.;Mirau,P. *Macromolecules*, 1993, *26*, 3049.
8. (a)Crowther,M.W.;Cabasso,I.;Levy,G.C. *Macromolecules*, 1988, *21*, 2924.
   (b)Mirau,P.A.;Tanaka,H.;Bovey,F.A. *Macromolecules*, 1988, *21*, 2929.
   (c)Mirau,P.A.;Bovey,F.A. *Macromolecules*, 1990, *23*, 4548.

9. Kwei,T.K.;Nishi,T.;Roberts,R.F. *Macromolecules*, 1974, *7*, 667.
10. Muller,G.;Stadler,R. *Makromol. Chem., Rapid Commun.*, 1992, *13*, 117.
11. Takegoshi,K.;Hikichi,K. *J. Chem. Phys.*, 1991, *94*, 3200.
12. Menestrel,C.L.;Kenwright,A.M.;Sergot,P.;Laupretre,F.; Monnerie,L. *Macromolecules*, 1992, *25*, 3020.
13. (a)Hashimoto,T.;Kumaki,J.;Kawai,H. *Macromolecules*, 1983, *16*, 641.
    (b)Hashimoto,T.;Itakura,M.;Hasegawa,H. *J. Chem. Phys.*, 1986, *85*, 6118.
14. Gelles,R.;Frank,C.W. *Macromolecules*, 1982, *15*, 1486.
15. Halary,J.L.;Ubrich,J.M.;Nunzi,J.M.;Monnerie,L. *Polymer*, 1984, *25*, 956.
16. Nishi,T.;Wang,T.T.;Kwei,T.K. *Macromolecules*, 1975, *8*, 227.
17. (a)Pines,A.;Gibby,M.G.;Waugh,J.S. *J. Chem. Phys.*, 1973, *59*, 569.
    (b)Schaefer,J.;Stejskal,E.O.;Buchdahl,R. *Macromolecules*, 1975, *8*, 291.
18. van Geet,A.L. *Anal. Chem.* 1970, *42*, 679.
19. McBrierty,V.J.;Douglass,D.C.;Kwei,T.K. *Macromolecules*, 1978, *11*, 1265.
20. Henrichs,P.M.;Tribone,J.;Massa,D.J.;Hewitt,J.M. *Macromolecules*, 1988, *21*, 1282.
21. Anderson,J.E.;Slichter,W.P. *J. Phys. Chem.*, 1965, *69*, 3099.

22. Stejskal,E.O.;Schaefer,J.;Sefcik,M.D.;Mckay,R.A. *Macromolecules*, 1981, *14*, 275.
23. Shultz,A.R.;Gendron,B.M. *J. Appl. Polym. Sci.*, 1972, *16*, 461.
24. Takegoshi,K.;McDowell,C.A. *J. Chem. Phys.*, 1987, *86*, 6077.
25. Cahn,J.W. *J. Chem. Phys.* 1965, *42*, 93.
26. Larbi,F.B.C.;Halary,J.L.;Monnerie,L. *Macromolecules*, 1991, *24*, 867.
27. Asano,A.;Takegoshi,K.;Hikichi,K. *Polym. J.*, 1992, *24*, 555.

Chapter 5 Poly(ethylene oxide)/$LiClO_4$ (PEO/$LiClO_4$) Blend

5.1 Introduction

Blend of poly(ethylene oxide) (PEO) and alkali metal salt shows a high ionic conductivity.[1] PEO/$LiClO_4$ blend in a lithium$(Li)^+$-ion concentration range of O/Li≥6/1 shows a conductivity higher than $10^{-5}\Omega^{-1}cm^{-1}$ at 50℃;[2-4] O/Li represents the ratio of PEO to $LiClO_4$. The ionic conductivity of PEO/$LiClO_4$ blend decreases rapidly with decreasing temperature. In order to understand such high conductivity of PEO/$LiClO_4$ blend, it is important to study the structure and the polymer/ion interaction.

DSC[3] and X-ray[5] studies showed that PEO/$LiClO_4$ blend has two kinds of PEO_XLiClO_4 crystalline complexes: stoichiometries of O/Li=3/1 and 6/1. PEO_XLiClO_4 represents a complex with $LiClO_4$ at a stoichiometry of O/Li=X/1. At Li^+-ion concentrations lower than O/Li=6/1, the blend has the crystalline pure PEO and PEO_6LiClO_4 complex phases. At concentrations higher than O/Li=6/1, the blend has crystalline PEO_6LiClO_4 and PEO_3LiClO_4 complex phases. The stoichiometry at eutectic point is found to be O/Li=10/1 at Li^+-ion concentrations less than O/Li=6/1, while at higher concentrations eutectic point is not observed.[5]

In the crystalline phase PEO is in the 7/2 helix and in the trans-trans-gauche (ttg) conformation of the CC-OC, CO-CC, and OC-CO bonds.[6] Recently, Chatani, *et al.* examined PEO/NaSCN complexes of O/Na=3/1 and 1/1.[7] They suggested that for O/Na=3/1 complex PEO is in a ttgttgtt$\bar{g}$ conformation and for O/Na=1/1

complex PEO is in a gt$\bar{g}\bar{g}$tg conformation.[7] They suggested that the conformation of the latter complex is more extended than the former. For crystalline PEO_XLiClO_4 complexes, PEO is believed to be in a similar conformation and to take a helical structure.

In this chapter, we describe the morphology, stoichiometry, and domain size of various PEO/$LiClO_4$ blends. Firstly, we assign the ^{13}C CP/MAS spectra by comparison with previous DSC[3] and X-ray[5] results. The ^{13}C spin-lattice relaxation (T_{1C}) is measured to study crystalline and amorphous phases in the blend. Secondly, the Li^+-ion mobility is investigated by ^7Li spin-lattice relaxation behavior (^7Li-T_1). From the observations of ^{13}C and ^7Li NMR, the stoichiometry is discussed. Finally, the ^1H spin-lattice relaxation behaviors in both the laboratory (T_{1H}) and rotating ($T_{1\rho H}$) frames are examined to study the domain size of PEO_XLiClO_4 complexes.

5.2 Experimental

A Materials

The weight average molecular weight of PEO is 20000. Anhydrous $LiClO_4$ was obtained from NACALAI TESQUE Inc. PEO and $LiClO_4$ were dissolved in anhydrous acetonitrile at a concentration of 10w/v%, and mixed at ratios of oxygen of PEO to Li (O/Li) of 20/1, 12/1, 8/1, 6/1, 3/1, and 1/1. The PEO/$LiClO_4$ blends were obtained by casting solutions on a glass plate under N_2 gas atmosphere at room temperature. The samples obtained were

dried under vacuum at 100℃ for 2-3 days and further dried under vacuum at room temperature for more than 3 weeks.

B NMR Measurements

All NMR measurements were made using a JEOL JNM-GX270 spectrometer operating at 67MHz for ^{13}C and 105MHz for ^7Li. The high-resolution solid-state ^{13}C NMR spectra were obtained by the combined use of cross-polarization (CP) and magic-angle-spinning (MAS).[8] The radio frequency (rf) field strength for both ^1H and ^{13}C was 55KHz. The spinning frequency was about 5.5KHz. T_{1H} was indirectly measured by well-resolved ^{13}C signals enhanced by CP after applying 180° pulse to ^1H nuclei (pulse sequence 3 of Figure 2-3 in chapter 2).[9] Similarly, $T_{1\rho H}$ was indirectly obtained by the ^{13}C signals with combined use of CP and the spin-locking to ^1H nuclei (pulse sequence 2 of Figure 2-3 in chapter 2).[10] ^{13}C spin-lattice relaxation time (T_{1C}) was obtained by the Torchia pulse sequence (pulse sequence 5 of Figure 2-3 in chapter 2).[11] The contact time for the CP signal enhancement was 100 or 500μs for the $T_{1\rho H}$ experiments. For the T_{1H} and T_{1C} experiments, the contact time is 100 or 500μs for O/Li=20/1, 12/1 and PEO, and for the other samples, 1 or 2 ms. The temperature calibration was done using proton signals of methanol under spinning at 5.5KHz.[12,13]

^7Li NMR spectra were obtained without MAS for samples sealed in glass tubes. ^7Li spin-lattice relaxation time (^7Li-T_1) was measured by the conventional inversion-recovery method with high-power proton decoupling (55KHz).

5.3 Results and Discussion

A ^{13}C CP/MAS NMR Spectra and Relaxation

Figure 5-1 shows the ^{13}C CP/MAS spectra of PEO/$LiClO_4$ blends and PEO. For pure PEO with a CP contact time of 100μs, the signal of crystalline phase is observed at 72ppm. When the contact time is 1ms, the signal of amorphous phase appears at 71ppm. With increasing amount of $LiClO_4$, the crystalline phase of pure PEO decreases. We could not observe the pure crystalline signal at 72ppm for O/Li$\leq$6/1. The amorphous peak at 71ppm (or 70ppm) is observed at all concentrations. The peak of amorphous phase appears at 1ppm higher field than that of crystalline phase. This is ascribed to the susceptibility difference between the two phases.[14]

New peaks are clearly observed at higher fields in a middle concentration range of O/Li=12/1-3/1. The efficiency of CP signal enhancement for O/Li=12/1-3/1 blends is much better than for pure PEO. At a concentration of O/Li=1/1, the high field shift peaks disappear and a singlet peak is observed at 71ppm. Although the chemical shift of this peak is equal to that of the amorphous PEO, the efficiency of CP signal enhancement of this peak is much better than that of the amorphous PEO. Therefore, this peak may be attributed to a new crystalline phase. In fact, previous studies pointed out an existence of a new complex in this concentration range.[3,5]

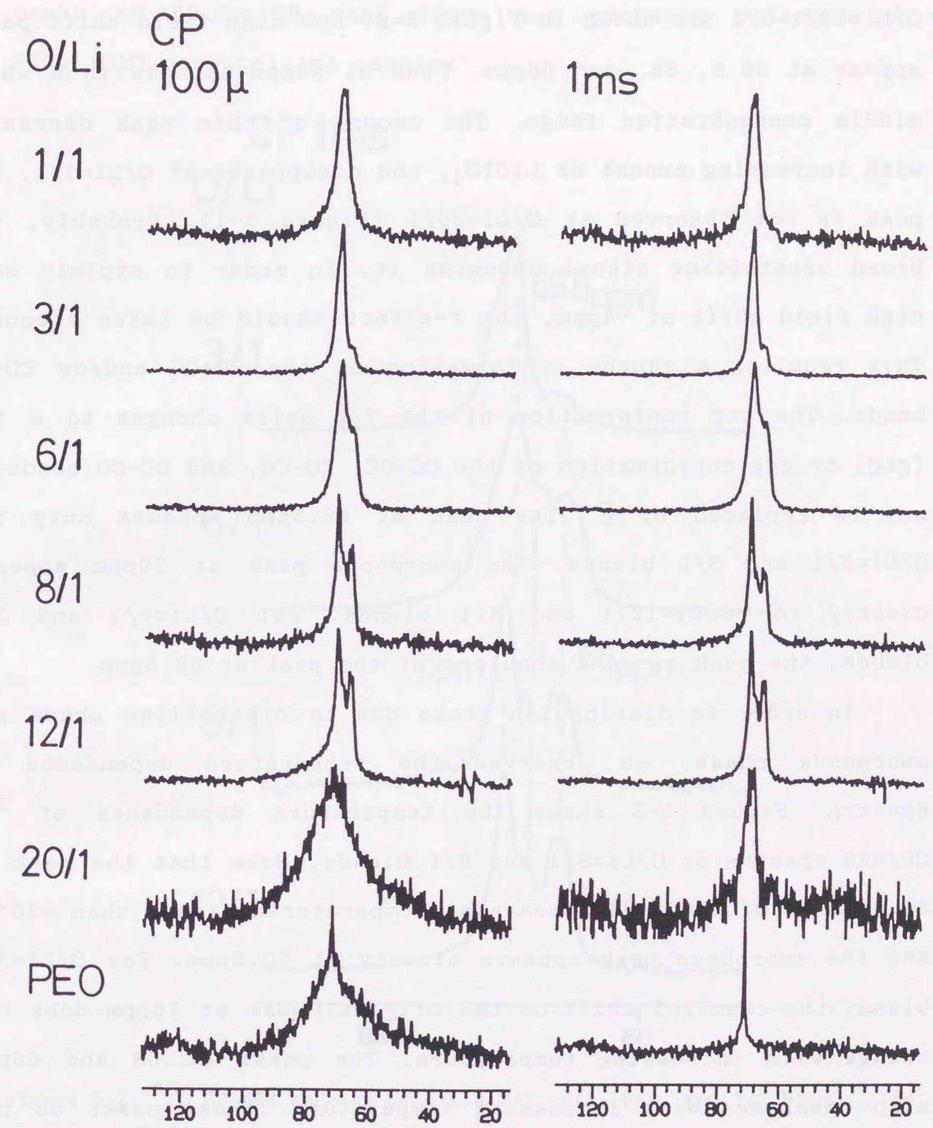

Figure 5-1. ^{13}C CP/MAS spectra of PEO/$LiClO_4$ blends and PEO. The ratio of O/Li is shown on the left side of the spectra. The contact time of CP signal enhancement is 100μs for the spectra on the left-hand side, and 1ms for those on the right-hand side.

The enlarged ^{13}C CP/MAS spectra at middle concentrations of O/Li=12/1-3/1 are shown in Figure 5-2. New high field shift peaks appear at 69.5, 68, and 66ppm. Peak at 66ppm appears in a whole middle concentration range. The amount of this peak decreases with increasing amount of $LiClO_4$, and disappears at O/Li=1/1. The peak is not observed at O/Li=20/1 (Figure 5-1). Probably, the broad crystalline signal obscures it. In order to explain such high field shift of ~4ppm, the *r*-effect should be taken account. This requires a gauche conformation at the CC-OC and/or CO-CC bonds. The ttg conformation of the 7/2 helix changes to a tgg (gtg) or ggg conformation of the CC-OC, CO-CC, and OC-CO bonds; g may be replaced by $\bar{g}$. The peak at 69.5ppm appears only for O/Li=6/1 and 3/1 blends. The amorphous peak at 70ppm appears clearly for O/Li=12/1 and 8/1 blends. For O/Li=6/1 and 3/1 blends, the peak is on a shoulder of the peak at 69.5ppm.

In order to distinguish peaks due to crystalline phase and amorphous phase, we observed the temperature dependence of spectra. Figure 5-3 shows the temperature dependence of ^{13}C CP/MAS spectra of O/Li=8/1 and 6/1 blends. Note that the peak at 69.5ppm of O/Li=6/1 disappears at temperatures higher than ~70℃, and the amorphous peak appears clearly at 70.6ppm. For O/Li=8/1 blend, the chemical shift of the original peak at 70ppm does not change with increasing temperature. The peaks at 68 and 66ppm also disappear with increasing temperature. Those peaks do not appear again when the temperature is lowered to 38℃. These results are consistent with those of O'Gara *et al.*[15] Furthermore, the peak at 66ppm appears after drying under vacuum for more than 3 weeks, while it does not appear for a week. This shows that it

takes a few weeks for the structure to be equilibrated. The new peaks at 69.5, 68, and 66ppm are probably related to the PEO_XLiClO_4 crystalline complex.

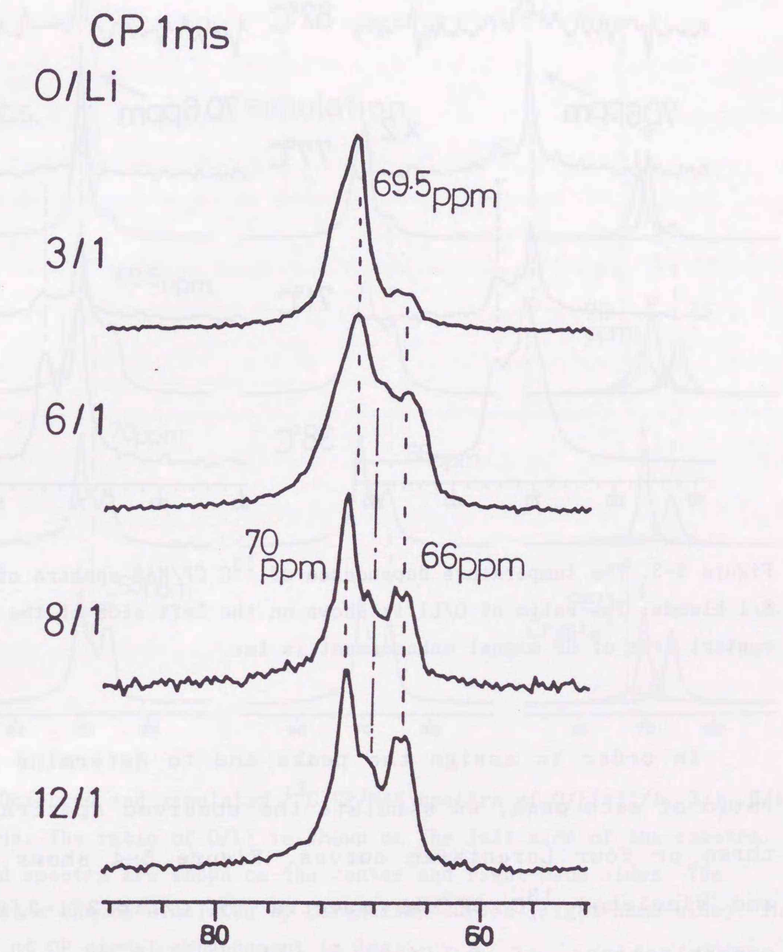

Figure 5-2. ^{13}C CP/MAS spectra of O/Li=12/1, 8/1, 6/1, and 3/1 blends. The ratio of O/Li is shown on the left side of the spectra. The contact time of CP signal enhancement is 1ms.

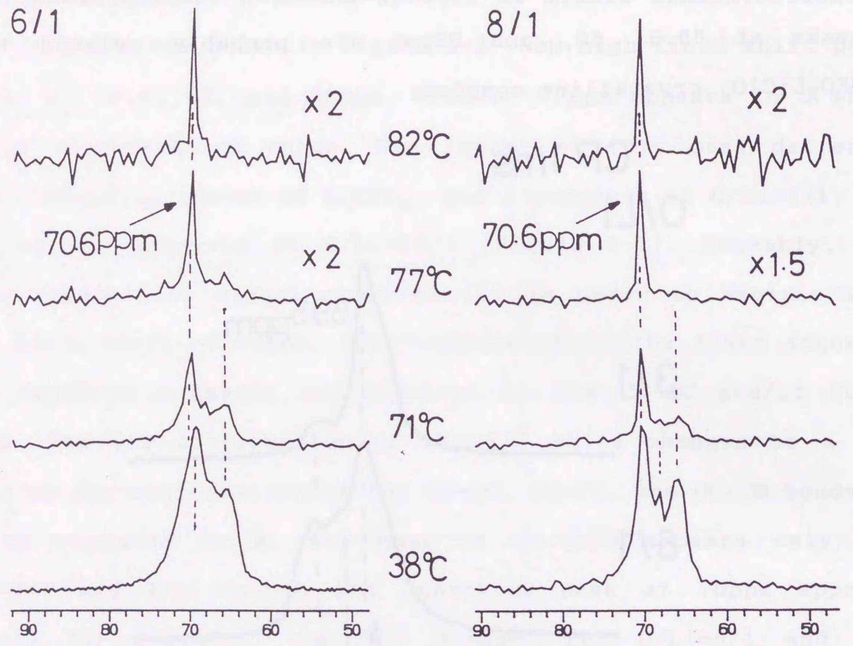

Figure 5-3. The temperature dependence of ^{13}C CP/MAS spectra of O/Li=6/1 and 8/1 blends. The ratio of O/Li is shown on the left side of the spectra. The contact time of CP signal enhancement is 1ms.

In order to assign the peaks and to determine the relative ratio of each peak, we simulate the observed spectra by a sum of three or four Lorentzian curves. Figure 5-4 shows the observed and simulated ^{13}C CP/MAS spectra of O/Li=12/1-3/1 blends. At concentrations of O/Li≦12/1, all the peaks show a similar dependence on the CP contact time. Although we simulate the observed spectra of CP contact time of 100μs, we can not find the difference more than 5% of relative intensity between the CP contact times of 100μs and 1ms. Therefore, the relative ratio of each peak is probably correct within an error of 5%.

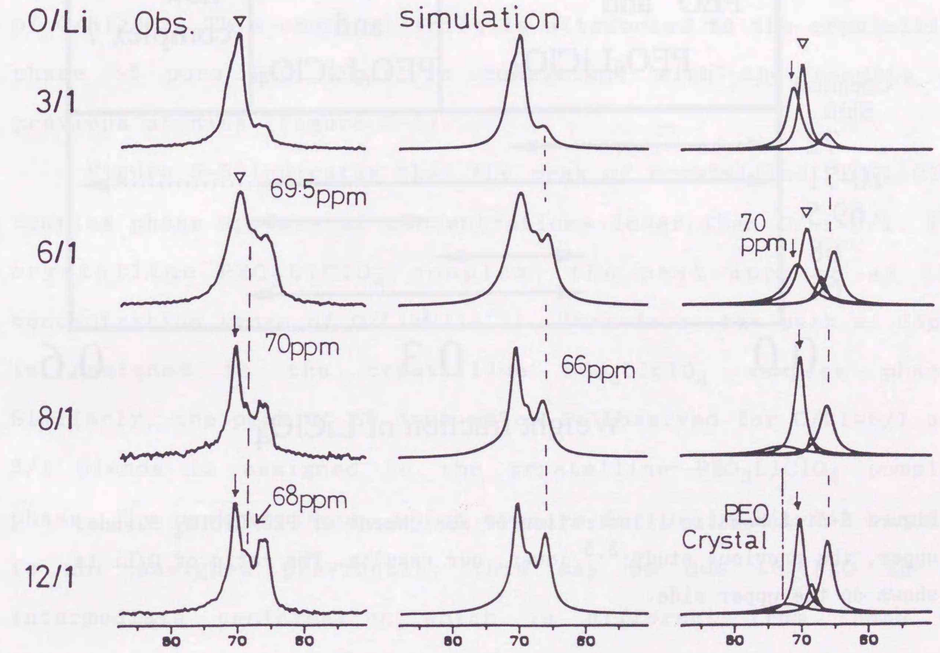

Figure 5-4. Observed and simulated ^{13}C CP/MAS spectra of O/Li=12/1, 8/1, 6/1, and 3/1 blends. The ratio of O/Li is shown on the left side of the spectra. The simulated spectra are shown on the center and right-hand sides. The observed spectra can be simulated by Lorentzian curves (right-hand side). The contact time of CP signal enhancement is 1ms.

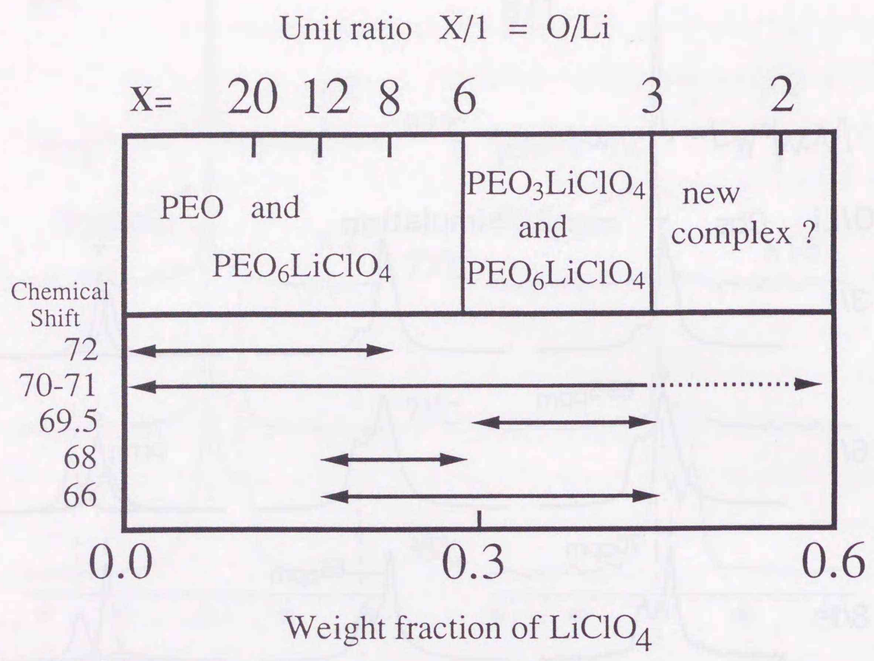

Figure 5-5. Schematic illustration of assignment of $PEO/LiClO_4$ blends. upper, the previous study;[3,5] lower, our results. The ratio of O/Li is shown on the upper side.

Observed peaks are at 72, 70-71, 69.5, 68, and 66ppm. We assign the peaks by comparison with previous studies. Figure 5-5 schematically summarizes previous DSC[3] and X-ray diffraction[5] studies of $PEO/LiClO_4$ blends. Our observation is also shown by arrows.

$PEO/LiClO_4$ blends may consist of amorphous pure PEO phase, amorphous PEO/Li phase in which Li^+-ions are dissolved (or dissociated) in PEO matrix, crystalline pure PEO phase, and crystalline PEO_XLiClO_4 complex phase. Figure 5-3 indicate that

the amorphous PEO/Li phase appears at 70-71ppm and that the amorphous pure PEO phase (very sharp peak) that appears at 71ppm does not appear. This is because the amorphous pure PEO phase becomes less mobile upon the addition of $LiClO_4$.

The peak at 72ppm is observed at lower $LiClO_4$ concentrations of $O/Li \geq 8/1$. This chemical shift is attributed to the crystalline phase of pure PEO. This is consistent with the results of previous studies (Figure 5-5).

Figure 5-5 indicates that the peak of crystalline PEO_6LiClO_4 complex phase appears at concentrations lower than O/Li=3/1. For crystalline PEO_3LiClO_4 complex, the peak appears at the concentration range of O/Li=6/1-3/1. Therefore, the peak at 66ppm is assigned to the crystalline PEO_6LiClO_4 complex phase. Similarly, the peak at 69.5ppm which is observed for O/Li=6/1 and 3/1 blends is assigned to the crystalline PEO_3LiClO_4 complex phase. The peak at 68ppm, which appears for O/Li=12/1-6/1 blends, is not assigned previously; this may be due to PEO in an intermediate conformation which is different from those of PEO_6LiClO_4 and PEO_3LiClO_4 complexes.

The relative ratio of each peak is listed in Table 5-1 together with the values of T_{1C}. The amount of the peak of 66ppm (PEO_6LiClO_4) decreases with increasing $LiClO_4$ and disappears at concentrations of $O/Li < 3/1$. This is consistent with the results of X-ray study.[5]

The study of chemical shift indicates that for the crystalline PEO_6LiClO_4 complex PEO takes a gauche conformation at the CC-OC and/or CO-CC bonds: tgg (gtg) or ggg structure. In the crystalline PEO_6LiClO_4 complex PEO is probably in a similar

conformation to that in PEO/NaSCN=1/1: gtg̅g̅tg conformation.[7] The conformation of PEO in the crystalline PEO_3LiClO_4 complex is close to that in the crystalline pure PEO phase, because the chemical shift of crystalline PEO_3LiClO_4 complex is similar to that of pure PEO. The conformation of PEO in the PEO_3LiClO_4 complex is similar to that of PEO/NaSCN=3/1 complex: ttgttgttg̅ conformation.[7] This suggests that PEO in the PEO_6LiClO_4 complex is in a more extended conformation than in the PEO_3LiClO_4 complex.

T_{1C} of each peak is obtained by the decay of magnetization of respective peak which is simulated by Lorentzian curves like Figure 5-4. The T_{1C} values are summarized in Table 5-1. The T_{1C} curve of pure PEO, which is obtained from casting anhydrous acetonitrile solution, is triple-exponential. The values are 0.20±0.06s for the amorphous phase (11%), 11±2s for the crystalline phase (53%), and 0.8±0.4s for the interphase (36%). The values of amorphous and crystalline phases are in agreement with previous data.[14,16] The existence of interphase is presumably due to a difference in preparation of sample.

The decay curve of the amorphous phase of $PEO/LiClO_4$ blends is mostly double-exponential. The short T_{1C} value of amorphous phase of O/Li=20/1-1/1 blends is ~0.2s and comparable to that of pure PEO. The long T_{1C} value is assigned to a part of dissolved Li^+-ions.

Table 5-1 Observed T_{1C} values of each peak for $PEO/LiClO_4$ blends and PEO; The fraction compared to whole system is also listed

O/Li	72	71-70	69.5	68	66
PEO	0.8±0.4 (36%)	0.20±0.06 (11%)			
	11±2 (53%)				
20/1		0.16±0.03*			
12/1	1.8±0.9 (15%)	0.1±0.2 (8%)		4.3±0.8 (12%)	0.3±0.2 (10%)
		11±4 (30%)			9±3 (26%)
8/1	0.35±0.07 (18%)	0.09±0.04 (13%)		3.6±0.8 (5%)	0.7±0.5 (6%)
		10±2 (32%)			14±10 (26%)
6/1		0.03±0.02 (8%)	0.9±0.8 (11%)	5.5±0.6 (9%)	2.2±0.8 (12%)
		8±1 (21%)	24±10 (27%)		13±4 (12%)
3/1		0.12±0.06 (10%)	2±1 (8%)		9±3 (11%)
		18±2 (37%)	28±4 (34%)		
1/1		0.3±0.1 (42%)			
		8±2 (58%)			

*; The value of O/Li=20/1 blend is observed only for amorphous region because of poor S/N

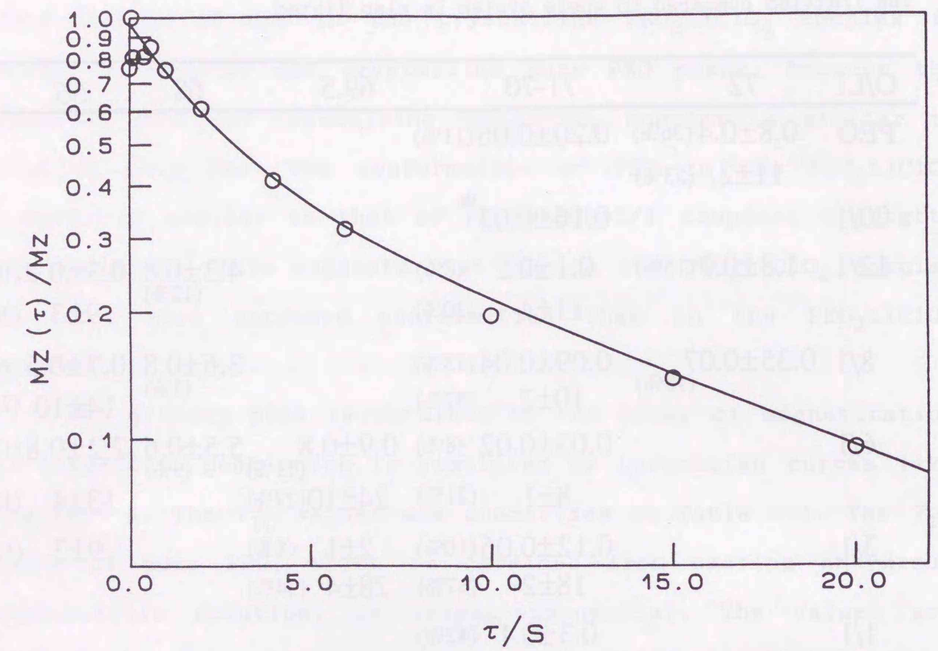

Figure 5-6. The observed T_{1C} decay curve of the peak at 66ppm (○) of O/Li=6/1 blend. The solid line is the "best fitted" one to conventional double-exponential curve. The T_{1C} values and the fraction of short T_{1C} are listed in Table 5-1.

Figure 5-6 shows the T_{1C} decay curve of the peak at 66ppm for O/Li=6/1 blend; this peak is assigned to the crystalline PEO_6LiClO_4 complex phase from ^{13}C CP/MAS spectra. The decay curve gives T_{1C} values of 2.2±0.8s (50%) and 13±4s (50%). For O/Li=12/1-6/1 blends, the T_{1C} decay is also double-exponential. On the other hand, the T_{1C} decay of O/Li=3/1 blend is single-exponential. The T_{1C} value is in agreement with the long value of those of O/Li=12/1-6/1 blends (Table 5-1).

Since ^7Li has a spin 3/2, the quadrupole interaction may be taken account of the T_{1C} curve. The T_{1C} is mostly governed by the dipole interaction of directly bonded protons. The quadrupole relaxation effect on ^{13}C nucleus is transmitted through the flip-flop process between ^7Li and ^{13}C spins and/or ^7Li and ^1H spins. When the flip-flop occurs very frequently, namely, the rate is an order of μs^{-1}, the quadrupole interaction can affect the ^{13}C relaxation process. This means that ^7Li NMR spectrum is not observable because of $T_2 \sim \mu s$. However, the T_2 rate obtained from the ^7Li spectra is an order of ms (Figure 5-8). Therefore, the quadrupole effect of ^7Li nucleus to T_{1C} is negligible.

The double-exponential decay indicates that the crystalline phase consists of two parts which have the same conformation. As compared with the results of pure PEO, the short and long T_{1C}'s are ascribed to mobile and rigid parts, respectively, of a PEO_6LiClO_4 chain. The rigid part probably directly interacts with Li^+-ions, while the mobile part does not. The value of short T_{1C} becomes longer with increasing amount of $LiClO_4$. This implies an increase in rigid phase: crystalline PEO_3LiClO_4 complex phase. In the crystalline PEO_6LiClO_4 complex phase of O/Li=3/1 blend, all oxygen atoms of PEO interact with Li^+-ion.

Similarly, the T_{1C} behavior of the peak at 69.5ppm is double-exponential; the short value is ~1s and the long value is ~20s. The peak at 69.5ppm is assigned to crystalline PEO_3LiClO_4 complex phase and appears only for O/Li=6/1 and 3/1 blends. This indicates that the PEO_3LiCLO_4 chain in the crystalline complex has two parts, interacting and not interacting with Li^+-ions.

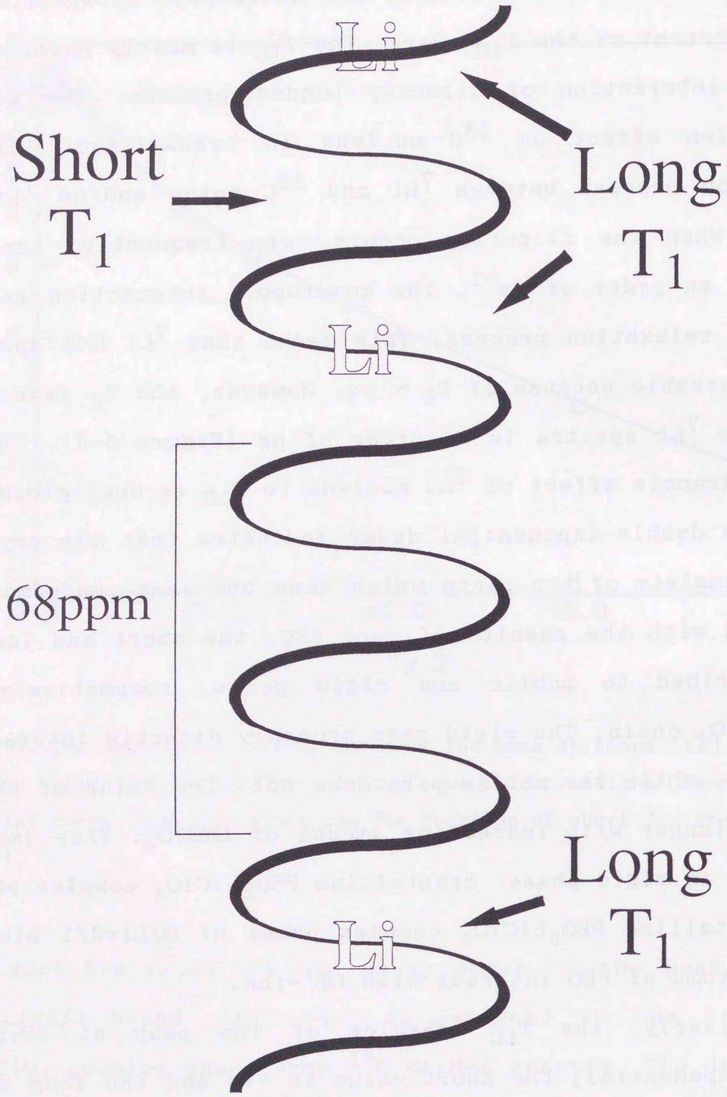

Figure 5-7. Schematic illustration of the PEO chain in PEO/$LiClO_4$ blends. The size of Li^+-ion and PEO chain is arbitrary.

For the peak at 68ppm of O/Li=12/1-6/1 blends, the T_{1C} decay curve is single-exponential. The value of 4s is in a range between short and long values obtained from the double-exponential curves at 66 and 69.5ppm. The chemical shift is also inbetween. The peak at 68ppm disappears at a high concentration of O/Li=3/1. On the basis of these results, we conclude that this peak is attributed to an intermediate phase. At low concentrations of $LiClO_4$, the amount of Li^+-ions are not enough to form the crystalline complex. The part which does not include Li^+-ions may remain. This part is probably ascribed to the peak at 68ppm.

Figure 5-7 shows schematically a model of PEO chain in the PEO_XLiClO_4 complex. From ^{13}C CP/MAS spectra and relaxation studies, we conclude that the PEO_XLiClO_4 complex (X=6 and 3) has mobile and rigid PEO parts with the same conformation. The rigid PEO part interacts with Li^+-ions and the mobile PEO part does not. Those parts have long and short T_{1C}'s, respectively. The peak at 68ppm is attributed to an intermediate phase which exists at lower concentrations of $LiClO_4$. With increasing amount of $LiClO_4$, Li+-ions migrate to the part and form PEO_XLiClO_4 complex. The peak at 68ppm disappears at higher concentrations of $LiClO_4$.

B ^{7}Li NMR Spectra and Relaxation

Figure 5-8 shows ^{7}Li NMR spectra with proton decoupling. The spectra of O/Li=3/1 and 1/1 blends are very broad and the half-intensity width is 1-2KHz. The spectra of O/Li=20/1-6/1 blends have two components, sharp and broad, with half-intensity widths of ~100 and ~500Hz, respectively. The signal of O/Li=8/1 blend apparently shows only the broad component. The sharp component is obscured by the broad component. The broad linewidth indicates the rigid component. Similar spectra were observed by Chung, *et al.*[17] The chemical shifts of sharp and broad components are -1.1 and -2.2ppm from the ^{7}Li resonance of LiCl aqueous solution, respectively. The chemical shift of $LiClO_4$ in the solid state is -3.7ppm and the half-intensity width is ~3KHz. When an atom becomes a cation, the chemical shift is expected to move to lower fields. Therefore, the broad component is ascribed to the complexes and the sharp component to the amorphous PEO/Li phase.

The ^{7}Li spectra without proton decoupling of O/Li=3/1 and 1/1 blends become broader than 3KHz. The broad component of O/Li=8/1 blend also becomes broader; the half-intensity width is ~4KHz (figures are not shown). This indicates that the broad component of O/Li=8/1 blend and O/Li=3/1 and 1/1 blends are less mobile than 55KHz; the PEO-Li^{+}-ion interaction is stronger than for other blends. This suggests that the PEO-Li^{+}-ion interacting part of the crystalline PEO_6LiClO_4 and/or PEO_3LiClO_4 complexes can be in exact stoichiometry. Details are described in section C.

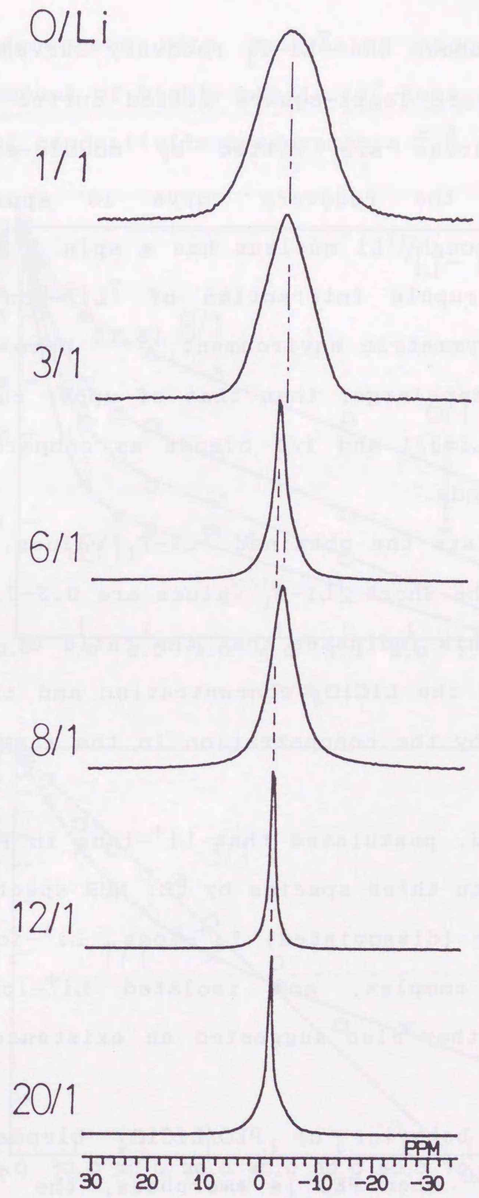

Figure 5-8. Observed ^{7}Li spectra with proton decoupling of PEO/$LiClO_4$ blends. The chemical shift is from LiCl aqueous solution. The ratio of O/Li is shown on the left side of the spectra. The spectra is observed under no MAS.

Figure 5-9 shows the ^{7}Li-T_1 recovery curves of the blends. The solid lines are least-square fitted curves to data points. The recovery curves are fitted by double-exponential. For O/Li=3/1 blend, the recovery curve is apparently single-exponential. Although ^{7}Li nucleus has a spin 3/2 and quadrupole moment, the quadrupole interaction of ^{7}Li$^+$-ion is very small because of high symmetric environment.[18,19] Note that τ of lower curves is one order larger than that of upper curves. ^{7}Li-T_1 is very long for O/Li=3/1 and 1/1 blends as compared with that of O/Li=20/1-6/1 blends.

Table 5-2 lists the obtained ^{7}Li-T_1 values. For O/Li=20/1-6/1 blends, all the short ^{7}Li-T_1 values are 0.3-0.4s and the long values are ~5s. This indicates that the ratio of short (or long) ^{7}Li-T_1 depends on the $LiClO_4$ concentration and the ^{7}Li-T_1 rates are not affected by the concentration in the range of O/Li=20/1-6/1.

O'Gara, *et al.* postulated that Li$^+$-ions in PEO/$LiClO_4$ blend can be divided into three species by ^{6}Li NMR spectroscopy.[15] They are highly mobile (dissociated) Li$^+$-ions, Li$^+$-ions existing in the crystalline complex, and isolated Li$^+$-ions. For their O/Li=2/1 sample, they also suggested an existence of aggregates of Li$^+$-ions.

The ^{7}Li-T_1 behavior of PEO/$LiClO_4$ blends reflects the mobility of PEO.[20] When PEO is amorphous, the ^{7}Li-T_1 value is short.[20] The short ^{7}Li-T_1 is, hence, attributed to highly mobile Li$^+$-ions in the amorphous PEO/Li phase. The long ^{7}Li-T_1 is attributed to rigid Li$^+$-ions in the crystalline complexes. The percentage of short component is more than 80% for O/Li=20/1 and

12/1. This decreases with increasing amount of $LiClO_4$. The decrease in amount of highly mobile Li$^+$-ions is in agreement with the results of conductivity measurements.[2-4]

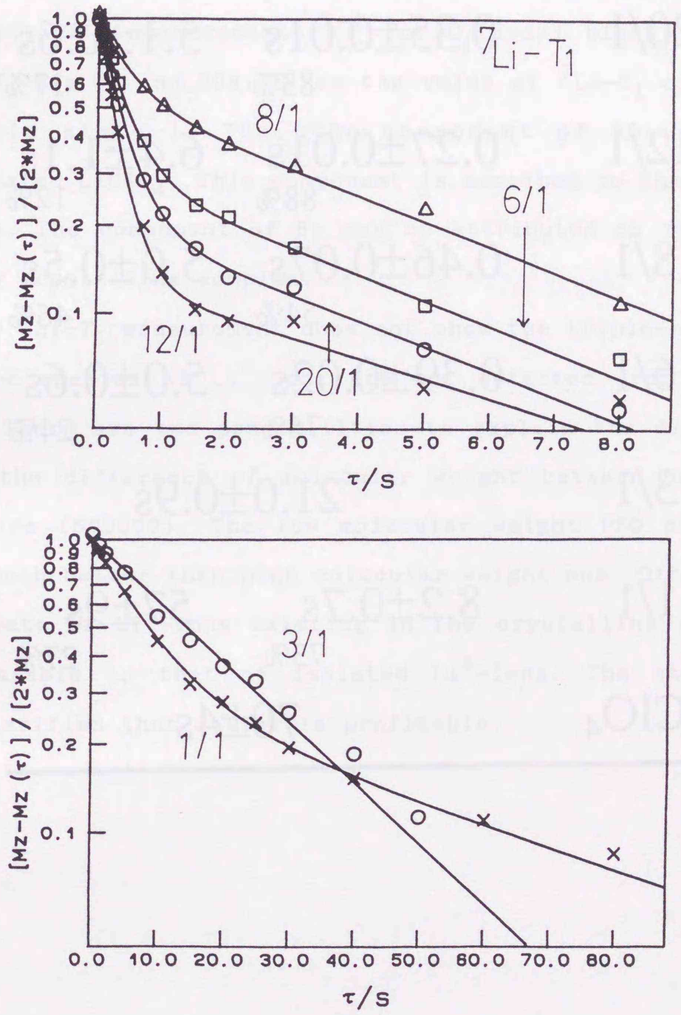

Figure 5-9. Observed ^{7}Li-T_1 recovery curves of PEO/$LiClO_4$ blends. upper, O/Li=20-1,12/1, 8/1, and 6/1; lower, O/Li=3/1 and 1/1. The solid lines are the "best fitted" ones to conventional double- or single-exponential curve.

Table 5-2 Observed ^{7}Li-T_1 values of PEO/$LiClO_4$ blends

Sample	Short	Long
20/1	0.35±0.01s 83%	5.1±0.6s 17%
12/1	0.27±0.01s 88%	6.4±1.1s 12%
8/1	0.46±0.07s 54%	5.0±0.5s 46%
6/1	0.39±0.02s 76%	5.0±0.6s 24%
3/1	21.0±0.9s	
1/1	8.2±0.7s 73%	57±9s 27%
$LiClO_4$	70±4s	

Since Li^+-ions in the amorphous PEO/Li phase of O/Li=3/1 blend is less mobile and have a similar ^{7}Li-T_1 value to the crystalline phase, it can not be detected. This small mobility is also observed by O'Gara, *et al.*[15] and consistent with the results of conductivity measurements.[2-4] For O/Li=1/1 blend, the values of ^{7}Li-T_1 are 8s and 60s. Since the value of ^{7}Li-T_1 of $LiClO_4$ in the solid state is 70s, the component of 60s is due to precipitated $LiClO_4$. This component is ascribed to the aggregated Li^+-ions. The component of 8s may be attributed to the Li^+-ions in a new crystalline complex.

Our ^{7}Li-T_1 measurement does not show the triple-exponential; the three species of Li^+-ions are not detected from the ^{7}Li-T_1 curves. There are two possibilities to explain the disagreement. One is the difference of molecular weight between ours (20000) and theirs (600000). The low molecular weight PEO may dissolve $LiClO_4$ much better than high molecular weight one. Otherwise, the ^{7}Li-T_1 rate of Li^+-ions existing in the crystalline complex may be comparable to that of isolated Li^+-ions. The stoichiometry study clarifies that latter is profitable.

C Stoichiometry of Complex

From the combined studies of ^{13}C and ^{7}Li NMR, we estimate the stoichiometry of each phase and examine the structure of $PEO/LiClO_4$ blends.

For O/Li=8/1 blend, 46% of Li^+-ions are less mobile (Table 5-2). Twenty-six percent of PEO form the PEO_6LiClO_4 complex (Table 5-1). Thus, 35% of Li^+-ions are needed. This indicates that the remaining 11% of Li^+-ions are ascribed to isolated ions, suggesting that the ^{7}Li-T_1 rate of Li^+-ions in the crystalline complex is comparable to that of isolated ions. Fifty-five percent of PEO belong to crystalline phase (Table 5-1) and 35% of Li^+-ions are interacting. This corresponds to the stoichiometry of O/Li=12/1. This is consistent with the stoichiometry of O/Li=10/1 at eutectic point suggested by X-ray study.[5] Fifty-four percent of Li^+-ions are dissolved in the amorphous PEO/Li phase. This corresponds to a concentration of O/Li~5/1 at which the conductivity is low.

On the other hand, for O/Li=12/1 blend, 12% of Li^+-ions are less mobile. Twelve percent of Li^+-ions can only form the PEO_6LiClO_4 complex using 6% of PEO. The results of ^{13}C measurements show that 26% of PEO is involved in the complex. Therefore, the amount of PEO is about three times larger than that of Li^+-ions. This is because O/Li=12/1 blend contains a small amount of $LiClO_4$ as compared with O/Li=8/1 blend.

For O/Li=6/1 blend, there are two complexes, PEO_6LiClO_4 and PEO_3LiClO_4. Twenty-four percent of Li^+-ions are less mobile. Twelve percent of PEO form the complex with the exact stoichiometry of O/Li=6/1, because Li^+-ions are already enough to

form the complex with the stoichiometry of O/Li=6/1.

For O/Li=3/1 blend, 6% of Li^+-ions are needed to form PEO_6LiClO_4 complex using 11% of PEO with the exact stoichiometry of O/Li=6/1.

These view-points for PEO_6LiClO_4 complex show that at low concentrations of O/Li>8/1, the amount of PEO is three times larger than that of $LiClO_4$; at concentrations higher than O/Li=8/1, the complex is in the exact stoichiometry of O/Li=6/1.

Similar relation holds on PEO_3LiClO_4 complex. For O/Li=3/1 blend, 34% of Li^+-ions form PEO_3LiClO_4 complex of 34% of PEO with the exact stoichiometry of O/Li=3/1. Forty percent of Li^+-ions are used for both PEO_6LiClO_4 and PEO_3LiClO_4 complexes. Remaining 60% of Li^+-ions are attributed to isolated ions, suggesting again that the ^{7}Li-T_1 rate of Li^+-ions existing in the crystalline complex is comparable to that of isolated ions.

O/Li=6/1 blend contains a small amount of $LiClO_4$ as compared with O/Li=3/1 blend. Remaining 12% of Li^+-ions form PEO_3LiClO_4 complex. Twelve percent of Li^+-ions can only form the complex with 6% of PEO. This suggests again that the amount of PEO is about three times more than that of Li^+-ions. The results of ^{13}C measurements show that 27% of PEO is involved in the complex.

In order to explain why the amount of PEO is three times greater than that of $LiClO_4$, a model for complex phase is proposed. Figure 5-10 shows a schematic illustration of the PEO_XLiClO_4 complex phase model; three columns of PEO chain surround $LiClO_4$ molecules.

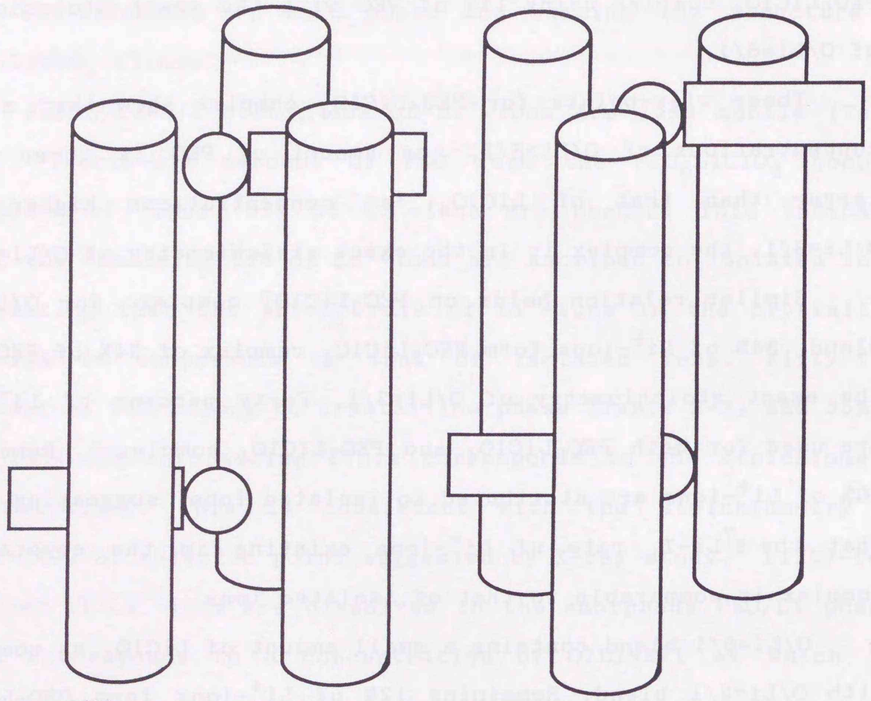

Figure 5-10. Three PEO columns model for the PEO_XLiClO_4 complex. The cylinder represents the PEO chain in Figure 5-7. The circle represents Li^+ and combined rectangle is ClO_4^-.

For PEO_6LiClO_4 complex, one column in Figure 5-10 has 12 units of PEO chain. Two units (2 oxygen atoms) of a column interact with a Li^+-ion. Other 4 units keep stiff comparable to the interactive part. When the $LiClO_4$ concentration increases, this 4-unit part is possessed by Li^+-ions. Similar views are presented for PEO_3LiClO_4 complex; for PEO_3LiClO_4 complex, one column in Figure 5-10 has 6 units of PEO chain.

Parker, *et al.* postulated a double helical model for PEO/KSCN and PEO/NaSCN.[21] Our observation, however, does not support a double helical model. If the PEO_XLiClO_4 complex consists of a double helix, we will observe that the amount of PEO is two times larger than that of Li^+-ions.

For O/Li=1/1 blend, 73% of Li^+-ions exist in the crystalline complex and the isolated state. Fifty-eight percent of PEO are less mobile. Robitaille and Fauteux predicted a new complex at concentrations higher than O/Li=3/1.[5] However, O'Gara, *et al.* suggested that O/Li=2/1 blend has the stoichiometry of O/Li=4.2/1 and other 53% is not dissolved.[15] If the present O/Li=1/1 blend includes the PEO_3LiClO_4 complex with the stoichiometry of O/Li=3/1, 53% of Li^+-ions are isolated ions. This is consistent with O'Gara, *et al.*[15] Therefore, O/Li=1/1 blend may consist of crystalline PEO_3LiClO_4 complex, but not new crystalline complex.

D Domain Size detected by T_{1H} and $T_{1\rho H}$

Table 5-3 and 5-4 list the T_{1H} and $T_{1\rho H}$ values, respectively, of each peak of PEO/$LiClO_4$ blends. In analogy with polymer/polymer blends, the heterogeneity can be investigated by ^1H spin-lattice relaxation behavior.

The observed T_{1H} curves are single-exponential except for 68 and 66ppm peaks of O/Li=6/1 blend. The T_{1H} value of the crystalline phase at 72ppm of PEO is close to that of the amorphous phase at 71ppm. The $T_{1\rho H}$ value of the crystalline phase is clearly one order of magnitude different from that of the amorphous phase. This indicates that PEO is homogeneous on several hundreds Å scale,[22] although the complete agreement of T_{1H} value is not achieved. Similarly, O/Li=12/1, 8/1, 3/1, and 1/1 blends are homogeneous on several hundreds Å scale. In addition, the blends have domains on several tens Å size.

Table 5-3 Observed T_{1H} values of each peak for PEO/$LiClO_4$ blends and PEO

O/Li	72	71-70	69.5	68	66
PEO	3.2±0.1	2.3±0.3			
20/1		0.9±0.2*			
12/1	2.9±0.5	1.8±0.1		2.2±0.4	1.8±0.1
8/1	0.8±0.1	0.72±0.04		1.4±0.2	1.0±0.1
6/1		3.0±0.2	3.6±0.4	2.0±0.3 (76%)	1.8±0.9 (70%)
				17±6 (24%)	11±8 (30%)
3/1		6.0±0.3	4.5±0.2		3.6±0.3
1/1		4.4±0.1			

*; The value of O/Li=20/1 blend is observed only for amorphous region because of poor S/N

However, O/Li=6/1 blend has domains on several hundred Å size. The double-exponential behavior of T_{1H} observed for 68 and 66ppm peaks probably suggests two domains with different size.

The results of $T_{1\rho H}$ measurements also suggest that PEO/$LiClO_4$ blends are heterogeneous on several tens Å scale.

Table 5-4 Observed $T_{1\rho H}$ values of each peak for PEO/$LiClO_4$ blends and PEO

O/Li	72	71-70	69.5	68	66
PEO	0.14±0.01	1.8±0.2			
20/1		0.21±0.01*			
12/1	0.27±0.03	33±7		14±3	0.8±0.4 (26%)
					62±22 (74%)
8/1	1.3±0.3 (54%)	24±2		36±14	31±4
	76±53 (46%)				
6/1		1.7±1.1 (30%)	4.7±3.1 (27%)	64±21**	1.4±0.8 (24%)
		84±16 (70%)	97±22 (73%)		75±11 (76%)
3/1		2.7±1.2 (37%)	90±10		21±4
		122±22 (63%)			
1/1		1.1±0.2 (58%)			
		67±12 (42%)			

*; The value of O/Li=20/1 blend is observed only for amorphous region because of poor S/N

**; The value at 68ppm of O/Li=6/1 blend is obtained by single-exponential fitting owing to scattering data. This scattering is due to its small intensity

References

1. (a)Fenton,D.E.;Parker,J.M.;Wright,P.V. *Polymer*, 1973, *14*, 589.
   (b)Weight,P.V. *J. Polym. Sci., Polym. Phys. Ed.*, 1976, *14*, 955.
2. Ferloni,P.;Chiodelli,G.;Magistris,A.;Sanesi,M. *Solid State Ionics*, 1986, *18&19*, 265.
3. Gorecki,W.;Andreani,R.;Berthier,C.;Armand,M.;Mali,M.;Roos,J.; Brinkmann,D. *Solid State Ionics*, 1986, *18&19*, 295.
4. (a)Watanabe,M.;Nagano,S.;Sanui,K.;Ogata,N. *Solid State Ionics*, 1986, *18&19*, 338.
   (b)Watanabe,M.;Nagano,S.;Sanui,K.;Ogata,N. *Polym. J.*, 1986, *18*, 809.
5. Robitaille,C.D.;Fauteux,D. *J. Electrochem. Soc.*, 1986, *133*, 315.
6. Takahashi,Y.;Tadokoro,H. *Macromolecules*, 1973, *6*, 672.
7. (a)Chatani,Y.;Okamura,S. *Polymer*, 1987, *28*, 1815.
   (b)Chatani,Y.;Fujii,Y.;Takayanagi,T.;Honma,A. *Polymer*, 1990, *31*, 2238.
8. (a)Pines,A.;Gibby,M.G.;Waugh,J.S. *J. Chem. Phys.*, 1973, *59*, 569.
   (b)Schaefer,J.;Stejskal,E.O.;Buchdahl,R. *Macromolecules*, 1975, *8*, 291.
9. Zumbulyadis,N. *J. Magn. Reson.*, 1983, *53*, 486.
10. Alla,M.;Lipmaa,E. *Chem. Phys. Lett.*, 1976, *37*, 260.
11. Torchia,D.A. *J. Magn. Reson.*, 1978, *30*, 613.
12. Takegoshi,K.;Hikichi,K. *J. Chem. Phys.*, 1991, *94*, 3200.
13. van Geet,A.L. *Anal. Chem.*, 1970, *42*, 679.

14. Dechter,J.J. *J. Polym. Sci., Polym. Lett. Ed.*, 1985, *23*, 261.
15. O'Gara,J.F.;Nazri,G.;MacArthur,D.M. *Solid State Ionics*, 1991, *47*, 87.
16. Zhang,X.;Takegoshi,K.;Hikichi,K. *Macromolecules*, 1992, *25*, 2336.
17. Chung,S.H.;Jeffrey,K.R.;Stevens,J.R. *J. Chem. Phys.*, 1991, *94*, 1803.
18. Wintersgill,M.C.;Fontanelle,J.J.;Calame,J.P.;Smith,M.K.; Jones,T.B.;Greenbaum,S.G.;Adamic,K.J.;Shetty,A.N.; Andeen,C.G. *Solid State Ionics*, 1986, *18&19*, 326.
19. Kim,D.-W.;Ryoo,B.-K.;Park,J.-K.;Maeng,K.-S.;Hwang,T.-S. *Polym. J.*, 1992, *24*, 509.
20. Donoso,J.P.;Bonagamba,T.J.;Panepucci,H.C.;Oliveira,L.N.; Armand,M. *J. Chem. Phys.*, 1993, *98*, 10026.
21. Parker,J.M.;Wright,P.V.;Lee,C.C. *Polymer*, 1981, *22*, 1305.
22. (a)McBrierty,V.J.;Douglass,D.C.;Kwei,T.K. *Macromolecules*, 1978, *11*. 1265.
    (b)VanderHart,D.L. *Makromol. Chem. Macromol. Symp.*, 1990, *34*, 125.
    (c)Asano,A.;Takegoshi,K.;Hikichi,K. *Polym. J.*, 1992, *24*, 555.

Chapter 6 General Conclusion

This dissertation presents an NMR approach to *polymer/polymer* and *polymer/lithium-salt blends*. Bisphenol A polycarbonate/poly(methyl methacrylate) (PC/PMMA) and polystyrene/poly(vinyl methyl ether) (PS/PVME) blends are analyzed. The analyzed polymer/lithium-salt blend is poly(ethylene oxide) (PEO)/$LiClO_4$ with O/Li=20/1, 12/1, 8/1, 6/1, 3/1, and 1/1. The results obtained here are as follows:

PC/PMMA blend

1. The inter-polymer ^1H NOE signals of PC/PMMA=5:5 blend in THF solution are clearly observed. The ^{13}C-T_1 temperature curves of the phenyl groups of PC and the methoxy group of PMMA of the blend shift as a whole to higher temperatures than those of pure PC and PMMA. These results suggest a close proximity between PC and PMMA in solution, and indicate an interaction between the phenyl groups of PC and the methoxy group of PMMA: n-π electron interaction.

2. The miscibility of PC/PMMA=3:7, 5:5, and 7:3 blends is investigated by T_{1H} and $T_{1\rho H}$ measurements in the solid state. The T_{1H} results reveal that the blends are homogeneous on a scale of 200-300 Å. However, we find that the blends are heterogeneous on a scale of 20-30 Å from the $T_{1\rho H}$ observation. The phase-separation process and the phase diagram are determined from the analysis of T_{1H} relaxation behavior on the assumption that no ^1H spin-diffusion between phase-separated domains occurs.

PS/PVME blend

1. We find that the dipole-dipole interaction is averaged by molecular motion and hence the ^1H spin-diffusion is hindered at temperatures much higher than T_g in spite of the homogeneous blend. At temperatures lower than T_g, the $T_{1\rho H}$ value of PS is in agreement with that of PVME. PS/PVME=5:5 blend is concluded to be homogeneous on a scale of 20-30 Å.

2. The phase-separation process at 140℃ is investigated by the $T_{1\rho H}$ decay behavior. The phase-separation is initiated by the spinodal decomposition; the rate is $0.5min^{-1}$.

PEO/$LiClO_4$ blend

1. The ^{13}C CP/MAS spectra reveal that the PEO_6LiClO_4 complex has a gauche conformation at the CC-OC and/or CO-CC bonds. The crystalline complexes, PEO_6LiClO_4 and PEO_3LiClO_4, consist of rigid and mobile PEO parts. The rigid part interacts with Li^+-ions, while the mobile part does not. From the combined studies of ^{13}C and ^7Li NMR, we find that the PEO_6LiClO_4 and PEO_3LiClO_4 complexes assume a structure in which $LiClO_4$ molecule is surrounded by three PEO chains.

2. The T_{1H} and $T_{1\rho H}$ measurements reveal that the O/Li=6/1 system is heterogeneous on a scale of several hundreds Å, but other blends are roughly homogeneous on the same scale. The PEO_XLiClO_4 crystalline complex has domains on a scale of several tens Å.

Acknowledgement

I am very grateful to Professor Kunio Hikichi of Department of Polymer Science, Faculty of Science, Hokkaido University for his cordial discussion, valuable advice, and kind encouragement.

I am also grateful to Dr. Kiyonori Takegoshi, present associate professor of Kyoto University, for his valuable and helpful discussion and kind encouragement.

I should like to thank Dr. Sakae Tsuda of NMR laboratory, present post-doctoral fellow of Alberta University in Canada, for his help in NMR experiments and kind encouragement. I also like to thank Professor Isao Tanaka for helpful guidance, and all members of Department of Polymer Science, Faculty of Science, Hokkaido University.

Finally, I wish to thank my parents for their kind and continuous encouragement. In particular, I am very grateful to my deceased father let me go to Doctoral Course.

List of Publications

I. Published in Journals

1. Inter-Polymer Interaction of Polymer Blend in Solution as Studied by NMR: Polycarbonate/Poly(methyl methacrylate)
Atsushi Asano, K. Takegoshi, and Kunio Hikichi,
Polymer Journal, 1992, 24, 473-477.

2. Solid-State NMR Study of Miscibility and Phase-Separation of Polymer Blend: Polycarbonate/Poly(methyl methacrylate)
Atsushi Asano, K. Takegoshi, and Kunio Hikichi,
Polymer Journal, 1992, 24, 555-562.

3. Carbon-13 NMR Spectral Assignments of Regioirregular Polypropylene Determined from Two-Dimensional INADEQUATE Spectra and Chemical Shift Calculations
Tetsuo Asakura, Nobuhiko Nakayama, Makoto Demura, and Atsushi Asano,
Macromolecules, 1992, 25, 4876-4881.

4. Solid-State ^{13}C NMR Analysis of Miscibility of Polymer Blends
Atsushi Asano, K. Takegoshi, and Kunio Hikichi,
Hyoumen, 1993, 31, 835-845. (in Japanese)

5. ^{13}C CP/MAS NMR Study on Miscibility and Phase-Separation of Polystyrene/Poly(vinyl methyl ether) Blend
Atsushi Asano, K. Takegoshi, and Kunio Hikichi,
submitted to Polymer.

6. ^{13}C CP/MAS and ^{7}Li NMR Study of PEO/$LiClO_4$ Blend
Atsushi Asano, K. Takegoshi, and Kunio Hikichi,
in preparation.

7. Analysis of Polymer Alloys
Atsushi Asano and Kunio Hikichi,
section 2 of chapter 2 in "Spectroscopy of Polymer Materials"
(temporary title)
Gijyutsu Jyouhou Kyoukai in Japan (in Japanese)
in preparation.

8. C-13 NMR Assignment of Regioirregular Polypropylene
Tetsuo Asakura, Atsushi Asano, and Nobuhiko Nakayama,
Reports on Progress in Polymer Physics in Japan,
1989, 32, 445-448.

9. NMR Study on the Polymer-Polymer Interaction of Polymer Mixture: PC/PMMA Blend
Atsushi Asano, K. Takegoshi, and Kunio Hikichi,
Reports on Progress in Polymer Physics in Japan,
1990, 33, 485-488.

10. Solid-State ^{13}C NMR Study of Polymer Blends.
1. Miscibility of PC/PMMA Blends
Atsushi Asano, K. Takegoshi, and Kunio Hikichi,
Reports on Progress in Polymer Physics in Japan,
1991, 34, 387-390.

11. Solid-State ^{13}C NMR Study of Polymer Blends.
2. Phase-Separation Process of PC/PMMA Blends
Atsushi Asano, K. Takegoshi, and Kunio Hikichi,
Reports on Progress in Polymer Physics in Japan,
1991, 34, 391-394.

12. Solid-State ^{13}C NMR Study of Polymer Blends.
3. Miscibility of PS/PVME Blends
Atsushi Asano, K. Takegoshi, and Kunio Hikichi,
Reports on Progress in Polymer Physics in Japan,
1992, 35, 489-492.

13. Solid-State ^{13}C NMR Study of Polymer Blends.
4. Phase-Separation Process of PS/PVME Blends
Atsushi Asano, K. Takegoshi, and Kunio Hikichi,
Reports on Progress in Polymer Physics in Japan,
1993, 36, 445-448.

14. Solid-State ^{13}C NMR Study of PEO/$LiClO_4$ Complexes
Atsushi Asano, K. Takegoshi, and Kunio Hikichi,
Reports on Progress in Polymer Physics in Japan,
1993, 36, 455-458.

II. Published in Conferences

1. NMR Study on the Polymer-Polymer Interaction of
Polycarbonate/Poly(methyl methacrylate) Mixture in Solution
Atsushi Asano, K. Takegoshi, and Kunio Hikichi,
39th Japanese National Polymer Conference; Spring Meeting,
Kyoto, Japan, May.29.1990
Polymer Preprints in Japan, 1990, 39(3), 398.

2. High-Resolution Solid-State ^{13}C NMR Study on Miscibility of
Polycarbonate/Poly(methyl methacrylate) Blends
Atsushi Asano, K. Takegoshi, and Kunio Hikichi,
39th Japanese National Polymer Conference,
Nagoya, Japan, Oct.17.1990
Polymer Preprints in Japan, 1990, 39(11), 3869-3871.

3. High-Resolution Solid-State ^{13}C NMR Study on Phase-Separation
Process of Polymer Blend
Atsushi Asano, K. Takegoshi, and Kunio Hikichi,
25th Japanese National Polymer Meeting of
Hokkaido and Touhoku, Sapporo, Japan, Feb.2.1991
Proceedings of 25th Polymer Meeting, 1990, page 52.

4. Phase-Separation Process of Polystyrene/Poly(vinyl methyl
ether) Blend studied by High-Resolution Solid-State ^{13}C NMR
Atsushi Asano, K. Takegoshi, and Kunio Hikichi,
40th Japanese National Polymer Conference: Spring Meeting,
Kyoto, Japan, June.2.1991
Polymer Preprints in Japan, 1991, 40(4), 1197.

5. High-Resolution Solid-State ^{13}C NMR Study on
Phase-Separation Process of PS/PVME Blend
Atsushi Asano, K. Takegoshi, and Kunio Hikichi,
26th Japanese National Polymer Meeting of
Touhoku and Hokkaido, Sendai, Japan, Jan.16.1992
Proceedings of 26th Polymer Meeting, 1991, page 15.

6. Solid-State NMR Study of Poly(ethylene oxide)/$LiClO_4$ Blend
Atsushi Asano, K. Takegoshi, and Kunio Hikichi,
41th Japanese National Polymer Conference: Spring Meeting,
Yokohama, Japan, May.29.1992
Polymer Preprints in Japan, 1992, 41(4), 1375.

7. Solid-State NMR Study on Phase-Separation of Polymer Blends
Atsushi Asano, K. Takegoshi, and Kunio Hikichi,
41th Japanese National Polymer Conference,
Morioka, Japan, Sep.29.1992
Polymer Preprints in Japan, 1992, 41(10), 4127-4129.

8. Solid-State NMR Study on Phase-Separation of PS/PVME Blend
Atsushi Asano, K. Takegoshi, and Kunio Hikichi,
4th SPSJ IPC 92, Yokohama, Japan, Dec.3.1992
Preprints of 4th SPSJ International Polymer Conference,
1992, page 251.

9. Solid-State ^{13}C NMR Study on the structure of PEO/$LiClO_4$
   Atsushi Asano, K. Takegoshi, and Kunio Hikichi,
   42th Japanese National Polymer Conference: Spring Meeting,
   Kyoto, Japan, May.31.1993
   Polymer Preprints in Japan, 1993, 42(4), 1362.

10. Phase-Separation of Polymer Blend as Studied by ^{13}C- and ^{2}D-NMR in Solids
    K. Takegoshi, Atsushi Asano, Akinori Tezuka,
    and Kunio Hikichi
    42th Japanese National Polymer Conference,
    Tokyo, Japan, Sep.21.1993
    Polymer Preprints in Japan, 1993, 42(10), 4147-4149.

11. Solid-State ^{13}C, ^{1}H, ^{7}Li-NMR Study of PEO/LiClO4 Complexes
    Atsushi Asano, K. Takegoshi, and Kunio Hikichi,
    42th Japanese National Polymer Conference,
    Tokyo, Japan, Sep.21.1993
    Polymer Preprints in Japan, 1993, 42(10), 4150-4152.

12. Spin Diffusion in Polymer Blends
    Atsushi Asano, K. Takegoshi, and Kunio Hikichi,
    32th NMR Conference, Tokyo, Japan, Nov.6.1993
    Preprints of 32th NMR Conference, 1993, page 307-308.